Top copy

THE AERODYNAMIC CHARACTERISTICS OF COMMERCIAL VEHICLES, USING TWO WIND TUNNEL MODELS OVER A MOVING GROUND

by

P.C. ADEY,
B.Sc.(Eng.), A.C.G.I.

of the Department of Aeronautics and Astronautics
University of Southampton
England

A thesis submitted for the degree of
Master of Philosophy

Feburary 1987

LIST OF CONTENTS

UNIVERSITY OF SOUTHAMPTON

ABSTRACT

FACULTY OF ENGINEERING AND APPLIED SCIENCE
DEPARTMENT OF AERONAUTICS AND ASTRONAUTICS

MASTER OF PHILOSOPHY

THE AERODYNAMIC CHARACTERISTICS OF COMMERCIAL VEHICLES, USING TWO WIND TUNNEL MODELS OVER A MOVING GROUND

by Philip Christopher Adey

Over the last fourteen years the Department of Aeronautics and Astronautics has investigated the aerodynamics of road vehicles, with particular attention to commercial vehicles. The 2.1m x 1.7m low speed wind tunnel, with its moving belt simulation of ground effect, has been the main facility for this research. Using this facility a series of tests were undertaken to examine the effect of various radii on a 1:8 scale idealized rigid truck model's cab and container leading edges at zero model yaw.

The requirement for testing large models over a moving ground plane, to increase the model Reynolds number and improve model detail, led to the construction and installation of a large 5.3m x 2.4m moving belt rig in the floor of the Department's new 3.5m x 2.6m wind tunnel. This moving ground is one of the largest in use for this type of vehicle testing, and its mechanical and aerodynamic development is discussed in detail.

In order to measure forces and pressures on road vehicle models in crosswinds, a technique using yawed models with rotating wheels on a yawed 2.0m x 1.1m moving ground was also developed in the 3.5m x 2.6m wind tunnel. This allowed tests on a 1:6 scale truck model in which both the model and moving ground have been yawed up to 15 degrees. It is believed that this is the first time that this technique has been used in road vehicle testing. The purpose of these tests was to quantify the effect wheel rotation and ground plane boundary layer has on the model, especially with the addition of simple aerodynamic 'add-on' devices to the model. To supplement the study, tests in the 2.1m x 1.7m wind tunnel were completed where the same pararmeters were studied at zero yaw.

LIST OF FIGURES

21 Drag results for 1:8 scale idealized rigid truck model in 2.1m x 1.7m wind tunnel

22 Surface pressure distribution around container leading edge

23 Container upper surface pressure distribution on 1:8 scale idealized rigid truck model in 2.1m x 1.7m wind tunnel

24 Container upper surface pressure distribution on 1:8 scale idealized rigid truck model in 2.1m x 1.7m wind tunnel

25 Lift and Pitch results for 1:8 scale idealized rigid truck model in 2.1m x 1.7m wind tunnel

26 Pressure plotting details for 1:6 scale rigid truck model

27 The effect of wheel rotation on container lower surface pressure distribution in 3.5m x 2.6m wind tunnel

28 The effect of wheel rotation on container lower surface pressure distribution in 3.5m x 2.6m wind tunnel

29 The effect of wheel rotation on container lower surface pressure distribution in 3.5m x 2.6m wind tunnel

30 The effect of wheel rotation on container lower surface pressure distribution in 3.5m x 2.6m wind tunnel

31 The effect of wheel rotation on container lower surface pressure distribution in 3.5m x 2.6m wind tunnel

32 The effect of wheel rotation on container lower surface pressure distribution in 3.5m x 2.6m wind tunnel

33 The effect of wheel rotation on container lower surface pressure distribution in 3.5m x 2.6m wind tunnel

34 The effect of wheel rotation on container lower surface pressure distribution in 3.5m x 2.6m wind tunnel

35 The effect of wheel rotation on container lower surface pressure distribution in 3.5m x 2.6m wind tunnel

36 The effect of wheel rotation on container lower surface pressure distribution in 3.5m x 2.6m wind tunnel

37 Types of rear wheel mudguarding for 1:6 scale rigid truck model

38 Effect of ground motion on drag changes with fixture of 'add-on' devices for 1:6 scale rigid truck model in 3.5m x 2.6m wind tunnel

39 Effect of ground motion on side f. changes with fixture of 'add-on' devices for 1:6 scale rigid truck model in 3.5m x 2.6m wind tunnel

40 Effect of ground motion on yawing m. changes with fixture of 'add-on' devices for 1:6 scale rigid truck model in 3.5m x 2.6m wind tunnel

41 Effect of ground motion on rolling m. changes with fixture of 'add-on' devices for 1:6 scale rigid truck model in 3.5m x 2.6m wind tunnel

42 Effect of ground motion for 1:6 scale rigid truck model in 3.5m x 2.6m wind tunnel

43 Effect of ground motion for 1:6 scale rigid truck model in 3.5m x 2.6m wind tunnel

44 Effect of ground motion for 1:6 scale rigid truck model in 3.5m x 2.6m wind tunnel

LIST OF PLATES

Plate

LIST OF SYMBOLS

C_D (Cd)*	drag coefficient
C_L (Cl)	lift coefficient
C_{LF}	front axle lift coefficient
C_{LR}	rear axle lift coefficient
C_M (Cm)	pitching moment coefficient
C_P	pressure coefficient
C_N (Cn)	yawing moment coefficient
C_R (Cr)	rolling moment coefficient
C_Y (Cy)	side force coefficient
q_∞	freestream dynamic pressure
Re	Reynolds number based on model length
Re_R	Reynolds number based on model circular radius
U_∞ (Vo)	freestream velocity
U/U_∞ (V/Vo)	local velocity deficit (ratio)
ΔC_B (dCb)	change of coefficient from a baseline value
δ	boundary layer thickness

*Alternative notation used in some figures in brackets.

ACKNOWLEDGEMENTS

The author wishes to express his grateful thanks to Mr. K. Burgin, for his patient encouragement and helpful discussions during the course of the work.

Further thanks are due to Professor G. M. Lilley and Mr. J. P. Beatham of the Department of Aeronautics and Astronautics and also to Mr. L. Gutteridge of Leyland Trucks Limited for their useful suggestions and comments.

The project could not have been completed without technical staff and I would particularly like to thank Mr. D. R. Browning, Mr. D. W. Davidson, Mr. M. Grinter, Mr. G. H. Moore and Mr. D. Whitham for their constant support and excellent workmanship.

Thanks are also due to Mr. L. J. Dykes of the Design Office of the Department of Aeronautics and Astronautics, for his contribution to the mechanical design.

The work was supported by the Science and Engineering Research Council.

CHAPTER 1
INTRODUCTION

1.1 A SHORT REVIEW OF COMMERCIAL VEHICLE AERODYNAMICS

Any car driver who uses a main road in this country or abroad, knows about commercial vehicle aerodynamics and their effects. Buffetting when being overtaken, or even when considerable distances behind a truck can be quite alarming. Generations of children have used the dirty backs of containers to place their point of view. A further aspect and one which is potentially lethal, is the spray generated by trucks that can obscure a driver's vision for vital moments.

The use of 'air-management' on road vehicles is not new: as far back as the nineteen twenties attempts at streamlining passenger cars, coaches and some trucks were made. However with the abundance of energy in the decades after World War II, the average truck was not the attention of aerodynamic treatment. The oil embargo by the Arabian States in 1973, legalisation, the Iranian crisis during 1979 and enforced competition with dwindling markets, changed the whole motor industry's outlook in the seventies. Aerodynamics became important as one of the most cost-effective methods of conserving fuel, by the reduction of aerodynamic drag.

Air resistance has the greatest effect at high speeds and thus significant fuel savings are obtained on vehicles which spend considerable time at high speeds. However, with some vehicles, for instance a typical ten ton box-van (having a drag coefficient of 0.60), appreciable drag losses can occur at speeds as low as 30mph (see Table 1).

Vehicle Speed (mph)	% Of Total H.P. Due To Aerodynamic Drag
30	31
50	55
70	71

Table 1

With a high proportion of freight being carried around the world by heavy goods vehicles, it became a necessity to understand the flow about these vehicles. Because of the prospect of quick returns, attention was initially given to the testing and development of drag reducing devices and fairings for mounting on standard production trucks. A vast amount of reseach has been published (see Bibliography) in America, Australia, Europe and Japan. Although there is much duplication, the effects of the following parameters, used for reducing the aerodynamic forces acting on commercial vehicles, are well documented:

(i) Cab-roof deflectors
(ii) Forebody shaping of cab and container
(iii) Effect of load types, heights and position
(iv) Shaping rear face of container
(v) Under-bumper airdams and container side panels
(vi) Sealing cab-container gap

The majority of the investigations were completed with detailed scale models in a wind tunnel, or actual trucks using a 'coast-down' or 'over-the-road' method of assessment. However, full-scale measurements are subject to many uncertainies; lack of precise environmental control, the difficulty of making accurate measurements on a moving, vibrating platform, and the difficulty of separating aerodynamic forces from those of other origin. The time and expense required for such testing resulted in the use of aeronautical facilities for vehicle research and the building of wind tunnels specifically for road vehicles, for example Kelly et al.(23)* and Egle et al.(13).

---

*Numbers in parenthesis designate References at end of paper.

In order that the wind tunnel represent road behaviour, the wind tunnel flow and model simulations must faithfully represent real life. The most important parameter being the necessary presence of a ground plane. As a vehicle moves over the road, both the air and the road are stationary, and thus no boundary layer exists on the road. In the wind tunnel, however, since the air moves relative to any fixed ground representation in the tunnel, a boundary layer is formed. Attempting to keep the wind tunnel ground plane boundary layer thin has resulted in three common techniques:

(i) A separate ground board

(ii) Floor mounting with upstream suction to remove the boundary layer

(iii) A moving ground plane

Of particular interest to Southampton University, has been the acceptance of the moving ground plane as a good simulation of the ground and an essential part of racing car and, to a lesser extent, passenger car testing. The interaction of underbody flows with such vehicles a major factor in their performance and safety.

In addition to racing and passenger car aerodynamics, research using the moving ground installation in the University's 2.1m x 1.7m wind tunnel has centred on the aerodynamics of bluff bodies (Refs. 16 and 21), reducing the aerodynamic drag of trucks (Ref. 2) and reducing the water spray from heavy vehicles (Refs. 1 and 3).

1.2 PRESENT INVESTIGATION

This report will present the progress achieved and results obtained from a research programme undertaken at Southampton University. The research completed was in accordance with the programme of work suggested by the Science and Engineering Research Council in Grant Reference GR/C/83432 and as such was directed at the aerodynamic design of heavy goods vehicles for drag reduction and spray suppression in crosswinds. The programme had four major avenues of work, as described below.

(i) Commissioning and development of a yawed moving ground plane.
(ii) Development of a large 5.3m x 2.4m moving ground plane.
(iii) The effect of varying cab and container leading edge radius on the flow field around an idealized rigid truck shape.
(iv) Assessment of the effects of wheel rotation and ground plane boundary layer on a rigid truck at zero and non-zero yaw angles.

The objective of the first two avenues of work was primilarily to provide unique facilities at Southampton University for the wind tunnel testing of commercial vehicles over a moving ground. Whilst the latter two avenues used these new facilities and established facilities, for the investigation of wind tunnel testing techniques and aerodynamic phenomenon.

A fuller introduction to each investigation is given at the start of the respective chapter.

CHAPTER 2
DEVELOPMENT OF WIND TUNNEL FACILITIES

2.1 INTRODUCTION

The research programme detailed in Chapter 1 required the development of two new facilities. This chapter establishes the level of development currently attained and the further developments, if any, which may be required. The reseach programme used the established 2.1m x 1.7m and the new 3.5m x 2.6m wind tunnels with two moving ground rigs. Each facility is individually discussed.

2.2 2.0m x 1.1m MOVING GROUND IN 2.1m x 1.7m WIND TUNNEL

2.2.1 Introduction

Over the last fourteen years, Southampton University has completed important research into the aerodynamics of road vehicles. The 2.1m x 1.7m wind tunnel, with its moving belt representation of a road surface, has been the main facility for this research. The requirement for a good simulation of ground effect was met with the installation of the 2.0m x 1.1m moving belt rig above the original wind tunnel floor. The speed of the belt is infinitely variable between 0m/s and its maximum speed of approximately 28m/s. The moving belt rig is fully described by Hurst(21), and is shown in Figure 1 and Plate 4.

This research programme has not attempted to further develop either the 2.1m x 1.7m wind tunnel nor its moving ground installation. Instead, at the commencement of the programme the velocity distribution above the belt was measured at various positions, to give a datum for future moving ground developments in the 3.5m x 2.6m wind tunnel; the optimum simulation for road vehicles being one which minimizes the bondary layer.

2.2.2 Experimental Arrangement

Two values of the boundary layer are used throughout this thesis to quantify the velocity distribution above the belt:

(i) The standard experimental boundary layer thickness (δ), defined as the distance from the belt surface to the point where the velocity in the boundary layer (U) is 98% of the freestream velocity (U_∞ : measured by a pitot-static probe, fixed to the tunnel's working section wall).

(ii) The velocity deficit (U/U_∞) at a height of 10mm above the belt surface (measurements closer than 10mm unobtainable in some investigations reported in 2.3 and 2.4).

Total pressure measurements of the ground plane boundary layer were made with a pitot rake positioned in an empty test section above the moving belt. The rake measured pressures at 5 and 10mm intervals,

to a height of 10 and 30cm, respectively. A mutitube manometer, positioned outside the tunnel, was connected to the rake by lengths of fine bore tubing. For all the results presented in 2.2 the centre of the lowest probe was 5mm above the belt surface.

Boundary layer traverses over the belt were taken, with and without leading edge suction and moving belt (2.2.3), with three air-belt speeds (2.2.4), at three downstream positions (2.2.5), and at three transverse positions (2.2.6). However, results presented in 2.2.3 were taken at a different time to those in 2.2.4/5/6 and thus absolute differences due to experimental error exist. Results were obtained at a synchronized air-belt speed of 26.2m/s with leading edge suction, unless otherwise stated.

2.2.3 Leading Edge Suction and Belt Movement

Often during wind tunnel investigations, using a moving ground facility, tests are repeated with the belt stationary in order to check the sensitivity of the model's force or pressure measurements to the ground plane boundary layer. Further boundary layer changes can be accomplished over the 2.0m x 1.1m moving ground by stopping the leading edge suction. To investigate the effect of these changes, together and individually, velocity profiles were measured with the four suction-belt variants at the centre of the belt (1.05m downstream of the front roller's crest). The results are presented in Table 2 (below) and in Figure 2(a).

	U/U_∞	δ(mm)
L.E.Suction Off & Belt Stopped	.787	74
L.E.Suction Off & Belt Moving	.795	82
L.E.Suction On & Belt Stopped	.952	14
L.E.Suction On & Belt Moving	.969	17

Table 2

The results show that the boundary layer over the belt depends largely on the leading edge suction. Without suction applied the boundary layer thickness increased by approximately five fold (ave. $\Delta\delta$= 63mm) and the average velocity deficit decreased by 0.17. Stopping the belt decreased the boundary layer thickness by a small amount

(ave. $\Delta\delta$= 6mm). However, because the moving belt surface caused the air next to the surface to accelerate, an improved velocity deficit with the belt moving was obtained at heights up to 10mm.

The dependence of the velocity profile on suction was a result of flow separation from the front suction box's leading edge (a circular 13mm radius). Without suction, the separation bubble formed did not reattach to the suction box, resulting in the large boundary layer measured over the belt. Applying suction removed this separation bubble, giving attached flow over the remaining chord of the suction box and subsequently a smaller boundary layer over the belt.

2.2.4 Air-Belt Speed

Results obtained with three different synchronized air-belt speeds, at the centre-line of the belt and the overhead balance (1.19m downstream of the front roller's crest), are presented in Table 3 (below) and in Figure 2(b).

Speed(m/s)	U/U_∞	δ(mm)
19.0	.979	12
23.3	.965	28
26.2	.954	34

Table 3

The velocity profiles at higher air-belt speeds showed an increased velocity deficit at the belt surface and throughout the boundary layer, thereby resulting in thicker boundary layers at higher Reynolds numbers. This does not, however agree with usual boundary layer dependence on Reynolds number, where the opposite is predicted. This suggests that there is insufficient suction, at higher speeds, to remove the separation bubble formed at the leading edge of the front suction box.

2.2.5 Downstream Position

Results obtained at three positions down the streamwise length of the belt's centre-line are presented in Table 4 (over) and in Figure 2(c).

Position	U/U_∞	δ(mm)
1(0.13m)*	.942	22
2(0.66m)	.950	29
3(1.19m)	.954	34

*distance downstream

Table 4

Position 1 was over the leading edge of the perforated base plate (on which the belt runs), 0.13m downstream of the front roller's crest. Position 3 was at the centre-line of the overhead balance (1.06m downstream of position 1) and position 2 was half-way between positions 1 and 3.

The results show the velocity deficit at the ground decreased with downstream position. This indicates that a layer of retarded air was present immediately above the belt at position 1, which was subsequenty accelerated by the belt's movement. This air probably orginated from outside of the tunnel, entering through the front suction box-belt gap. At heights greater than 15mm from the belt's surface the results indicate another layer of air, whose thickness increased with distance downstream. This being the boundary layer originating from the end of the front suction box.

2.2.6 Transverse Position

Results obtained at three transverse positions across the belt are presented in Table 5 (below) and in Figure 2(d).

Position	U/U_∞	δ(mm)
1(28cm)*	.946	42
2(53cm)	.954	34
3(78cm)	.983	0

*distance across belt

Table 5

Position 2 was at the centre-line of the belt and the overhead balance, while positions 1 and 3 were 25cm to the left and right of the belt's centre-line, respectively (looking downstream at the belt).

The velocity profiles showed large changes in the boundary layer obtained at these three positions. The variation of velocity deficit and boundary layer thickness, was greater than those found in 2.2.3 and 2.2.4. The distribution measured at position 3 gave the most favourable figures obtained during this investigation. The cause of these variations was the front suction box, which due to poor design and deterioration, produced inconsistent boundary layers transversely across the belt.

2.2.7 Conclusion

Even though boundary layer changes, either by air-belt speed or distance downstream, were found, variations of the velocity profile due to the quality of the front suction box design, were more substantial.

With the present moving belt rig, the normal turbulent boundary layer on a usual fixed ground representation of a road surface was eliminated and a local velocity distribution within 6% of freestream measured. However, with an improved front suction box design, a maximum velocity deficit of 2% could be obtained.

2.3 YAWED 2.0m x 1.1m MOVING GROUND IN 3.5m x 2.6m WIND TUNNEL

2.3.1 Introduction

In real life a truck's flow field is dominated by cross-winds. The 2.1m x 1.7m wind tunnel is suitable for up to 1:6 scale rigid and 1:8 scale articulated truck models in yawed flow. However the moving ground is 1.1m wide and cannot be yawed due to the structure of the wind tunnel, which has the conventional corner fillets of an aeronautical wind tunnel. Therefore, to simulate cross-winds, the model alone is yawed and the resultant forces measured. Fixed wheels are fitted to the model and the tunnel floor boundary layer is removed by the moving belt, leading slot and suction box. This technique was used for tests described in Chapter 3.

Therefore to simulate cross-winds by yawing the moving ground with the model, the 3.5m x 2.6m wind tunnel had to be used; this technique being essential if rotating wheels are to be attached to the model.

2.3.2 November 1984

During November 1984, the 2.0m x 1.1m moving ground was first transported to the 3.5m x 2.6m wind tunnel. The belt surface was positioned flush with the tunnel floor so that the tunnel's original cross-section area was not reduced, the installation being shown in Plate 1(b). The 2.1m x 1.7m wind tunnel front sucton box was placed ahead of the moving ground, with a new suction box positioned along the ground's windward side. Both suction boxes were flush with the belt's surface, as shown in Plate 1(a). The moving ground had a maximum yaw angle of 22.5 degrees.

Mechanically the yawed moving ground was successful, flatness and tracking of the belt being completely adequate. With a tunnel air-belt speed of 26.2m/s, velocity profiles were measured above the belt surface at the centre-line of the belt and the overhead balance (1.05m downstream of the front roller's creast). The same procedure as described in 2.2.1 was used.

The results for zero degrees yaw, Figure 3(a), showed an unacceptable velocity deficit (U/U_∞= 0.803) and thick boundary layer (δ= 119mm). Obviously the suction fans were incapable of removing the

tunnel floor boundary layer: the front suction fan being the same as used in the 2.1m x 1.7m wind tunnel installation, and the side suction fan being the one used, in the same installation, for the belt suction.

2.3.3 May 1985

The next test session with the yawed moving ground, held during May 1985, was completed with the belt surface raised 13cm above the original tunnel floor. The large front suction box and fan from the 5.3m x 2.4m moving ground rig were incorporated ahead of the ground, thus enabling the tunnel floor boundary layer (δ = 75mm) to be ducted out of the tunnel through a 75mm high gap under the large suction box (Figure 4). The front and side suction boxes were positioned as during November 1984, but raised to be flush with the belt surface. The suction for the small (2.1m x 1.7m wind tunnel) suction box was provided by the same fan used before. However, the side suction fan was replaced by three smaller fans, each rated at 28.3m^3/min. at 0.15m W.G.Press. Unfortunately raising the moving ground limited the maximum obtainable yaw angle to 17.5 degrees.

Velocity profiles were again measured, under the same conditions as used during November, in order to establish the effect of the modifications. Initially tests were completed studying the leading edge radius on the large front suction box, and also the length and position of porous material on the surface of the three suction boxes. The final configuration had a velocity deficit of 0.942. Then the belt was yawed to 15 degrees and velocity profiles were measured along the centre-line of the overhead balance at 12.7cm intervals transversely across the belt. The results obtained are presented in Table 6 (over) and in Figures 3(b), 3(c) and 3(d).

Transverse distance(cm)	U/U_∞	δ(mm)
12.7	.931	21
25.4	.804	97
38.1	.955	125
50.8	.965	112
63.5	.946	42
76.2	.967	16
88.9	.965	18
101.6	.965	18

Table 6

The lack of suction where the side and the small front suction boxes joined, resulted in the poor velocity distribution at 25.4cm across the yawed belt, whilst a joint between the two centre suction chambers of the large front suction box gave rise to the thick boundary layers measured at 38.1 and 50.8cm across the yawed belt. This joint stopped the appliance of suction through a 3.5cm wide strip along the centre-line of the tunnel. However, at larger distances across the belt the velocity deficit became smaller and the boundary layer thickness decreased. Thus the boundary layer over much of the yawed belt was equal to that measured over the unyawed 2.1m x 1.7m wind tunnel installation. The facility was subsequently pronounced adequate for testing to be commenced, using a 1:6 scale truck model.

2.3.4 July and October 1985

Further yawed ground tests were conducted in July and October 1985. The installation was kept unchanged from that used during May, except a new suction fan (described in 2.4) was used in conjuction with the large front suction box. To assess the effect of the new suction fan, during October velocity profiles were taken transversely across the unyawed belt, firstly along the centre-line of the overhead balance, Figure 5(a), and secondly 51cm upstream of the balance centre-line, Figure 5(b). The results, which were only taken up to a height of 60mm, are also presented in Table 7 (over).

Transverse distance(cm)	U/U_∞	δ(mm)
12.7*	.985	0
25.4	.985	0
50.8	.948	>60
76.2	.973	15
101.6	.966	19

*not shown in Figure 5(a)

(a)

Transverse distance(cm)	U/U_∞	δ(mm)
25.4	.985	0
50.8	.947	>60
76.2	.976	13
101.6	.980	10

(b)

Table 7

The cause of the relatively poor boundary layer at 50.8cm across the belt was the large front suction box and was due to the same reasons discussed in 2.3.3. However, the other velocity profiles gave excellent velocity deficits, now smaller than those measured in May and those measured over the unyawed 2.1x 1.7m wind tunnel installation, and with negligible boundary layer thickness. The 2.0m x 1.1m yawed ground installation was thus completely satisfactory and no further development was conducted.

2.4 5.3m x 2.4m MOVING GROUND IN 3.5m x 2.6m WIND TUNNEL

2.4.1 Description of the moving ground

The use of large scale models, to improve the absolute measurement at a higher Reynolds number and to allow more representative detail on the model, resulted in the development of a large moving ground, with boundary layer control, in the 3.5m x 2.6m wind tunnel. The moving ground is shown in Figure 1 and Plate 2. When this facility is required for use in the wind tunnel, a six meter length of the working section floor is removed. The moving belt, mounted in its steel framework, is raised into position with the belt surface 15cm above the test section floor level so that the belt's surface is above the tunnel floor boundary layer. The P.V.C. belt is 2.44m wide and the distance between the crests of the two 46cm diameter end rollers is 5.30m. The upper half of the belt rests on a flat perforated base plate which is positioned at the same height as the roller crests. The upper surface of the base plate is anodized in an attempt to reduce the frictional forces between the belt and plate. The base plate is perforated so that any tendency of the belt to lift or flap, is countered by applying suction through four streamwise independent suction chambers mounted under the plate. The lower half of the belt loop is supported by three rollers, two intermediate 23cm diameter idle rollers positioned 76cm inboard of the two 46cm end rollers, and a tensioning roller positioned at the belt's mid-length.

The belt is powered by an internally mounted 100 H.P. hydraulic motor which drives the downstream end-roller through a toothed transmission belt. The speed of the belt is manually monitored using an electronic tachometer fitted to the upstream end-roller. Tracking (control of the belt's transverse movement) was initially achieved by manual vertical skewing of the upstream end-roller (belt tension varying across the belt's width).

Immediately upstream of the belt a front suction box is fixed to the tunnel floor, level with the belt's surface. The suction box spans the width of the tunnel and has a chord of 56cm. Under the complete length of the suction box is a 95mm high gap which allows the tunnel floor boundary layer (δ= 75mm) to be expelled out of the tunnel. The suction box also ensures that an acceptable leading edge

stagnation point is obtained with subsequent attached flow, and then that no new boundary layer develops over its chord by applying suction (see 2.4.4).

2.4.2 August 1984

Initial running of the new moving ground took place during August 1984. Unfortunately due to severe vibrations, testing was abandoned. Poor performance of the moving ground was caused by the 15cm diameter tensioning roller. This roller could not keep the unsupported belt continuously in tension with its sliding assembly mounting, thus resulting in the belt 'slapping'.

2.4.3 March 1985

Before the next series of tests, during March 1985, the small tensioning roller and mounting was replaced with a 23cm diameter roller mounted on two trailing arms (similar to the 2.0m x 1.1m moving ground design). However during the first day of development, a split hydraulic line covered the belt's undersurface with oil. Even after extensive cleaning of the belt, slippage of the driving roller occurred at a belt speed of 21.4m/s. The attachment of '3M grit-tape' to the driving roller reduced slippage, and belt speed was limited to 23.8m/s because of belt tracking problems (a result of incorrect belt tensioning) and vibrations of the ground's frame. Re-positioning the tensioning roller by small amounts, addition of weights and springs to the roller to add further tension, proved to have little effect once slippage was overcome.

With a tunnel air-belt speed of 23.8m/s, velocity profiles over the belt surface were measured (again using the procedure described in 2.2.1). The velocity distribution obtained 25cm off the belt's centre-line and at the centre-line of the overhead balance (2.53m downstream of the front roller's creast), which is presented in Figure 6(a), had a thick boundary layer (δ= 210mm) with a large velocity deficit (U/U_∞= 0.842).

2.4.4 May and September 1985

The above result placed doubt on the front suction box's effectiveness. Therefore during May 1985, in conjunction with testing of the yawed 2.0m x 1.1m moving ground, smoke flow visualization on the suction box was carried out. This showed the flow was separating from the leading edge radius of the suction box. In addition the suction applied along the suction box's chord was not removing the resulting separation bubble and hence giving the poor velocity profiles previously measured over the ground. To resolve this a cambered elliptical leading edge (or drooped nose) was placed over the original leading edge radius. The new leading edge was found to give the required attached flow during further flow visualization. Also during May, velocity profiles over the yawed ground were improved with suction only applied through a 15cm chord of porous material, starting 15cm from the leading edge of the suction box. Originally the whole of the upper surface of the suction box was porous.

These front suction box developments were incorporated with the 5.3m x 2.4m moving ground during September 1985. Addionally a new suction fan for the front suction box was bought for the tests. The fan had a superior specification (85.0m^3/min. at 1.02m W.G.Press.) than the original fan. Modifications to the tensioning roller swinging arms were also implemented. An improved spring assembly (to add further tension to the belt) and a motorcycle damper (to reduce vibration of the roller) were fitted to each arm.

With the belt running at 27.4m/s, a strobe light showed severe vibrations in the mounting points of the tensioning roller swinging arms and the ground's frame in the vacinity. To alleviate this a strengthening beam was bolted across the ground's frame at the mounting points of the swinging arms. The modified moving ground subsequently reached speeds of 28.6m/s without vibration, with strong vibration starting at speeds above 30m/s. Further strobe studies at this speed showed bending of the tensioning roller to be causing these vibrations.

To assess the front suction box modifications, velocity profiles were completed at the same position as during March but at a synchronized air-belt speed of 26.2m/s. The profile obtained, which is

also presented in Figure 6(a), had a velocity deficit of 0.931 and a boundary layer thickness of 73mm.

2.4.5 March 1986

In an attempt to further reduce the severe vibrations, and improve the ground ground plane boundary layer, a number of modifications were carried out on the moving ground during March 1986. Firstly the 23cm diameter tensioning roller was replaced with a new 46cm diameter roller, of similar design, but having a higher standard of construction and superior dynamic balancing (to 2000 r.p.m.). This replacement roller was hoped to remove any vibrations set up by the previous roller's flexing. Secondly, to supplement the frame strengthening completed during September 1985, further strengthening between the moving ground's frame at the mounting points of the tensioning roller's two trailing arm damper/spring assembies (where the most severe vibration occurred) and the floor, and bracing between the leg supports of the ground, were fabricated. Finally, the belt's lateral tracking system was redesigned so that this was achieved by manual vertical skewing of the upstream intermediate idle roller. This development was found to work entirely satisfactory and because the upstream end-roller was subsequently fixed with the roller's creast, front suction box and perforated base plate, level throughout all periods of wind tunnel testing, this was hoped to improve the velocity distribution above the belt.

To quantify any flow quality improvements above the belt, surface velocity profiles were re-measured. However, although during static 'wind-off' tests belt speeds of 38.1m/s were reached, this was not possible with the tunnel air synchronized with the belt because of catastrophic belt lift. Thus velocity profiles were obtained at a synchronized air-belt speed of 26.2m/s, when belt lift at the rear of the perforated base plate was only minimal. The results of these tests are presented in Figure 6 and discussed below.

(i) At heights up to 75mm above the belt, the velocity distribution obtained 25cm off the belt's centre-line and at the centre-line of the overhead balance, also presented in Figure 6(a), showed an improvement in comparison with that obtained during September 1985. However, unaccountably at heights above 30mm from the

belt the U/U_∞ values asymptoted to approximately 0.98, compared to the September value of 0.99 at heights above 90mm.

Therefore, although the velocity profile obtained during March 1986 was not quite up to the standard of those obtained over the 2.1m x 1.7m wind tunnel's moving ground installation, a significant improvement had been acomplished during the development programme, as summerized in Table 8 (below).

Test Session	U/U_∞	δ(mm)
March 1985	.842	210
September 1985	.931	73
March 1986	.945	45

Table 8

(ii) Results obtained at three transverse positions across the belt are presented in Table 9 (below) and in Figure 6(b).

Position	U/U_∞	δ(mm)
1(0.97m)*	.945	45
2(1.22m)	.890	88
3(1.47m)	.932	34

*distance across belt

Table 9

Position 2 was at the centre-line of the belt and the overhead balance, while positions 1 and 3 were 25cm to the left and right of the belt's centre-line, respectively (looking downstream at the belt).

The velocity profiles showed large changes in the boundary layer obtained at these three positions, reinforcing the findings reported in 2.4.3. The cause of the relatively poor boundary layer at the centre-line of the belt was the large front suction box for the reasons discussed in relation to the yawed 2.0m x 1.1m moving ground (2.3.3).

(iii) Results obtained at two positions down the streamwise length of the belt are presented in Table 10 (over) and in Figure 6(c).

Position	U/U_∞	δ(mm)
1(1.27m)*	.899	34
2(2.53m)	.932	34

*distance downstream

Table 10

Position 2 was at the centre-line of the overhead balance (2.53m downstream of the front roller's creast). Position 1 was half-way between Position 2 and the front roller. Both positions were 25cm to the right of the belt's centre-line (looking downstream at the belt).

The results show the velocity deficit up to 30mm above the belt decreased with downstream position, which indicates that a layer of air accelerated by the belt's movement was present above the belt. This also being similar to that observed over the 2.1m x1.7m wind tunnel installation (2.2.4).

2.4.6 Conclusion

At the time of writing* further modifications are planned for the 5.3m x 2.4m moving ground. These are:

(i) A new front suction box (to reduce ground plane boundary layers and to produce negligible transverse variations)

(ii) A larger belt suction fan and the drilling of more suction holes towards the rear of the perforated base plate (to overcome belt lift).

Having implemented these changes, testing at air-belt speeds of 30m/s, with improved ground plane boundary layers and minimal belt lift, should be possible during the summer of 1986.

*May 1986

2.5 BALANCE REPEATABILITY

While development and assessment of ground plane simulation facilities was being carried out during 1984/5, a parallel investigation studying the performance of force measuring balances in both the 2.1m x 1.7m and 3.5m x 2.6m wind tunnels, the three component strain gauge dynamometer and a new strut mounted drag measuring balance was completed. This investigation had two avenues of work, calibration and repeatability. The results arising from the latter are presented here.

In both wind tunnels, road vehicle models are mounted above a moving ground from an overhead balance. The two overhead balances give measurements of the lift and drag forces, and the pitching moment. The 2.1m x 1.7m tunnel mechanical balance is fixed and thus can only give wind co-ordinate measurements, while the 3.5m x 2.6m tunnel load cell balance can be yawed giving body co-ordinate measurements. In order to obtain, side force, yawing and rolling moments, the three component strain gauge balance is mounted in the model tested.

The repeat tests were runs completed with a particular vehicle configuration on successive runs, or at different times during a day, or on different days, or a combination of these three (without removing the model from the tunnel between any of the tests). The majority of the repeats done in the 2.1m x 1.7m wind tunnel were taken during research described in Chapters 3, 4 and 5, over the 2.0m x 1.1m moving ground with negligible ground boundary layer. The repeats done in the 3.5m x 2.6m wind tunnel were taken during the development disussed in 2.3 and 2.4, with associated poor ground boundary layers. Two models were used in the investigation, 1:6 and 1:4 scale models of a rigid truck (typical results are given in 3.3).

The results for the four balances, presented in Table 11, give the average coefficient change for all the repeat runs made during particular test sessions. Additionally, Table 11 lists the number of repeat runs that were completed, from these it should be noted that the number of repeats done in the 5.3m x 2.6m wind tunnel were generally smaller (and also taken over shorter periods of time) than those in the 2.1m x 1.7m wind tunnel.

2.1m x 1.7m Tunnel Balance

Date	Configurations	Repeats	ΔC_L	ΔC_D	ΔC_M
8/84	20	48	.0029	.0057	.0020
9/84	11	22	.0051	.0056	-
4/85	1	23	.0044	.0073	.0039
8/85	2	38	.0054	.0055	.0031
8/85	9	18	.0013	.0016	.0008
9/85	34	68	.0015	.0011	.0008
1/86	11	22	.0023	.0011	.0007

3.5m x 2.6m Tunnel Balance (* = 25mV)

Date	Configurations	Repeats	ΔC_L	ΔC_D	ΔC_M
11/84	5	12	.0118	.0778	.0274
3/85	2	12	.0082	.0340	.0183
7/85	1	3	.0136	.0165	.0140
	1	3	-	.0498*	-
9/85	4	16	.0050	.0113	-
	2	6	-	.0144*	-

Strain Gauge Dynamometer

Date	Configurations	Repeats	ΔC_Y	ΔC_N	ΔC_R
9/84	11	22	.0209	.0035	.0087
11/84	5	12	.0050	.0034	.0157
10/85	76	152	.0070	.0081	.0059

Strut Balance

Date	Configurations	Repeats	ΔC_D
9/85	6	22	.0047
10/85	76	152	.0046

Table 11

The 25mV quoted for two of the 3.5m x 2.6m balance drag measurements, refers to the maximum output of a new load cell used during these tests (all other tests used a 50mV load cell).

The repeatabilities above will be considered after comparing them with the following values reported by Cooper et al.(8) and Cooper

et al.(11) at different wind tunnels in Europe and America.

Reference(8): zero yaw average repeatability obtained at four North American wind tunnels (bad lift repeat due to results at a particular tunnel).

	ΔC_L	ΔC_D	ΔC_M	ΔC_Y	ΔC_N	ΔC_R
+/-	.011	.002	.004	.005	.003	.005

Reference(11): zero yaw drag repeatability obtained at the following establishments.

	ΔC_D
National Research Council, Canada	+/- .001
National Maritime Insitute	+/- .005
Fachhochscchule, Aachen	+/- .004
Cranfield	+/- .005
M.I.R.A.	+/- .002

Inspection of all the above results showed the 2.1m x 1.7m tunnel balance exhibited excellent repeatability in all three components. The balance's drag repeatability being better than three of the five tunnels used by Cooper et al.(11) and similar to the remaining two tunnels.

The 3.5m x 2.6m tunnel balance initially gave an unacceptable drag (ΔC_D= 0.0778) and pitching moment (ΔC_M= 0.0274) repeatability. During the period of assessment the level of repeatability improved substantially (eventually ΔC_D= 0.0113 and ΔC_M= 0.0140). This was strange since no particular corrective work was done on the balance in this period. The improved repeatability was probably a result of two factors, firstly the reduced time scale over which repeat runs were obtained in the later tests, and secondly improved wind tunnel testing techniques as the author's experience of using the balance grew over the assessment period. The lift coefficient repeatability throughout the period was always less than 0.0140. Replacement of the original drag load cell (50mV) with a new load cell (25mV) having a sensitivity nearly three times that of the original, did not give better repeats.

As a result, in its present state the 3.5m x 2.6m tunnel balance was found to be of very limited use for road vehicle testing, the balance, designed for large downforces obtained from aeroplane models, lacks repeatability when measuring modest forces. Although if

corrective work on the balance was carried out, and the repeatability continued its present improving trend, this situation would change.

Because of this a new drag measuring load cell balance was constructed for tests in the 3.5m x 2.6m wind tunnel. The balance, which is placed above the model in the mounting strut, gave substantially improved drag repeatabilities (ΔC_D= 0.0047) in comparison with the overhead balance of the 3.5m x 2.6m wind tunnel. Subsequently it was decided that all future testing in the 3.5m x 2.6m wind tunnel would utilize this balance in preferance to the tunnel's overhead balance.

Repeatability obtained from the strain gauge dynamometer during September 1984 was acceptable, except for high sideforce values. Slack in the model's mounting strut pivot assembly was thought to be a contributing factor and modifications to the pivot bearings were completed before the November 1984 tests. The sideforce repeatability subsequently improved, however to the detriment of the rolling moment values. A new pivot assembly was then manufactured, but unfortunately the dynamometer could not be used with the new mounting during the later tests.

As a consequence of this study, to enable confident use of force results obtained during testing in either tunnel, coefficients presented in this report are given to three decimal places.

CHAPTER 3
1:6 SCALE RIGID TRUCK MODEL

3.1 INTRODUCTION

Before commencing the latter two avenues of research proposed in Chapter 1, a preliminary programme investigating fundamental changes in wind tunnel testing of a commercial vehicle was deemed necessary.

Gutteridge(19) had suggested parameters, such as ground plane boundary layer and model-ground clearance, caused the variation of results he obtained from five wind tunnels in the U.K. In addition to these parameters, the effect of yaw, Reynolds number, transition and a turbulence generating grid, were studied. Even though it was feared that the result of some of these changes would be small, a comprehensive set of results would be a useful foundation for, and comparison with, future research.

The model used in this investigation, a 1:6 scale rigid truck (loaned by Leyland Vehicles Limited), was one of the two models reported by Gutteridge and is shown in Figure 7. The wooden model had a square edged container, and a cab with interchangeable forebodies giving either sharp or radiused leading edges. An airdam for both cab radii was available. The model had no surface detail, and chassis detail was simply modelled having no cooling flow and fixed wheels.

3.2 EXPERIMENTAL ARRANGEMENT

The results reported here were obtained from experiments carried out in the University's 2.1m x 1.7m wind tunnel with its 2.0m x 1.1m moving ground. The tests (unless otherwise stated) were all performed at a synchronized air-belt speed of 26.2m/s, giving a Reynolds number of 1.96×10^6 (based on model length). This Reynolds number being just greater than one-sixth of the full-scale value at 55 m.p.h. Except for the results reported in 3.4, dynamic-head was measured by two pitot-static probes, fixed to the tunnel wall, in the freestream alongside the model.

The model was attached to the three component overhead balance of the wind tunnel by a circular vertical strut (38mm diameter), which passed through a hole in the container's roof. The pitching moment was transmitted to the balance by a length of wire attached to the rear of the container. The three component strain gauge dynamometer was mounted in the model's container, giving measurements of the side force, yawing and rolling moments.

The area blockage ratio was 7.7% based on the model and mounting strut frontal areas (5.8% based on the model alone). No blockage correction was applied to the results, these being presented in the body co-ordinate system (similar to the M.I.R.A. axis system) shown in Figure 8.

The pitching moment coefficients showed unacceptable scatter at yaw. This was caused by the pitch wire, which was attached to the model off the container's centre-line, a distance which increased with yaw. This made the model unstable in pitch, but also resulted in a rolling moment interaction in the pitch wire, measured by the overhead balance. Even though the interaction was taken into account in the data reduction, this proved insufficient, resulting in the unreliable pitching moment coefficients at yaw. Thus reference to pitching moment coefficients at yaw will not be made in Chapter 3. In future, to obtain pitching moments at yaw the overhead balance must be modified to enable the pitch wire to be mounted from the balance off the tunnel's centre-line.

The full six aerodynamic forces and moments were measured at yaw angles of 2.7, 5.0, 10.0, 15.5 and 20.2 degrees, while three components (drag, lift and pitch) were only measured at zero yaw (assuming zero side force at zero yaw). Tare drag and lift forces were measured on the exposed strut, which was in the presence of the model, for all configurations at each yaw angle.

In order to determine the local surface flow on the model, flow visualization was completed using surface tufts applied to the roof and leeside of both the cab and container.

3.3 CAB CONFIGURATIONS AT YAW

The flow around a typical full-scale commercial vehicle travelling along a road is dictated by crosswinds. Thus tests in a wind tunnel should be carried out with the model yawed relative to the wind to check that for example, a fuel saving aerodynamic device does not cause any degradation of the truck's handling characteristics. However, a moving ground plane only gives a simulation of a vehicle operating in a no-wind condition. A crosswind would produce a velocity profile that depends largely on the contour of the ground as well as other obstructions near the road. Nevertheless, yaw tests over a moving ground plane give an indication of the sensitivity of the vehicle's lateral forces and moments for particular configurations of the vehicle.

For any truck like body the drag coefficient arises mainly from the differences between the mean pressure coefficients on the front and rear surfaces, while the side force and lift coefficients result from the differences in pressure between the two sides and between the upper and lower surfaces, respectively. The distribution of these pressure differences over the relevent surfaces determines the yawing, pitching and rolling moments. The variation of these forces and moments with yaw, for the 1:6 scale model, are presented in Figure 9.

For the four configurations tested (except the square cab with airdam at 2.7 degrees), C_D increased up to a yaw angle of 15.5 degrees. At 20.2 degrees, while C_D values for either cab with an airdam attached remained similar to those at 15.5 degrees, drag with the two standard cabs fell. For all yaw angles, the drag with the square cab was larger than that with the round cab, and the addition of an airdam to either cab increased the model's drag (except with the round cab at 5 degrees and less).

Lift coefficients with the two square cab configurations increased steadily throughout the yaw range. The round cab, after an initial decrease in lift up to 5 degrees, also showed a rapid C_L increase at larger yaw angles. However, placing the airdam on the round cab dramatically reduced this increase of C_L with yaw angle. The model with round cab consistently had a larger lift than with the square cab, and the addition of an airdam always reduced lift (nearly

always resulting in an overall model downforce).

The side force, yawing and rolling moment coefficients were all nearly linear with yaw angle, the slopes of the side force and rolling moment curves were positive while the slope of the yawing moment curve was negative. With the square cab, or addition of either airdam, lower side forces and higher negative yawing moments were measured, suggesting that the lateral centre of pressure was further downstream for these cases.

Also the square cab, or addition of either airdam, resulted in lower rolling moment coefficients. However, at large yaw angles the trends became indistinguishable.

At zero yaw, surface tuft observations indicated that no flow separation occurred around the round cab's vertical 32mm radiused edges and separation from the 8mm edges did not re-attach ahead of the cab's base, giving rise to two contrasting flow regimes on the cab's sides. However, from the horizontal 32mm radius to the rear of the cab roof, intermittant separated and fully-attached flow was observed. Whilst with the square cab, the oncoming flow separated from all of the front edges, without re-attachment occurring on the cab. The separated region even extending downstream on to the container's lower sides before re-attaching. Shielding from the square cab's separation bubble gave rise to an intermittant separated and fully-attached flow on the container's roof and upper sides, which extended approximately 150mm downstream from the leading edge. Although the size of these regions on the container were similar with the round cab, the separated flow had become dominate.

On yawing the model, with either cab, little change of the cab roof and leeward cab side flows were observed to those at zero yaw. Separation on the container roof lengthened along the leeward longitudinal edge and shortened along the windward longitudinal edge. With the round cab, the separated region on the container's upper leeward side increased in size, extending towards the container's base and floor. Two factors contributed to this, firstly, cross-flow and secondly, air passing through the cab and container gap, both increasing separation from the container's upper vertical leeward edge. However, as a result of cab roof separation shielding, this was not observed with the square cab, instead separation from the vertical leeward cab edge dominated the container's lower side, with only a

small increase of the upper separated region.

Additionally, for all yawed and non-yawed model configurations, attached flow was always observed towards the rear of the container's roof and leeside.

Even though flow impingement on the container forebody caused a greater container drag with the round cab in comparison with the square cab. Flow acceleration around the round cab's radiused edges, thus reducing high stagnation pressures on the cab's forebody, and increased pressure on the cab's base due to the increased gap flow (especially at yaw), gave a lower model drag than with the square cab's sharp edges. Beyond 15.5 degrees yaw, movement of the stagnation point on the cab face gave rise to large flow accelerations around the cab's windward leading edge, thus resulting in a slight drag reduction. Additionally at yaw, increased cab and container leeside separation from the edges of the square cab should have resulted in larger side forces, however this was not the case, instead the opposite was obtained

Carr(4) on a simple rectangular body, found intense localized suctions resulting from separation at the vertical windward edge. Presumably, the 1:6 model's cab and container had separated regions on their windward sides, which were more predominant with the square cab. The resulting suctions counteracted the increased side force due to leeside separation, giving a lower overall side force. These suctions also gave rise to the larger negative yawing moment coefficients obtained with the square cab.

The airdam's purpose was to shield uneven chassis structure from direct flow, thus reducing the model's drag. Gilhaus(18) showed that when a truck experienced cross-flow, the airdam's effectiveness fell as the shielding effect diminished. The airdam on the round cab only gave a 1.7% drag reduction at zero yaw (ΔC_D= -0.013) which is smaller than the usually reported reductions of up to 10%. The cause of this being the model's relatively smooth chassis, the small drag reduction obtained with shielding of the chassis was counteracted by a high stagnation pressure on the airdam's forebody. At yaw the situation worsened, with reduced chassis shielding but large forebody pressures still present. While, flow acceleration and/or separation, around the windward vertical edge of the two airdams resulted in higher negatve yawing moments. Additionally, by shielding the yawed

model's chassis the airdam reduced leeside separation, giving the lower side forces obtained with fixture of either airdam.

The general increase of lift with yaw angle was a result of lift on the container. Carr(4) found strong vortices springing from the inclined leading and windward edges of a yawed square edged model. On the yawed 1:6 model, these vortices caused large suctions on the container roof. Additionally cross-flow under the container created high pressure regions where the flow met obstructions (eg. longitudinal chassis members, petrol tank, etc.). The smaller C_L with the square cab in comparison with the round cab was a result of differences in cab-roof and cab-bumper separations. The reduction of lift produced with either airdam was due to the airdam relieving high pressure on the chassis structure, giving lower surface pressures under the cab and container.

3.4 CORRELATION OF YAWED DRAG COEFFICIENTS

Previous investigations studying the effect of cross-winds on road vehicles in the 2.1m x 1.7m wind tunnel were hampered by the lack of drag force measurements at yaw. To resolve this situation a three component strain gauge dynamometer was constructed, whose design was detailed by Newell(26). Using the dynamometer, a vehicle's yawed body co-ordinate drag can be obtained by summing the overhead balance's wind co-ordinate drag and the dynamometer's body co-ordinate side force. Because the dynamometer was virtually unused, the sensitivity and repeatability (see 2.5) of the yawed coefficients was very pleasing.

In order to validate the yawed drag coefficient values, results were compared to those of Gutteridge(19), who tested the same 1:6 scale model at three other wind tunnels in the U.K. Results are presented in Figures 10 and 11 for the four cab and airdam configurations. The M.I.R.A. blockage correction was applied to the results, which used a freestream dynamic-head measured by a pitot-static probe (fixed to the tunnel wall) ahead of the model.

Correlation between the Southampton results and the other tunnels was very good, especially with those of establishment C with either airdam fitted. Therefore the yawed drag force was measured to acceptable accuracy using the combination of overhead balance and internally mounted dynamometer. The afore mentioned correlation of absolute measurements is surprising (and perhaps lucky!) when possible inconsistences between the tests at the two different wind tunnels are listed, as below.

(i) Area blockage ratio: 7.7% at Southampton
1.6% at C

(ii) Ground plane boundary layer: ground board at C

(iii) Support interference

(iv) Flow quality in the working section

(v) Measurement of dynamic-head

(vi) Positioning of the model with respect to the freestream direction and to the ground

Because a vehicle aerodynamist faces difficulties when requiring absolute values, he primarily uses difference quantities in

this work. The measured differences between configurations are of first importance in vehicle development, and are more likely to reflect full-scale than are absolute magnitudes. The relationship between model and full-scale coefficient magnitudes is a function of model detail and wind tunnel simulation. It is for these reasons that throughout this report little emphasis is placed on the absolute measurement of the aerodynamic forces and no blockage correction was applied to any of the results (except those above).

3.5 REYNOLDS NUMBER

The model with round and square cabs was tested at all yaw angles, with synchronized air-belt speeds of 19.0, 20.7, 22.2, 23.3, 25.0 and 26.2m/s, giving Reynolds numbers (based on model length) of 1.43, 1.55, 1.67, 1.75, 1.88 and 1.96 x 10^6, respectively.

On inspection of the average results (which are not presented, except for particular results in 3.6 and 3.11 specific to other investigations) the only significant trends were observed in drag values, namely the following gradual reductions of C_D with increasing Reynolds number:

(i) 3.6% : round cab at 10.0 degrees (ΔC_D= -0.030)
(ii) 2.9% : round cab at 15.5 degrees (ΔC_D= -0.026)
(iii) 3.0% : square cab at 10.0 degrees (ΔC_D= -0.025)

Flow visualization showed at the lower Reynolds numbers the flow around the round cab's horizontal upper leading edge separated, with re-attachment occurring on the cab's roof just ahead of its base. Only at a Reynolds number of 1.88 x 10^6 was the intermittant separated and fully-attached cab roof flow first observed (as described in 3.3). No change of the flow around the square cab was observed, with increasing Reynolds number, to that described in 3.3.

However, at zero yaw using the same model, Gutteridge(19) at one establishment found evidence of Reynolds number effects with the round cab at higher speeds than tested here (up to Re = 3.70 x 10^6). The primary cause being further changes of the boundary layer separation on the round cab's radiused edges. Similarly, Gilhaus(17) and Cooper(10), using simple models with varying edge rounding, found that radiused models were highly Reynolds number dependent at high Reynolds numbers. Cooper(6) found changes in force and moment coefficients, with increased Reynolds number, for an articulated lorry, whose drag dropped to a steady value at a Reynolds number (based on model length) of 6.50 x 10^6 (U_∞= 67m/s).

Therefore specific Reynolds number effects are dependent on the vehicle tested, in particular the type of edges present on the model. The maximum speed used in this investigation was limited by the moving ground, belt lift becoming a major problem at speeds above 27m/s. Speeds of 26.2m/s give a Reynolds number of 0.66 x 10^6 (based

on model width) for the 1:6 scale model, however, this is slightly less than the minimum value advised by the S.A.E. Recommended Practice(31). Additionally work by Cooper et al.(8, 9, 10, & 11) has suggested a minimum test Reynolds number considerably higher than the S.A.E. recommendation.

In conclusion, a requirement to test the 1:6 model at higher air-belt speeds is apparent if the effect of Reynolds number is to be clearly identified (ie. fully attached flow on the round cab's roof). However, insufficient data is presently available to establish a minimum test Reynolds number. The required value is certainly a function of model configuration and detail, and it is possible that no clearly definable, 'limiting' value exists for many vehicles (including the 1:6 scale model).

3.6 TRANSITION

The effect of transition on the non-yawed model with round and square cabs, at the same six Reynolds numbers used in 3.5, is presented in Figure 12. Wire transition was applied with masking tape in an open loop on the cab's forebody, approximately 20mm in from the cab's vertical and upper horizontal leading edges. Gauge 22 wire (0.7mm diameter) was chosen because of its use by previous investigators in the University's wind tunnels, for example Gutteridge(19).

Throughout the Reynolds number range transition resulted in an 8.7% reduction of the model's lift with the round cab (ave. ΔC_L= -0.007) and an 8.2% reduction of downforce with the square cab (ave. ΔC_L= 0.006). A 1.7% drag increase (ave. ΔC_D= 0.012) obtained with transition on the round cab was, similar to lift changes, consistent for all Reynolds numbers. The drag with the square cab was generally decreased by a smaller 0.3% (ave. ΔC_D= -0.002). Pitching moment coefficients exhibited similar trends to those of drag coefficient.

Transition is commonly used to eliminate laminar boundary layer separation by tripping the boundary layer into turbulence, upstream of the former's separation, thereby simulating a higher Reynolds number. Thus transition should not effect the square cab because separation was fixed at the cab's sharp edges. Flow visualization confirmed this, with flow changes only being observed when transition was applied to the round cab. With increased Reynolds number, similar cab roof changes to those observed on the round cab without transition (3.5) were found with transition applied. But with transition at a Reynolds number of 1.96×10^6 the cab roof flow became fully attached, with no signs of any separation. The intermittant nature of flow on the round cab's roof at Re = 1.88×10^6, with and without transition, probably resulted in the high C_D values at this Reynolds number.

However, this flow change was not quantified by force measurements, the coefficient change with transition at the highest Reynolds number being similar to those obtained throughout the Reynolds number range, as commented on above and shown in Table 12 (over):

$Re(x10^6)$	ΔC_L	ΔC_D
1.43	-.011	.007
1.55	-.006	.012
1.67	-.006	.009
1.75	-.007	.013
1.88	-.005	.022
1.96	-.005	.011

Table 12

This is a similar result to that found in 3.5, when a change of the cab roof flow at larger Reynolds numbers was not shown by the force measurements. Therefore, this would seem to indicate that the changes of flow field with transition, or Reynolds number, are more subtle than surface tuft flow visualization would lead to believe.

The general coefficient changes with transition on the round cab probably resulting from reduced cab roof suctions and decreased shielding of the container's forebody. Because transition had a greater effect on the radiused cab, transition was only applied to the round cab during tests described in 3.7 and 3.8.

3.7 TRANSITION AT YAW

To supplement the study of transition with Reynolds number at zero yaw, transition was applied to the yawed model with the round cab. The same transition type and method of application were used as described in 3.6. Results are presented in Figure 13.

A 1.5% increase of model drag with transition at zero degrees yaw (ΔC_D= 0.011) was lost at small yaw angles, while drag reductions of the order of 5% were obtained at higher yaw angles (ΔC_D= -0.043 at 20.2 degrees). The effect of transition on the model's lift became appreciable at 15.5 and 20.2 degrees, an increased lift of 39.0% (ΔC_L= 0.058) and 13.5% (ΔC_L= 0.026), respectively, being obtained with transition applied.

Increased side forces and smaller negative yawing moments with transition at yaw angles greater than 10 degrees, suggests an upstream movement of the lateral centre of pressure. No appreciable changes of rolling moments were measured.

Because shielding of the container's forebody by cab roof separation became less effective at yaw, the effect of transition, by further reducing shielding, was decreased at small yaw angles. Flow visualization on the model at yaw indicated no surface flow changes (apart from attached cab roof flow) with and without transition. Therefore, with transition, flow acceleration around the cab's radii became more significant at larger yaw angles, giving rise to a reduced cab forebody drag. The increased side forces and lower yawing moments with transition, probably resulted from delayed separation on the cab's vertical windward radii, thus giving smaller suctions on the windward cab side.

3.8 TRANSITION TYPES

The final investigation of transition studied the effect of two additional types of transition, firstly, 18 gauge wire (1.2mm diameter and applied in the same manner as the 22 gauge wire had previously) and secondly, carborundum. The latter transition is commonly used in aeronautical wind tunnel investigations and consists of carborundum grit stuck to the model surface. The size of grit was chosen using the relationship proposed by Pope and Harper(29), which gave a suitable grit diameter of 0.23mm (grades 70 or 80 carborundum). Since the University already had grade 60 carborundum (0.30mm diameter) in stock and any differences between the carborundum grades was thought to be negligible. A 10mm wide band of grade 60 carborundum was used, at the same position as the wire transition had been applied.

The effect of these two transition types, on the round cab at zero degrees yaw, are shown in Figure 14. The results will be compared to those with 22 gauge wire transition (3.6), which were obtained two weeks previously.

The 18 gauge wire and carborundum gave opposing effects, the wire increasing the lift and drag of the round cab, while the carborundum generally resulted in the opposite. However, at the higher Reynolds numbers, the appliance of carborundum changed the model's coefficients by a reducing amount. Table 13 (below) gives the average change in coefficients, on applying the three transition types, throughout the Reynolds number range.

	ΔC_L	ΔC_D
18 gauge wire	.008	.006
22 gauge wire	-.007	.012
60 carborundum	-.007	-.005

Table 13

Table 13 shows a confused situation, with opposing effects between different wire transitions for lift, and between wire and grit transitions for drag. Further experimental work using different types of transition and their positioning, needs to be completed before any conclusions can be drawn from this series of tests.

3.9 TURBULENCE GENERATING GRID

A turbulence generating grid was placed at the inlet of the wind tunnel's test section, one metre upstream of the moving ground rig. The 70cm x 70cm grid was constructed using lengths of circular tubing (16mm diameter) in a 10cm vertical and horizontal lattice. No measurements of the turbulent intensity, resulting from the grid, are available. Tests were performed at three synchronized air-belt speeds (19.0, 23.3 and 26.2m/s) with the round cab at zero yaw. The results obtained are presented in Figure 15 and the average coefficient changes with the grid's presence, throughout the Reynolds number range, are shown below:

$$\Delta C_L = -0.018 \ (22.8\%)$$
$$\Delta C_D = -0.171 \ (24.0\%)$$
$$\Delta C_M = -0.045 \ (23.0\%)$$

Previous investigations concerning turbulence in wind tunnels are sparse. However, Cooper(6), and Cooper and Campbell(7) obtained increased drag values with two truck models in the presence of turbulence, which compared favourably with previous full scale (turbulent) too wind tunnel (smooth) studies. Additionally, drag reductions from cab mounted deflectors were lessened with turbulence, while the performance of container mounted fairings was virtually unaffected. Cooper concluded that drag values obtained in turbulent flow depended on the magnitude of the turbulence, the nature of the yaw curve, and the pitch-angle sensitivity of the vehicle.

Work by Stollery and Garry(34), and Gilhaus(17) concentrated on the effect of turbulence as a flow-trip, affecting flow separations and re-attachments. Stollery and Garry found increasing drag of a trailer with increasing turbulence intensity. A result of reduced shielding of the trailer forebody by the cab roof separation. While Gilhaus found increased airflow turbulence reduced the critical Reynolds number of a rounded coach model, giving drag reductions below the critical Reynolds number.

The results reported in this investigation confirm that variations using turbulence generating grids in wind tunnels can be large. The dramatic reduction in all three coefficients obtained with the 1:6 scale model could be, similar to Gilhaus, attributed to a

lowering of the model's critical Reynolds number. However, no flow visualization was completed on the model with the grid in position, and without values of the flow field resulting from the grid and given the grid's small size, further discussion would be futile.

3.10 GROUND CLEARANCE

Ground clearance is another important parameter in model testing. Figure 16 shows the effect of increased clearance on lift, drag and pitching moment coefficients at zero yaw. In addition to the coefficients at a wheel-belt clearance gap of 6mm, further coefficients were obtained at clearances of 12 and 19mm. The coefficients were corrected to allow for variations in the exposed length of the mounting strut and for vertical displacement of the model relative to the origin of co-ordinates used in calculating moments.

Lift showed the greatest sensitivity, for the two standard cabs C_L decreased rapidly up to a ground clearance of 12mm and then at a slower rate to the larger clearance. For the 13mm increase in ground clearance, the lift reduced by 88.8% (ΔC_L= -0.072) with the round cab, and by 85.0% (ΔC_L= -0.052) with the square cab. However, adding an airdam to either cab resulted in the loss of this lift reduction with increasing clearance, thus giving a smaller downforce associated with fixture of an airdam on either cab.

The effect of increasing the ground clearance from 6 to 19mm on the drag is summarized below:

(i) ΔC_D with fixture of airdam on the round cab reduced from -0.013 to zero;

(ii) ΔC_D with fixture of airdam on the square cab increased from 0.008 to 0.028;

(iii) ΔC_D difference between the round and square cabs reduced from 0.015 to 0.004.

The above lift and drag variations with the two standard cabs were caused by a change of the stagnation pressure distribution over the cab's forebody, probably associated with an increase of cab bumper separation at the larger clearances. Additionally, the larger airdam drag was a result of increased onset flow as ground boundary layer shielding reduced.

3.11 GROUND PLANE BOUNDARY LAYER

To investigate the effect of ground plane boundary layer, tests throughout the Reynolds number range using the four belt and leading edge suction configurations (see 2.2.2) were completed on the model with both round and square cabs. The results are presented in Figures 17 and 18, and the average changes in C_L and C_D (in comparison with those obtained without suction and the belt stopped) are shown in Table 14 (below):

	Round Cab		Square Cab	
	ΔC_L	ΔC_D	ΔC_L	ΔC_D
Suction Off, Belt Moving	-.038	-.007	-.020	-.014
Suction On, Belt Stopped	.007	.022	.008	.012
Suction On, Belt Moving	-.023	.017	-.034	.010

Table 14

General trends which were not model configuration dependent were:

(i) reduced boundary layer thickness, achieved by suction or, to a lesser extent, by stopping the belt, increased drag;

(ii) reduced velocity deficit, achieved with the moving belt, decreased lift.

Addressing the problem of road surface simulation, the drag results with suction and the belt moving or stopped were very similar (especially with the square cab), thus adequate ground simulation for the model's drag was obtained with upstream suction. This was not the case with the model's lift, the moving belt, as well as the suction, having a substantial effect. However, for the present model, the moving belt's improved velocity deficit introduces an error in the ground representation by allowing more airflow through the wheel-belt clearance gap and so causing a reduction in the wheel lift.

Thus when requiring the correct road simulation for the basic 1:6 scale truck, reduced ground boundary layer shielding of the chassis, provided by upstream suction, is only essential. However, this statement disregards the correct wheel flow, which was obtained

with wheel rotation on the moving belt and is reported on in Chapter 5.

3.12 BELT SPEED

Continuing the theme of ground plane boundary layer effects, the aerodynamic coefficients of the 1:6 scale model (round cab) were obtained at ten differing belt speeds. With the tunnel air speed maintained at 26.2m/s, tests were conducted at belt speeds of 18.8, 20.6, 21.3, 22.4, 23.1, 24.0, 24.4, 24.9, 25.6 and 26.2m/s. The results are presented in Figure 19.

Both the lift and drag coefficients generally reduced as the belt speed increased from 18.8m/s. However, at 26.2m/s the coefficients suddenly increased, the drag reverting to the lower belt speed values.

Due to limited time, the gradual change of the ground plane boundary layer with belt speed was not measured. But boundary layer measurements in 2.2.2 showed that the effect of stopping the belt (with upstream suction) was to slightly decrease the boundary layer thickness (3mm) and to worsen the velocity deficit (0.017). Thus similar changes of the boundary layer can be assumed to partially occur during the tests reported here. Additionally, associated with 3.11 the effect of stopping the belt, at an air speed of 26.2m/s, was obtained and is shown below:

$$\Delta C_L = 0.029$$
$$\Delta C_D = 0.003$$
$$\Delta C_M = -0.010$$

The increased lift is a result of reduced wheel-belt clearance gap flow and the increased drag is due to reduced ground boundary layer shielding of the model's chassis. Thus, with decreasing belt speed, the values presented in Figure 19 were reverting to those with the belt stopped.

The increase of C_L and C_D (and subsequently C_M) at the higher speeds can only be explained by belt lift. Unfortunately the model was positioned towards the rear of the perforated base plate, so low pressure associated with the model's wake could have pulled the belt upwards, resulting in a change of the base flow and in particular, the wheel-belt gap flow.

CHAPTER 4
1:8 SCALE IDEALIZED RIGID TRUCK MODEL

4.1 INTRODUCTION

This part of the research programme was an attempt to obtain further understanding on the flow field around an idealized shape relevent to commercial vehicles, while using a moving ground simulation of the road surface. A rigid truck, and in fact most commercial vehicles, consist basically of two simple rectangular bodies in tandem. Studies using different fundamental representations of commercial vehicles have been published in the past and the scope of the work relevent to the present investigation is summarized below.

Carr(4) studied the effect of variations in edge radius, ground clearance and yaw angle on the aerodynamic characteristics of simple rectangular bodies. Not surprisingly, the square edged body's flow field was dominated by regions of separated flow originating from the model's leading edges. However, adequate rounding of the edges was found to prevent the formation of these separated regions, giving a 70% reduction in drag and additional reductions of other forces and moments.

Studying a similar leading edge radius-to-width phenomenon to that of Carr, Hucho et al.(20) showed that 1:4 scale wind tunnel tests of two delivery vans predicted a radius to achieve the maximum drag reduction, was twice that actually required on the full-scale vehicles. Recent work by Cooper(10) showed drag reductions obtained on a simplified box model with front edge rounding to be highly Reynolds number dependent. The drag coefficients of Cooper's models reduced to an asympotic, plateau value at a critical Reynolds number, that was also seen to reduce with increasing radius. In addition, Cooper found the critical Reynolds numbers increased with yaw angle, with the largest change obtained at the smaller radii.

The above authors reported solely on the radius-to-width phenomenon for simple body shapes and the error attributable to Reynolds number. However, the aerodynamics of commercial vehicles is also highly dependent on the interference between the cab and

container. Roshko and Koenig(30), and later Kramer et al.(24), studied this problem using sharp edged circular and rectangular bodies, representing cab and container forebodies. Varying the gap and the diameter ratio of two circular bodies gave large drag variations, a result of the first body's wake either impinging on, or shielding, the second body, the optimum drag occurring when the wake of the first body corresponded directly to the forebody of the second body. Further measurements with rectangular bodies showed the same quantitive drag behaviour as circular bodies.

Work by Allen(2) and recently Cowperthwaite(12), both studied the effect of cab-container interference and leading edge radii, using the same box represention of a truck. Allen found considerable flow differences with square and rounded cabs at various cab-container gaps. Increasing the cab-container gap resulted in a larger model drag. This increase was more pronounced when the front edges of the cab were radiused, eventually the drag of the radiused model became higher than the drag with square edges at the larger gap widths. These results demonstrating the pitfalls that can occur when radiusing the front edges of a cab, while Cowperthwaite extended Allen's work to consider leading edge radii on both the cab and container, and also the effect of container pitch angle. Increasing the leading edge radii of the cab increased the drag of the container, but simultaneously reduced the drag of the cab. The overall changes of drag depended on the container leading edge radii, curvature of these edges reducing the drag.

Kangas(22), using a 1:10 scale articulated truck model which was more realistically detailed than any of the models used in the above investigations, reported the effect of various leading edge cab radii. He supported the views of Hucho et al.(20), in that small-scale wind tunnel data would lead to the selection of an optimum radius that is larger than actually needed. Additionally, Kangas presented results which showed that the optimum radius (for minumum drag) was larger at large yaw angles than at small yaw angles, regardless of any Reynolds number effects.

This chapter will present results obtained with a newly constructed idealized rigid truck model. Using the model, attempts have being made to investigate the effect of various radii on the model's edges at zero yaw. The idealized truck consists of basically

two rectangular boxes, simulating the cab and container of a rigid truck, placed against each other in tandem. The model was designed so as to exhibit some of the real flow characteristics of a rigid truck, but additional complicating factors such as wheels, wheel arches, engine cooling and chassis detail were omitted. The model has zero cab-container gap and the cab and container have the same width. Because of this the lower vertical leading edges of the container are shielded by the cab and, with the container's rear edges, were the only edges on the model not radiused.

4.2 MODEL DETAILS

A recurrent deficiency in many previous reports studying the aerodynamics of basic shapes, is the small number of radii that were systematically wind tunnel tested. However, before a range of radii could be selected, a criteria which would determine when the boundary layer would separate from a radiused edge of the model, needed to be established using findings from previous investigations.

From investigations carried out on bodies with rounded leading edges, Gilhaus(17) and Cooper(10) both suggested the flow around the leading edge was a function of the Reynolds number Re_R (based on the circular radius R). Gilhaus, that Re_R should be greater than 1.10×10^5 for attached flow (a radius of 64mm on the present model), while Cooper proposed that the critical Reynolds number was a constant, where:

$$Re_R = 1.30 \times 10^5$$

Cooper found his data collapsed to this approximation and also correlated well with data from other sources. Using this expression a critical radius of 76mm for the idealized truck is obtained.

The above use of Re_R is based on the established use of the same Reynolds number in predicting the flow nature around a circular cylinder. However, the flow around a cylinder is not analogous to that around a surface radius on any vehicle (or bluff body). For a vehicle it is only with a sufficiently large adverse (positive) pressure gradient, depending on the previous history of the boundary layer, that the boundary layer will separate. Both Gilhaus and Cooper, in using a criterion based solely on Re_R, had neglected the boundary layer development from a stagnation point and the presence of an adverse pressure gradient. Therefore, it is extremely doubtful whether a single value of Re_R can be used to assess with exact certainty the flow around, for example, a circular leading edge of a cab.

The model dependency on the flow around a radius is indicated from observations by the following investigators:

(i) Carr(4) found that an adequate leading edge radius to prevent the formation of separation bubbles was 61mm (20% model width and $Re_R=1.78 \times 10^5$), although a model with a radius of 91mm (30% model width and $Re_R=2.67 \times 10^5$) had a slightly reduced drag.

(ii) Allen(2) using a cab leading radius of 24mm (8% model width

and Re_R=0.39 x 10^5) found flow separating from the radiused leading edge with re-attachment ahead of the cab's base.

(iii) Cowperthwaite(12) had attached flow with leading edge radii of 28 and 30mm, for the cab and container, respectively (10% model width and Re_R=0.90 x 10^5).

Assessing the above experiences (and those of Refs. 20, 22 and 28) and in the absence of any reliable flow separation criterion, a maximum circular leading edge radius of 120mm (40% model width and Re_R= 2.06 x 10^5) was chosen for the cab. However, because attached flow over the leading edges of the container depends on the cab-container interference in addition to container leading edge radius, a maximum radius of 60mm was chosen for the container. Finally, although the primary attention of this study was the effect of leading edge radii at zero yaw. Further tests at yaw were planned when the effect of both leading edge radii and moderate longitudinal edge rounding would be investigated*. Carr observed that an adequate longitudinal edge radius was approximately 10% of the model height for minimum yawed forces and moments. Therefore, a maximum allowable radius of 40mm was built into all longitudinal edges of the model, thus enabling tests, using two leading radii and two longitudinal radii, where totally different flow fields would be present around the model's edges at yaw.

A total of eight cabs were built, the cabs having vertical and horizontal leading edge radii of 0, 10, 20, 30, 40, 60, 90 and 120mm (0mm = square edge). Each cab was built as single block with no interchangeability between the leading and longitudinal radii. The 90mm and 120mm radii were sculptured from automotive clay and fitted to a prototype cab, which resulted in the 90 and 120mm cabs being 120mm longer than the other cabs. One container was constructed to facilitate testing of container leading edge radii of 0, 10, 20, 30, 40 and 60mm. The vertical and horizontal leading edge radii were built as single blocks, which fastened onto the front of the container. Cab and container leading edge radii of 0, 10, 20, 30 and 40mm were constructed with cab and container longitudinal edge radii of 0, 10, 20, 30 and 40mm, respectively. Larger cab and container leading edges were built with longitudinal edges of 40mm.

*These tests, which were partially completed, are not presented.

4.3 DETERMINATION OF MODEL DIMENSIONS

For testing in the 2.1m x 1.7m wind tunnel facility, several factors (listed below) had to be taken into account before the overall dimensions of the model could be determined.

(i) The model had to allow a suitable length of belt ahead of the model, to ensure a satisfactory oncoming flow.

(ii) The model had to allow a suitable length of belt behind the model, firstly, to facilitate proper development of the model's near wake, and secondly, to ensure that the back of the model was not over the rear of the perforated base plate (on which the belt runs) where belt lift might occur.

(iii) The model had to be such that at yaw it did not encroach over the side regions of the belt, where the flow could prove unsatisfactory.

(iv) The model-tunnel area blockage ratio had to be under 5%, to allow accurate measurement of forces and moments.

As a result, a total model length of 890mm was determined, allowing a maximum yaw angle of 20 degrees to be possible in the 2.1m x 1.7m wind tunnel over the 2.0m x 1.1m moving ground. Using the dimensions of the 1:6 scale truck model (Figure 7) as representative of rigid trucks, the length, width and height of the idealized model's cab and container were determined, the scale of the model being 0.13 (approximately 1:8 scale).

The model is shown in Plate 3 and its principle dimensions are given in Figure 20.

4.4 EXPERIMENTAL ARRANGEMENT

The results reported here were obtained from experiments carried out in the University's 2.1m x 1.7m wind tunnel with its 2.0m x 1.1m moving ground. The tests were all performed at a synchronized air-belt speed of 26.2m/s, giving a Reynolds number of 1.52×10^6 (based on model length). Dynamic-head was measured from two pitot-static probes fixed in the freestream alongside the model.

The model was hung from the tunnel's overhead balance by a circular vertical strut (25mm diameter) which passed through a hole in the container's roof, as shown in Plate 4(a). The pitching moment was transmitted to the overhead balance by a thin rod attached to the model in the rear of the container.

The area blockage ratio was 5.5% based on the model and mounting strut frontal areas (3.4% based on the model alone). No blockage correction was applied to the results, which are presented in the body co-ordinate system shown in Figure 8. Although lift and pitching moment results are of little importance in commercial vehicle aerodynamics, they are discussed here to aid understanding of the model's flowfield. Tare drag and lift forces were measured on the exposed strut and pitch rod in the absence of the model.

Tests were completed at zero model yaw angle and ground clearance was set at a value likely to be encountered in real life (120mm under container). The eight cabs (0, 10, 20, 30, 40, 60, 90 and 120mm leading radii) and five container leading edge radii (0, 20, 30, 40 and 60mm), with the cab's and container respective longitudinal radii, were used. Due to limited time, container leading radii of 20, 30 and 40mm were not tested with the 90 and 120mm cabs.

In order to determine the local surface flow on the model, flow visualization was completed and measurements of the container's surface pressure distribution were taken. Flow visualization, using smoke and surface tuft methods, was carried out on most configurations with container leading radii of 0 and 60mm. Surface pressures along the centre-line of the container's roof, and around the container's 0 and 60mm horizontal leading edge radii, were measured. To remove any flow interference along the container's centre-line (from the usual vertical mounting strut) for these tests the model was mounted from a circular sting (57mm diameter) which passed through a hole in the container's base, as shown in Plate 4(b). The method of pressure

measurement and data reduction, was the same as that described in 5.2.1.

Because results at zero degrees yaw are primarily dependent on the leading vertical and horizontal edges, to identify the cab and container configurations their respective leading edge radii are quoted.

4.5 DISCUSSION OF EFFECTS OF CAB AND CONTAINER ROUNDING

4.5.1 Reynolds number

A major disadvantage of smoke flow visualization in the 2.1m x 1.7m wind tunnel, is that the tunnel cannot be run at its usual air speed of 26.2m/s because the smoke plume breakes down. For this reason all smoke flow visualization reported in this chapter was completed at an air speed of 20.0m/s.

To validate the observations using smoke and also to briefly investigate the effect of Reynolds number on the model, five cabs with the 0mm container were tested at synchronized air-belt speeds of 20.0, 23.0 and 26.2m/s, giving Reynolds numbers (based on model length) of 1.16, 1.34 and 1.52 x 10^6, respectively.

Predictably no variation in the force and moment coefficients, which are shown in Table 15 (below), were found.

Cab(mm)	ΔC_L	ΔC_D	ΔC_M
0	.004	.003	.001
30	.005	.005	.001
60	.004	.005	.001
90	.003	.006	.001
120	.003	.001	.001

Table 15

Thus air speeds greater than 26.2m/s are required if Reynolds number trends similar to those observed by Cooper(10) are to be identified. Although there is insufficient data to predict the minimum test speed required to establish any Reynolds number effects. The absence of Reynolds number dependency between 20.0 and 26.2m/s, however, did authenticate the smoke flow visualization.

4.5.2 Drag results

The effect of different cab and container radii on the model's C_D are presented in Figure 21 and summarized over:

(i) Effect of cab radius was generally much greater than that of container radius.

(ii) Increasing cab radius reduced drag at a steadily declining rate, although the drag increased slightly with the 0mm container / 90 and 120mm cabs.

(iii) The 20mm container always reduced drag compared with the 0mm container, however, this effect diminished with small cab radii. Increasing the container radius above 20mm had only a small effect.

Flow visualization indicated the presence of a crescent shaped separation bubble on the cab roof for all configurations tested (separation starting slightly further upstream on the cab centre-line). Large cab radii would usually result in attached cab roof flow, however, unexpectedly a separation bubble was present throughout, this being due to the model's zero cab-container gap (flow over the cab-container roofs being analogous to that over a forward facing step). The extent to which the bubble shielded the container forebody was reduced with increasing cab radius. Thus with the square cab, the bubble shielded the container forebody and the airflow matched the container roof. Surface pressure measurements, presented in Figure 22, around the centre-line of the 0 and 60mm container's horizontal leading edges, quantified this observation. However, positive pressures towards the roof of either container indicated a small region where the 0mm cab's separation bubble did not shield the container's forebody.

On the 0mm container's roof, attached flow was observed with the 0mm cab. Changing the 0mm cab for the 30 or 40mm cabs gave rise to an intermittent separated and fully-attached flow, which was more severe towards the roof's longitudinal edges (a smaller separation bubble off the cab's centre-line giving reduced shielding). Fixture of the 60, 90 and 120mm cabs, with their reduced container forebody shielding, resulted in flow separation from the 0mm container's horizontal leading edge with re-attachment occurring approximately 150, 200 and 230mm downstream, respectively. This was in agreement with surface pressure measurements: suctions at the leading edge of the 0mm container being less with the 0mm cab than with any radiused cab (Figure 23). However, pressure differences between the 0 and 60mm cabs were reduced with container radiusing. Container radiusing had

little effect with the 0mm cab, but with the 60mm cab significant reductions in leading edge suction were obtained (Figure 24). Flow visualization, with the 60mm container, showed attached flow on the container's roof for all cabs.

As the cab's radius increased, the observable separated region down the cab's side became less, until with the 60mm cab (and subsequently the 90 and 120mm cabs) no separation originating from the cab's vertical leading edges was evident. The attachment of flow down the side of the 60mm cab (Re_R=1.03 x 10^5) were very close to the predictions of Gilhaus(17). Separation on the 30 and 40mm cabs only occurred over the lower middle region of the cab side (for the 40mm cab, separation was only indicated by a single tuft), while attached flow was observed on the 0mm cab along the longitudinal edges and the lower vertical leading edges. Also for each cab, flow deflected around the cab roof separation region, caused a general down-flow on the cab's upper sides which extended downstream on to the container.

The cab and container have the same width, thus the cab's vertical radius dictated the nature of the flow down the lower side of the model. Similar to the roof observations, the 60mm container gave attached flow along the upper side of the container. With the 0mm container, only the 0mm cab gave attached flow (resulting from container forebody shielding), for all other cabs a separated region extended a short distance downstream (200mm maximum).

Surface pressure measurements towards the container's base remained nominally unaffected by changes in forebody configuration, highlighting the dominance of the forebody flow field. This was confirmed with flow visualization, attached flow being observed for all configurations over the latter 450mm of the container. Assuming the drag due to energy losses in recirculating regions of separated flow were negligible, the following deductions concerning the drag trends can be made.

The drag decrease with increased cab radius was due to flow acceleration around the larger radii, causing a reduction of the extensive high stagnation pressure present on the smaller cab radii forebodies. However, this drag decrease was counteracted by drag resulting from the exposed container forebody (this being most noticeable with the 0mm container).

Similarly, with large cab radii, the drag decrease with

increased container radius was due to a reduction of the stagnation pressure over the container forebody (note the drag differences between the 0 and 60mm containers with the 120mm cab). The loss of this reduction with smaller cab radii because the container forebody had become completely shielded, removing the stagnation pressure.

4.5.3 Pitching Moment Results

Pitching moment coefficients, presented in Figure 25, showed similar variations with cab and container radii to those of drag coefficient. The pitching moment reflected the drag since, with the origin of co-ordinates at the belt's surface, it is primarily due to the drag vector acting roughly in the middle of the model.

4.5.4 Lift Results

The effect of different cab and container radii on the model's C_L are presented in Figure 25 and summarized below:

(i) All lift measurements were negative, (ie. indicating downforce).

(ii) Increasing cab radius decreased downforce, although this reduction started to asymptote with cab radii of 20mm and greater.

(iii) For all cab radii downforce changed little with container radii of 60 and 40mm, but smaller container radii gave slightly increased downforces, except for the 0mm container where the opposite was found with the 60, 90 and 120mm cabs.

To determine the influence of the step (formed between the container's undersurface and the cab's base), the model's undersurface was made smooth. This was achieved by placing an underbody on the container, which matched the lower surface of the cab. With a cab radius of 40mm, it was subsequently found that 60% of the model's downforce was a result of flow separation from the step.

Although little flow visualization was carried out under the model, smoke showed flow separating from the 0mm cab's lower horizontal edge, hence creating a low pressure region under the cab. Increasing the cab's radius reduced the separation's size, resulting in reduced suctions and thus the smaller downforces obtained with

larger cab radii. Negative pressures accompanying the turning and acceleration of flow around the larger container radii gave rise to further, but smaller, downforce reductions. However, this was reversed with the 60, 90 and 120mm cabs, where flow separation from the 0mm container's leading edge produced a greater lift than that associated with flow acceleration on the 60mm container. The drop in lift between the 90 and 60mm cabs was probably a result of the increased length of the 90mm cab and requires further investigation.

4.5.5 Effect of Transition

Tests on container radii of 20 and 30mm were repeated with transition (grade 60 Carborundum) applied to all cabs except the 90 and 120mm configurations. A closed loop of transition was placed on each cab's forebody, approximately 20mm in from the leading edges. The drag results obtained are presented in Figure 21. Drag coefficient changes were only reproduced since negligible changes to the other coefficients were measured (max. ΔC_L= 0.004 and ΔC_M= -0.009).

For both containers tested, transition only affected the intermediate cabs (10, 20, 30 and 40mm) by substantial amounts (ie. ΔC_D>0.01). The reduction in drag is due to the elimination of laminar boundary layer separation when the transition to a turbulent boundary layer occurs upstream of the former separation. Changes of boundary layer separation with transition effecting both the cab roof separation bubble (and subsequently the container forebody shielding) and the high pressure area on the cab's forebody. No effect was obtained from the 0 and 60mm cabs because flow separation was fixed at the sharp edges and no flow separation occurred at the radiused edges, respectively.

4.6 CONCLUDING REMARKS

The research has produced fundamental results on the effect of cab and container radii where, to date, little systematic work has been reported. Of special interest are the drag savings due to attached flow, obtained with simple rounding of the cab and container. The maximum drag reduction of 56.5% (ΔC_D= 0.407) being obtained when changing the 0mm cab and container for the 120mm cab and 60mm container.

However, with the tandem body studied here, the effect of edge rounding, not only in preventing flow separation, but also by altering the cab-container interference, has been closely examined. With the 60mm container a maximum 53.6% drag reduction (ΔC_D= 0.362) was obtained with the 120mm cab, whilst with the 0mm container a maximum 32.5% drag reduction (ΔC_D= 0.234) was obtained with the 60mm cab.

Finally, the measurements presented in this paper should provide a useful test case for some of the Computational Fluid Dynamic codes now being developed.

CHAPTER 5

YAWED GROUND AND ROTATING WHEEL RESEARCH

5.1 INTRODUCTION AND TECHNIQUES

A section of the research programme attempted to assess how a rotating wheel affects a commercial vehicle's flow field, when conducting cross-wind tests. To do this, the moving ground must be yawed with the yawed model, if the model has rotating wheels attached. This type of test has not previously been reported on. A literature search found few reports exist even concerning the aerodynamics of rotating wheels. The few that are in existence concentrate on the characteristics of isolated wheels, and the effect of varying the ground clearance under the wheel, which is only applicable directly to vehicles with exposed wheels (such as racing cars).

Cogotti(5) using driven wheels close to the ground with a foam rubber insert filling the wheel to tunnel floor gap, reported on experimental work completed on isolated and totally exposed wheels. With the wheel in contact with the ground, the drag coefficient of the rotating wheel was slightly lower than that of the stationary wheel. Moreover, the lift coefficient was found to be always positive, that is to say, the wheels were exhibiting lift in both rotating and static cases, but the rotating wheels' lift was less than the static one. Cogotti also found that the amount of wheel lift was strongly dependant on the quality of sealing between the wheels and ground, a small air leakage under the wheels producing a noticeable decrease in wheel lift. This was in agreement with earlier work by Stapleford and Carr(32) who found a small gap under the wheels could produce a complete reversal of the sign of lift. Using a moving ground plane simulation, Stapleford and Carr found this lift change increased. The moving ground increased the airflow through the wheel clearance gap and so caused a venturi, resulting in large negative pressures.

Fackrell and Harvey(14 & 15) in their two reports looked closely at a wheel on a moving ground. By integrating the surface pressure measurements around the wheel's circumference, the rotating wheel's lift and drag were found to be less than the stationary wheel's value (the same result as that of Cogotti, and Stapleford and Carr). Even though smoke flow visualization showed the boundary layer

remained attached over the stationary wheel much further around its surface than the rotating wheel. This did not result in the usually expected higher base pressures for the rotating wheel, in fact the opposite occurred. Over the rear and particularly the top surface, the stationary wheel had regions of increased negative pressure compared to the rotating wheel. Rotation of the wheel also produced a sharp rise in pressure at the moving ground-wheel contact point. These pressure distributions resulted in the force reductions obtained with wheel rotation.

The above results, however, deal with the aerodynamic characteristics of isolated wheels (such as racing cars). Cogotti in his report on wheel aerodynamics, continued to describe some results obtained with wheels mounted on a passenger car body and a simple two-wheeled body. Rotation of the four passenger car wheels produced a slight decrease of vehicle drag (ΔC_D= -0.005) and increase of lift (ΔC_{LF}= 0.019 & ΔC_{LR}= 0.002). Using the two-wheeled body, slight increases in both drag and lift were obtained with wheel rotation. The opposing drag changes for the two models was suggested to be caused by different wheelhousing shape, wheel position, different oncoming flow angles at the wheels and wheelhouse interference on the car body.

In an attempt to quantify the effect of wheel and wheelhousing airflow has on tyre power losses, Oswald and Browne(27) measured the airflow direction and velocity around a passenger car tyre in an on-the-road environment. They concluded that the flow pattern, although complex, was similar to the flow over an almost non-rotating tyre in a wheelhousing. This conclusion typifies the approach vehicle aerodynamics have historically used when representing the true operating conditions of vehicle wheels in the wind tunnel. A fixed wheel, with a small clearance gap below the wheel, being claimed as a satisfactory simulation for partially enclosed wheels. Stapleford and Carr(33) recommended a wheel-ground clearance gap between 0 and 2% of the wheel diameter for wheels of normal width. For large, exposed fixed wheels, Cooper(9) suggested the use of a simple spoiler (positioned 140 degrees clockwise from the tyre contact point) would simulate the major effects of a rotating wheel's forward separation point.

The theoretically ideal case of rotating wheels in contact with a moving ground surface has no earlier reports, chiefly because of the difficulty of measuring the aerodynamic forces in this

condition. The contact of the wheel on the ground precludes force balance measurements, of a model with rotating wheels, due to ground reaction forces.

This problem was satisfactorily solved at Southampton by mounting the wheels of scale wind tunnel models from the side of the tunnel. The wheels were independent of the model, which was mounted on the overhead balance. Forces on the isolated wheels were obtained by direct measurement and this added to the forces measured on the model. This method is used today in many European wind tunnel/moving ground facilities and by some customers using the University's 2.1m x 1.7m wind tunnel. But this technique has two main drawbacks, firstly the wheel mounts have to be strain gauged in order to measure wheel drag. Secondly the mountings and external wheel axles produce an unrealistic flow down the model's side.

These drawbacks resulted in a new technique where balanced wheels with low rolling resistance are attached to the model by a swinging, trailing arm suspension. This allows wheel drag to be transmitted to the model but no vertical force, while the wheel is running on the moving belt. By taking a balance reading before blowing air over the model, but with the belt moving, any non-aerodynamic drag of the wheel is established which is then taken from the air-blown measurements.

Such a wheel assembly was fitted to the 1:6 scale Leyland rigid truck model used in the tests reported in Chapter 3. Four nylon wheels, the same size and profile as the model's original fixed wheels were used, each with their own trailing arm suspension. A locking device fitted to each suspension arm allowed the wheels to be locked in a raised position off the moving belt, enabling the original wooden fixed wheels to be replaced on the model exactly as the rotating wheels, but with a 6mm wheel flat on the wheel's undersurface.

In addition to the wheel assembly, the vehicle's underbody was more realistically modelled. New underbody detail, shown in Plate 5(b), included engine with exhaust pipe, chassis with cross members, propeller shaft, spare wheel, battery, air-cylinders, side and rear bumper bars. Front wheelhousings were cut into the cab in which the front wheels were mounted, the rear wheels being isolated under the container.

The new detailed 1:6 scale rigid truck model, with round cab only and shown in Plate 5(a), was used in three wind tunnel

investigations, all studying the effect of wheel rotation and ground plane simulation on the model's aerodynamics. The first series of tests used the model positioned over the yawed moving ground facility (2.3). Measurements of the static pressure along the container's lower surface were taken, thus examining the effect of the flow from the two rear wheels on the container. The second series of tests determined the effect of wheel rotation and ground plane boundary layer on the model's aerodynamic forces at zero yaw in the 2.1m x 1.7m wind tunnel. Thirdly, the second study was extended to examine the effect of wheel rotation and ground plane boundary layer with the model yawed, using the yawed moving ground facility. However, in view of the uncertainty of the forces at yaw on the rotating wheel assembly used in the first two studies, and their subsequent effect on the yawed model, the rotating wheels in the third study were mounted from the side of the wind tunnel in the presence of the model. The aerodynamic forces measured, thus did not include the wheel forces.

5.2 YAWED STATIC PRESSURE INVESTIGATION

5.2.1 Experimental Arrangement

The results reported here were obtained from experiments carried out during May 1985 in the 3.5m x 2.6m wind tunnel, with the 2.0m x 1.1m yawed moving ground facility. The facility and ground plane boundary layers are fully described in 2.3.

The tests were conducted with the tunnel-air and ground-belt speeds synchronized at 23.3m/s, giving a Reynolds number of 1.75×10^6 based on model length. No correction for belt-air yaw angle was made on speeds. The area blockage ratio was 4.1% based on the model and mounting strut frontal areas (2.3% based on the model alone). The model was hung from the wind tunnel's overhead balance by a circular vertical strut (25mm diameter) which passed through the container roof.

Measurements of the static pressure along the container's lower surface were taken, thus examining the effect of the flow on the container from the two rear wheels. Fifty pressure tapping holes were placed along the container's lower surface in five longitudinal rows, as shown in Figure 26. The five rows of tappings, from the windward container side to the leeward container side, are described as A,B,C,D and E, respectively. Rows A and E were 20mm, and B and D were 80mm, from the container sides. Row C was on the centre-line of the container, between the two longitudinal chassis members (which ran the whole length of the model). The tappings were connected by lengths of fine-bore tubing (1.5mm internal diameter) to a portable two transducer Scani-valve pressure monitoring system, which was placed in the model's container. Tubes with tunnel total and static pressure, together with a control line and air pressure line (to power the system) were passed into the model down the back of the mounting strut, resulting in no extra interference on the model's flow field.

The pressure data were reduced to coefficient form using:

$$C_p = (p-p_\infty)/q_\infty$$

where 'p' is a local surface pressure, 'p_∞' and 'q_∞' are the reference values of static and dynamic pressure measured from two pitot-static probes fixed in the freestream alongside the model.

Firstly, tests with rotating wheels, with the model and moving ground, at yaw and zero yaw, were completed. These tests were repeated with fixed wheels, with the addition of model yawed, moving ground zero yaw. Only one yaw angle of 15 degrees was used. Most runs were repeated with an airdam fitted (as used in Chapter 3), which gave a front ground clearance of 33mm (for the basic cab clearance was 65mm).

Before examining the effect of wheel rotation on the lower surface pressure distribution (5.2.5), a study of the pressure distributions at zero degees yaw (5.2.3) and at 15 degees yaw (5.2.4) has been completed. Although no flow visualization was undertaken, leaving some details of the flow's exact nature unknown, it is hoped to remedy this in the near future.

5.2.2 Repeatability

In order to establish a level of confidence in the portable Scani-valve measuring unit, four repeat runs were completed with the two model configurations at 15 degrees yaw. Subsequently the average pressure coefficient change for the fifty tappings was found to be 0.007, which was adequate for the planned testing.

In addition to the model's surface pressures, during each test the two transducers sampled the freestream static pressure once (at the start) and dynamic pressure three times (at regular intervals). To assess the variation of dynamic pressure, an average value was calculated from all the tests completed during May 1985 (as shown below).

Transducer 1 : variation of q_∞ = 9mV (0.7%)

Transducer 2 : variation of q_∞ = 3mV (2.1%)

The higher percentage variation q_∞ for transducer 2 was a result of its lower maximum output voltage in comparison with transducer 1. Even so, the above variations of q_∞ were negligible and the pressure coefficients were calculated taking the last measured dynamic pressure into account.

5.2.3 Zero degrees yaw (reference to Figures 27, 28, 29, 30 & 31)

Symmetry was obtained between the results along rows A and E, and rows B and D, for the two configurations with rotating wheels. This had not been assumed since the chassis components are asymmetric. However, slight differences in the pressure coefficients directly above the fixed wheel were found (ΔC_p= 0.05). These were a result of different wheel-container gaps between the two rear wheels, which had been set as similarly as possible during wind tunnel testing.

In addition to the afore mentioned symmetry, there was also close agreement between the results along rows A and B, and rows D and E. The only differences were for rows B and D, with rotating wheels, a slightly reduced suction ahead of the rear wheels (which was smaller with addition of airdam and slightly larger with fixed wheels). This was a result of pressure build-up in front of the rear wheels, which did not occur along rows A and E due to their positioning.

For the basic model with rotating wheels, the pressure distribution obtained along rows A, B, D and E had three distinct regions.

(i) As distance from the container's leading edge increased the suction decreased. Thus down-flow between the cab and container formed a separation region under the container at its forward horizontal edge. The recirculation reduced in size along the container's length, with possibly re-attachment occurring before the blockage of the rear wheel slowed the flow.

(ii) Above the wheel the suction increased due to separation from the wheel's rotation (see 5.2.5)

(iii) Downstream of the wheel, decreased suction was found as the wheel's separation region diminished with possible attached flow before the container's base.

The addition of the airdam only marginally changed this general flow pattern, however it did initially give a reduced suction at the container leading edge which then gave way to an increased suction ahead of the rear wheel,and additionally, less suction over and immediately behind the wheel. These effects resulting from the

reduced airflow under the cab with the airdam fitted. Suction measurements obtained along the container's centre-line (row C) gradually reduced downstream of the leading edge. Half way along the container the pressure steadied and stayed constant for the remainder of the container, presumably indicating attached flow over the latter half of the container. Without the airdam, although generally the same occurred along the container's centre-line, the pressures were more scattered. This was probably a result of flow acceleration around the chassis components (ie. cross members and rear axle) by the faster air originating from under the cab, which was absent in the presence of the airdam.

5.2.4 Fifteen degrees yaw (reference to Figures 27, 28, 29, 30 & 31)

At yaw the flow under the model became highly asymmetric. Along the windward rows (A & B) the distribution was dominated by a build up of positive pressure ahead of the rear wheel, caused by cross-flow under the container being obstructed by the rear wheel and the longitudinal chassis members (which unlike in real life, had no gap between them and the container).

In comparison to the zero yaw results, from above the rear wheel to the container's base, along row A the added effects of separation from the container's longitudinal edge and enhanced wheel rotational separation (more air passing around the wheel) gave a consistantly lower pressure. While along row B, although similar increased suctions due to wheel separation were obtained behind the wheel, in absence of the longitudinal separation the pressure quickly reverted back to the zero yaw value.

Along the leeward rows (D & E) a general increased suction was obtained, a result of flow separation from the longitudinal chassis (especially ahead of the rear wheel along row D) and separation from the rear wheel (behind and above the rear wheel along row E). Also noticeable towards the container's base, along rows B, D and E, was a reduction of pressure due to the influence of the wake flow.

Along the centre-line (row C) separation from the chassis caused a near constant suction along the container. Similarly, but not as affectively as at zero yaw, the airdam smoothed any variations of C_p. The airdam also slightly lowered the pressure ahead of the rear axle.

Along the two windward rows (A & B) the airdam resulted in slightly increased suctions over the rear half of the container, these effects being generally smaller than those at zero yaw. However, at the container's leading edge the airdam reduced the pressure significantly. To a smaller extent the same occurred on the two leeward rows. The greatest effect of the airdam was observed along row D, where suction was substantially increased ahead of the wheel.

5.2.5 Wheel rotation (reference to Figures 32, 33, 34, 35 & 36)

The static pressure directly above the wheel was found to be lower for the fixed wheel in comparison to the rotating wheel case, at both 0 and 15 degrees yaw. The cause of this lower pressure was a result of the boundary layer remaining attached to the fixed wheel, much further around its surface than to the rotating wheel. The small wheel-container gap (25mm) was partially blocked by the rotating wheel separation; while for the fixed wheel, flow through the venturi shaped gap produced a lower static pressure on the container.

At zero yaw the difference in C_p between the rotating and the fixed wheel was greater along rows B and D (ave. $\Delta C_p = 0.25$). Behind the wheel the suction associated with the fixed wheel was quickly lost as the venturi effect vanished, while the rotating wheel's separation extended further downstream.

At yaw, the difference between the rotating and fixed wheel increased along the windward rows (row B: $C_p = 0.77$); the suction associated with the rotating wheel separation only slightly increasing, while the suction due to the fixed wheel venturi dramatically increased as more air passed under the yawed model.

Predictably no effect of wheel rotation was observed along the container's centre-line, the chassis shielding any changes of flow field.

Along rows D and E the pressure difference between the rotating and fixed wheels changed little in comparison to zero yaw. However, flow separation from the chassis consistantly reduced all of the pressures and also destroyed the differing wake flows. Additionally, there were differences with wheel rotation ahead of the rear wheel, suction with the fixed wheel being slightly greater than with the rotating wheel. This probably arose from different wake flows of the front wheels with rotation. Differences between the results

with the fixed wheel/yawed belt and fixed wheel/non-yawed belt were also measured in the same region (the suction with the yawed belt being slightly greater), ground plane boundary layers with belt angle being the likely cause.

Fixing the airdam onto the cab resulted in the removal of the above yawed/non-yawed belt differences and also reduced the change of pressure with wheel rotation directly above the wheels along row E.

5.2.6 Summary

The study provided a basic understanding of the underbody flow and the effect of model yaw on that flow. Pressure measurements vividly showed regions of high pressure and high suction, on the windward and leeward sides of the chassis, respectively, these pressures being a cause of the model's sensitivity to yaw.

Attempts to investigate the rotating and fixed wheel flow fields were handicapped by a lack of pressure tappings in the region above the wheel.

However, static pressure measurements on the container's lower surface, showed that the effect of rear wheel rotation is very localised and strongly yaw dependent. Although pressures directly above the wheel altered substantially with wheel rotation, the effects did not propagate downstream; measurements at the container's base remaining unchanged by wheel rotation. This suggests that any drag changes resulting from rear wheel rotation (5.3) are due to different pressure distributions around the wheel, and not wheel interference on the container.

5.3 ZERO YAW FORCE INVESTIGATION

5.3.1 Experimental Arrangement

The results reported here were obtained under the same tunnel conditions as previously used for the original semi-detailed model described in 3.2, except for the following details:

The model was hung from a thinner vertical strut (25mm diameter at the container's roof), which attached directly to the model with an improved pivot assembly. The strain gauge dynamometer was not used as tests were only completed at zero yaw. Drag and lift forces, and pitching moment were measured, the pitching moment by a thin rod attached to the model in the rear of the container. Because of limited time, tare drag and lift forces were measured on the exposed strut and pitch rod in the absence of the model. Results are presented in the body co-ordinate system shown in Figure 8.

Tests on three 'add-on' devices designed to improve the aerodynamic performance of existing commercial vehicles were carried out, followed by a comparison of three different types of rear wheel mudguarding. The 'add-on' devices were as follows:

(i) Cab roof mounted deflector of flat, rectangular shape having no curvature, a 15 degree (from the vertical) downstream lean and a vertical height half the cab roof to container roof distance. The deflector could be mounted in one of four positions at distances from the cab's upper horizontal leading edge of 31, 66, 102, and 137mm (described in this section as deflectors 1, 2, 3 and 4, respectively).

(ii) Five under bumper airdams giving front ground clearances of 33, 23, 18, 13 and 8mm (described in this section as airdams* 2, 3, 4, 5 and 6, respectively). All airdams were vertical, covering the whole cab lower horizontal leading edge, wrapping just around the cab's vertical leading edges.

---

*No airdam 1 designation for reasons explained in 5.4.

(iii) Two vertical side skirts, running the whole length of the container from the rear of the front wheel mudguard, to the back of the container, with side ground clearances of 60 and 35mm (described in this section as side skirts 1 and 2, respectively). The side skirts had apertures adjacent to the wheels allowing the whole of the wheel to be seen from the side. Both side skirts were always tested with airdam 2 fitted to the cab.

The three types of mudguard tested are shown in Figure 37. Mudguard 1 covered the upper 180 degrees of the rear wheel, giving a ground clearance of 65mm at the mudguard tip, while mudguards 2 and 3 both had ground clearances of 70mm at the mudguard tips. The three mudguards represent the most commonly seen types of mudguard on commercial vehicle rear wheel assemblies. Each mudguard had a width equal to that of the rear wheel (76mm) and had no side valancing. Mudguard 1 was 12.5mm thick and made of wood, while mudguards 2 and 3 were made of 0.7mm thick, flat aluminium plate.

Firstly, tests (with moving belt and leading edge suction) were completed with rotating and then fixed wheels, on the baseline (standard) model and with each deflector, airdam, side skirt and mudguard individually fitted. Secondly, with fixed wheels on the baseline model, and each airdam and side skirt individually fitted, tests were completed with the ground belt stopped and leading edge suction off.

In as much as the main purpose of this investigation was to determine the effect that wheel rotation and ground plane boundary layer has on the aerodynamic characteristics of a truck in a wind tunnel test. The discussion is limited primarily to the change of drag (ΔC_D), front axle lift (ΔC_{LF}) and rear axle lift (ΔC_{LR}) coefficients, with wheel rotation and ground plane boundary layer, and the variations in model configurations that may have a bearing on, or a relationship, to these quantities. However, data showing the aerodynamic benefits of these devices are discussed briefy. No attempt was made to use devices optimized for minimum vehicle drag (for instance the delfectors used did not necessarily give attached flow over the roof and sides of the container), the dimensions of the devices were determined using previous experience and after consultation with Leyland Vehicles Limited.

5.3.2 Baseline Model

With fixed wheels, the following averaged values were measured:

$$C_D = 0.768 \quad C_{LF} = 0.452 \quad C_{LR} = -0.355$$

The following differences between the results measured with fixed and rotating wheels were found:

$$\Delta C_D = -0.006 \quad \Delta C_{LF} = -0.011 \quad \Delta C_{LR} = -0.051$$

Thus with the baseline model, rotation of the four wheels produced a small decrease of the model's drag (0.8%) and front axle lift (2.4%), and a slightly larger decrease of rear axle lift (14.4%). These results show the same trend as observed by Fackrell and Harvey, and thus can be explained in a similar manner. It must be noted that the rotating wheel assembly does not allow measurement of the lift produced by the rotating wheel, only its drag. Therefore the reduced lift, shown above, is a result of the loss of the fixed wheel's lift and the differing interferences of the fixed and rotating wheel's wakes upon the model. However, in 5.2 a fixed wheel, in comparison to a rotating wheel, was found only to result in an increased suction on the container directly above the rear wheels. Thus, the higher rear axle lift of the model with fixed wheels was a result of the larger wheel lift, which counteracted any increased localized suction on the container. Two reasons probably caused the greater reduction of lift at the rear axle, firstly the large width of the rear wheels (twice that of the front wheels) and secondly, the rear wheels were isolated while the front wheels were mounted in wheelhousings.

For the baseline model with fixed wheels, the following differences between the results measured with stopped and moving ground belt were obtained:

$$\Delta C_D = 0.022 \quad \Delta C_{LF} = 0.003 \quad \Delta C_{LR} = -0.031$$

Here, in comparison to the stopped belt, the moving belt increased drag by 2.9%, nearly four times of that which the rotating wheels decreased drag. The moving belt also resulted in a 0.7%

increase of front axle lift and a larger 8.7% decrease of rear axle lift. The increased drag and decreased total lift of the model was a result of more air passing under the model with the reduced ground plane boundary layer of the moving ground (2.2.2).

5.3.3 Deflector

A cab-roof deflector's function is to relieve high container forebody pressures by matching the flow between the cab and container roof. As such, deflector 1 produced the best result with a 20.8% drag reduction ($\Delta C_D = -0.160$).

Rotating the wheels compared to the fixed wheel case produced the differences presented in Table 16 (below).

Deflector	ΔC_D	ΔC_{LF}	ΔC_{LR}
1	-.007	-.020	-.050
2	-.009	-.016	-.054
3	-.007	-.013	-.054
4	-.005	-.011	-.054

Table 16

With reference to Table 16, the different deflector positions did not cause ΔC_D and ΔC_{LR} to change significantly. Both were unchanged from the baseline model without deflector (5.3.2). ΔC_{LF} values were the same as the baseline model only with deflector 4, forward movement of the deflector resulting in an increased ΔC_{LF}. This suggests that with the deflector placed forward, the reduced downflow between cab and container resulted in increased lift on the fixed front wheels and/or altered the wheel wake interference characteristics of the two wheel types.

5.3.4 Airdam

With fixed wheels, lowering the front ground clearance of the model from 65mm to 23mm (fitting airdam 3) gave a 4.9% drag reduction ($\Delta C_D = -0.038$), but with smaller clearances (airdams 4, 5 and 6) no further drag benefit was obtained. The same model with rotating wheels showed similar drag reductions using airdams 2 and 3, but with smaller

front ground clearances (airdam 4, 5 and 6), the drag continued to fall. So that, airdam 6 with rotating wheels gave a 6.4% drag reduction (ΔC_D= -0.049). Fixture of airdam 2 to the rotating wheel model reduced the small total lift of the model to practically zero (C_L= 0.012). While for the fixed wheel model, airdam 3 achieved similar results (C_L= 0.015).

Rotating the wheels compared to the fixed wheel case produced the differences presented in Table 17 (below).

Airdam	ΔC_D	ΔC_{LF}	ΔC_{LR}
2	-.012	-.001	-.012
3	-.007	.007	-.008
4	-.012	.002	-.006
5	-.012	-.001	-.005
6	-.018	-.003	-.002

Table 17

With reference to Table 17, the results show fixture of any airdam to the model increased the reduction of drag obtained with wheel rotation, most notably with the smallest front ground clearance. Additionally any airdam dramatically reduced the lift reduction at the front and rear axles (for instance with airdam 3, an increase of front axle lift and a total lift change of only 1.6% of that of the baseline model).

With stopped ground the model gave the same drag reduction for airdams 2, 3 and 4 as the moving ground. But unlike the moving ground case, at smaller ground clearances the drag of the model increased slightly. The decrease of front ground clearance had little effect on the model's total lift with stopped ground. The differences between the results measured with stopped and moving ground belt are presented in Table 18 (over).

Airdam	ΔC_D	ΔC_{LF}	ΔC_{LR}
2	.025	-.030	-.070
3	.023	-.049	-.063
4	.021	-.056	-.065
5	.018	-.053	-.063
6	.015	-.041	-.062

Table 18

With reference to Table 18, the drag increase with moving ground was similar to that of the baseline model (5.3.2), although a general decrease of ΔC_D was obtained with smaller front ground clearances. The decrease of lift with the moving ground was much larger than the baseline model, especially at the front axle. Thus lowering the front ground clearance to a height above the belt where larger changes of boundary layer occurred with stopped/moving belt, made the model's lift more sensitive to ground plane changes.

5.3.5 Side-Skirts

A side-skirt is primarily for use at yaw, where, drag reductions due to reduced crossflow under the vehicle, give smaller regions of separated flow on the leeward side. However, reductions of drag at zero yaw are obtained by reducing air spillage from underneath the container, giving a smoother flow alongside the vehicle.

Fixture of either side-skirt to the model, with rotating or fixed wheels, resulted in similar drag reductions of 1.2% (ΔC_D = -0.009). With the ground stationary and fixed wheels, the side-skirt drag reduction increased slightly to -0.014.

Rotating the wheels compared to the fixed wheel case produced the differences presented in Table 19 (below).

Side Skirt	ΔC_D	ΔC_{LF}	ΔC_{LR}
1	-.014	.002	-.005
2	-.010	.010	-.004

Table 19

With reference to Table 19, both skirts reduced ΔC_{LR} compared to the baseline with airdam 2 model, however with skirt 2 and, to a lesser extent, skirt 1, an increase of ΔC_{LF} with wheel rotation was measured. Thus, although the magnitude of the total lift change was less than the baseline model, rotating the wheels with side-skirt 2 produced a lift increase, this suggesting that both side-skirts modified the front wheel flow.

The side-skirts increased total model lift with rotating or fixed wheels. However, with the stopped ground, addition of side-skirt 1 produced no lift change compared to the baseline model. Subsequently the lift of the model with skirt 2 increased similarly to the moving ground case. The differences between the results measured with stopped and moving ground belt are presented in Table 20 (below).

Side Skirt	ΔC_D	ΔC_{LF}	ΔC_{LR}
1	.030	-.025	-.048
2	.029	-.023	-.051

Table 20

Refering to Table 20, the drag increases with moving ground were slightly larger than that of the baseline model. While front axle decreases with moving ground were slightly smaller, large reductions of ΔC_{LR} were found in comparison to the baseline model.

5.3.6 Mudguards

All three types of mudguard produced more model drag. With fixed wheels, fixture of mudguard 1 gave the smallest drag increase (0.8%) and mudguard 2 the largest drag increase (1.7%). However, rotating the wheels only changed the drag with mudguard 1 fitted by a minimal amount, while drag reductions similar to those of the baseline model were obtained with mudguards 2 and 3 fitted (see table 21).

Mudguard	ΔC_D	ΔC_{LF}	ΔC_{LR}
1	-.001	-.014	-.025
2	-.007	-.016	-.024
3	-.007	-.013	-.020

Table 21

The result of this was that with rotating wheels fixture of mudguard 3 gave the smallest increase of drag, as shown in Table 22 (below).

Mudguard	1	2	3
Fixed Wheels (ΔC_D)	.006	.013	.009
Rotating Wheels (ΔC_D)	.011	.012	.008

Table 22

Thus, although drag increases due to mudguard presence are small, the size of this increase is dependent on wheel rotation for some particular mudguard shapes (ie. mudguard 1).

With rotating wheels, fixture of mudguards 1 and 3 produced increases of total lift, whilst there was little change of lift with mudguard 2. However, when wheel lift was measured with the fixed wheel assembly, for all cases the total lift was reduced with any mudguard present. Placement of a mudguard over the rear wheel also reduced the loss of rear axle lift, obtained with wheel rotation, by roughly half. The change of front axle lift with wheel rotation was similar to the baseline model, this being expected since no changes to the front wheel assembly were made.

Thus, the lift reduction measured with a mudguard over the fixed rear wheels, was a result of the wheels' reduced lift with mudguards present, counteracted by the mudguard's lift. The effect of wheel rotation on the mudguard lift could not be measured with the wheel assembly.

5.3.6 Summary

The purpose of this study was to present detailed zero yaw force measurements indicating the sensitivity of a typical truck model to wheel rotation and ground plane changes in the University's 2.1m x 1.7m wind tunnel. It did not attempt to provide details of the flow under the 1:6 scale model, which caused the variations of measurements obtained. That would necessitate flow visualization and local flow measurements, even more extensive than those examined in 5.2

The drag of the model with rotating wheels was always found to be less than with fixed wheels. Only the addition of front under-bumper airdams (especially airdam 5) and mudguard 1, altered the change of drag substantially. These drag changes can be directly related to the drag of the rotating wheel in comparison with the fixed wheel. But the changes in lift quoted with wheel rotation can only be used as an indication of the model's sensitivity to wheel rotation (wind tunnel testing where a rotating wheel's lift is measured has not yet been developed).

For the configurations tested, reducing the ground plane boundary layer by operating the belt at freestream velocity resulted in a decrease of the model's total lift and an increase of drag. The drag change with ground plane boundary layer being greater than that with wheel rotation for all configurations except airdam 6. Increased drag with a smaller boundary layer thickness was a result of a larger dynamic pressure to which the model's underbody was exposed. The boundary layer with the belt stopped and suction off (clear tunnel, at the centre of the belt: δ= 74mm) being similar to the front ground clearance of the model (65mm). The large effect on the model's lift with any airdam attached is not fully understood, but was probably a result of the increased air flow under the truck with the moving belt and the rate of loss of energy of the air flowing under the truck which was greatly reduced. However, it must be emphasized that the boundary layer over the textured surface of the stopped belt was thicker than which would be obtained over the smooth, hard-surface ground plane normally used in wind tunnel vehicle tests. Therefore, the differences presented here between the moving and the stopped belt should not be related to possible differences between the moving belt

and fixed ground methods of testing.

In addition to the above study, the author has been a participant in several similar investigations, where the effect of wheel rotation and moving ground have been measured. These tests have used completely different types of vehicles and model sizes, but using the same testing procedure and facility. The findings can be compared with those already presented to give the reader further knowledge and understanding of the changes possible. Results, presented in Table 23 (below), are given for the baseline configuration of each model.

Vehicle	Effect	ΔC_D	ΔC_{LF}	ΔC_{LR}
1	Wheel Rotation	.008	.005	.006
1	Moving Ground	.017	-.002	-.012
2	Moving Ground	.020	-.024	-.252
3	Moving Ground	.004	-.015	-.048
4	Moving Ground	.090	.354	.256

Vehicle 1 = 1:5 Van (detailed)
Vehicle 2 = 1:4 Racing Car (idealized)
Vehicle 3 = 1:4 Estate Car (idealized)
Vehicle 4 = 1:5 Racing Car (detailed)

Table 23

5.4 YAWED FORCE AND MOMENT INVESTIGATION

5.4.1 Experimental Arrangement

The results reported here were obtained from experiments carried out in the 3.5m x 2.6m wind tunnel, with the 2.0m x 1.1m yawed moving ground facility. The tunnel conditions (air-belt speed, model mounting, etc.) were the same as described in 5.2.1. However, in view of the uncertainty of the forces at yaw on the rotating wheel assembly used in 5.2 and 5.3, and their subsequent effect on the yawed model. The rotating wheels were mounted from the side of the wind tunnel, in the presence of the model, in order to measure yawed model forces. The aerodynamic forces presented here, thus do not include wheel forces

Because repeatable force measurements could not be obtained using the 3.5m x 2.6m tunnel's overhead balance (see 2.5), drag values were obtained using a direct measurement load cell balance positioned within the vertical mounting strut of the model. Measurements of sideforce, yawing and rolling moments were obtained from the three component strain gauge dynamometer (mounted in the model's container). Tare drag forces were measured on the exposed strut in absence of the model. No blockage correction was applied to the results (presented in the body co-ordinate system shown in Figure 8) and zero sideforce was assumed at zero yaw.

Similar to the study reported in 5.3, tests on 'add-on' devices were carried out, these were as follows:

(i) Three under-bumper airdams, with front ground clearances of 48, 33 and 8mm (described in this section as airdams 1, 2 and 6, respectively).

(ii) Two vertical side skirts, with side ground clearances of 60 and 35mm (described in this section as side skirts 1 and 2, respectively).

Airdams 2 and 6, and both side skirts, were the same devices (with the same numerical designation) used in 5.3. Whilst airdam 1 was constructed to the design guidelines described in 5.3.1.

Tests were completed with the baseline model, and each airdam and side skirt individually fitted, at yaw angles of 0, 2.5, 5.0, 10.0

and 15.0 degrees. Additionally tests with airdam 2 and side skirt 2 simultaneously fitted were carried out. Each model configuration was tested over the yawed ground plane with little boundary layer and rotating wheels (belt velocity = U_∞), and with a boundary layer and stopped wheels (belt velocity = 0). For all tests boundary layer suction was maintained.

In as much as the main purpose of this investigation was to determine the effect that ground plane boundary layer has on the aerodynamic characteristics of a yawed truck in a wind tunnel test, the discussion is limited primarily to the effects of the boundary layer on the model and those variations in model configuration that may have a bearing on or relationship to the effect of the boundary layer. However, a comparison with the values obtained from the tests reported in 5.3 are discussed first.

5.4.2 Tunnel-to-Tunnel Drag Comparison

A comparison of drag coefficient results obtained with the 1:6 scale model in the 2.1m x 1.7m wind tunnel (5.3) and the 3.5m x 2.6m wind tunnel is reported. Firstly, a comparison of results obtained in both tunnels is considered with the ground belt moving and boundary layer suction on. In this condition the empty tunnel boundary layers over each installation were very similar (the velocity distribution in the 2.1m x 1.7m wind tunnel being slightly less favourable except along the belt's centre-line), and thus direct comparison between both facilities was possible. Model drag coefficients for the configurations duplicated in both tunnels are given in Table 24 (below).

	Wind Tunnel		
	2.1m x 1.7m	3.5m x 2.6m	ΔC_D*
Baseline	.762	.668	-.094
Baseline + airdam 2	.726	.671	-.055
Baseline + airdam 6	.713	.673	-.040
Baseline + airdam 2 & side skirt 2	.718	.663	-.055

*$\Delta C_D = C_D$(3.5m x 2.6m) - C_D(2.1m x 1.7m)

Table 24

Clearly drag differences between the two tunnels were highly model configuration dependent. Drag values obtained in the 3.5m x 2.6m wind tunnel were between 5.6 and 12.3% (ΔC_D= -0.040 and -0.094) less than the drag in the 2.1m x 1.7m wind tunnel. The two major causes of this were:

(i) area blockage ratio 7.7% in the 2.1m x 1.7m tunnel
4.1% in the 3.5m x 2.6m tunnel

(ii) wheel drag (and drag of the trailing arm assembly) was measured in the 2.1m x 1.7m wind tunnel tests, but not in the 3.5m x 2.6m wind tunnel tests.

Other possible sources of tunnel-to-tunnel differences are:

(i) flow quality in the working section
(ii) dynamic-head measurement
(iii) ground plane boundary layer profiles over the two ground installations in presence of the model.

Therefore, it can be concluded that comparison of absolute drag values from tunnel-to-tunnel was unlikely in the first place. However, and perhaps overall more importantly, was any comparison of differences between configurations established? The following differences between the drag coefficient of the baseline model and with the 'add-on' devices fitted were calculated from the results in Table 24.

	Wind Tunnel	
	2.1m x 1.7m	3.5m x 2.6m
Airdam 2	-.036	.003
Airdam 6	-.049	.005
Airdam 2 + Side skirt 2	-.044	-.005

Table 25

With reference to Table 25, airdam 6, which gave the largest drag reduction (6.4%) in the 2.1m x 1.7m wind tunnel, resulted in a slight drag increase (0.7%) in the 3.5m x 2.6m wind tunnel. This

suggests that the beneficial drag difference with fixture of any airdam in the 2.1m x 1.7m wind tunnel was largely due to shielding of the model's wheels from the oncoming flow, which because wheel drag was not measured, this was not found in the 3.5m x 2.6m wind tunnel. This difference accounting for the very poor correlation between the two tunnels shown in Table 25.

Finally, a comparison of drag coefficient differences between the results measured with stopped and moving ground belt in both tunnels, is presented in Table 26. The lack of any boundary layer data over the yawed ground with the belt stopped, precluded any direct comparison of results between the two facilities with stopped belt. But any similarity of trends with the removal of boundary layer in both tunnels would be indicated.

	Wind Tunnel	
	2.1m x 1.7m	3.5m x 2.6m
Baseline	.022	-.009
Baseline + airdam 2	.025	0
Baseline + airdam 6	.015	-.002
Baseline + airdam 2 & side skirt 2	.029	.009

Table 26

Clearly little similarity between the two tunnels with boundary layer removal was found. For example, belt motion for the baseline model increased drag by 2.9% in the 2.1m x 1.7m wind tunnel, but in the 3.5m x 2.6m wind tunnel a drag decrease of 1.3% was obtained. Again a likely cause of this was the different wheel mountings used in each tunnel. Given the wheel's proximity to the ground, the predominate effect of the boundary layer probably occurs on the wheels. Whilst these effects were measured in the 2.1m x 1.7m wind tunnel, they were not in the 3.5m x 2.6m wind tunnel.

5.4.3 Effectiveness of 'Add-On' Devices with and without Ground Motion

Figures 38, 39, 40 and 41 present graphically the yawed coefficient differences between the baseline and the baseline model

with an 'add-on' device(s) fitted. Two difference characteristics are given for the four force and moment coefficients of each configuration, firstly, with the ground belt stopped, and secondly, with the belt moving. Comparison of each pair of characteristics enables the influence belt motion has on the effectiveness of the devices to be determined for the present model (without wheel force measurements).

The flow changes, and resulting aerodynamic forces, associated with addition of airdam and/or side skirts have been reported in 3.3 and 5.3. Hence, the following discussion is completed with reference to those sections.

(i) Drag

Figure 38(a): with the stopped belt all three airdams gave small drag reductions at 0 and 2.5 degrees yaw (in addition to airdam 6 at 5.0 degrees). The largest drag reduction, 1.8%, was gained with fixture of airdam 1 at zero degrees (ΔC_D= -0.012). At the two largest yaw angles, drag values greater than that of the baseline model were obtained with all three airdams (except airdam 1 at 10.0 degrees), the highest drag increase associated with airdam 6 (7.7% at 15.0 degrees) and the smallest with airdam 1 (3.5% at 15.0 degrees).

Figure 38(b): with belt motion fixture of airdam 1 resulted in a 0.4% drag reduction at zero degrees yaw (ΔC_D= -0.003), however, airdams 2 and 6 resulted in drag increases of 0.4 and 0.7% (ΔC_D= 0.003 and 0.005), respectively. At yaw, drag increased with fixture of either three airdams, the overall result at 15.0 degrees (airdam 6 = 7.6% and airdam 1 = 5.1%) being similar to that with the belt stopped.

Figure 38(c): both side skirts reduced drag throughout the yaw range, except for side skirt 1 at 15.0 degrees. The maximum drag coefficient reductions obtained at 5.0 degrees with side skirt 1 and 2 corresponding to maximum drag reductions of 3.6 and 4.0% (ΔC_D= -0.026 and -0.029), respectively. The cumulative effect of fitting both airdam 2 and side skirt 2 simultaneously were drag reductions of 3.4 to 1.8% (ΔC_D= -0.023 and -0.014) between 0 and 10.0 degrees, and a drag increase of 2.6% (ΔC_D= 0.022) at 15.0 degrees yaw.

Figure 38(d): in comparison with the belt stopped, the performance of the side skirts altered little with belt motion, except for both side skirts at 5.0 degrees yaw and side skirt 2 at 15.0

degrees yaw. Firstly, at 5.0 degrees the drag coefficient reductions were much less pronounced, maximum model drag reductions of 2.1 and 3.0% (ΔC_D= -0.015 and -0.021) were obtained for side skirt 1 and 2, respectively. Secondly, whereas at 15.0 degrees with the belt stopped, fixture of side skirt 2 resulted in a 0.9% drag decrease (ΔC_D= -0.008), with the belt moving a drag increase of 1.7% was obtained (ΔC_D= 0.015). More significantly, with airdam 2 and side skirt 2 fitted drag reductions of only 0.7 and 0.3% (ΔC_D= -0.005 and -0.002) were obtained at 0 and 2.5 degrees yaw, respectively, whilst a 1.4% drag increase at 10.0 degrees (ΔC_D= 0.011) rose to a substantive 6.4% increase at 15.0 degrees (ΔC_D= 0.055).

(ii) Sideforce

Figure 39(a): fixture of any airdam on the model reduced the sideforce. Although fixture of airdam 2 reduced the sideforce slightly more than airdam 6 at 5.0 degrees (33.0% in comparison with 28.1%), generally greater sideforce reductions were obtained with smaller front ground clearances. The reductions obtained at 15.0 degrees with airdam 1, 2 and 6 being 5.1, 9.4 and 15.2% (ΔC_Y= -0.049, -0.090 and -0.145), respectively.

Figure 39(b): these sideforce reductions were generally slightly decreased and more clearly defined with the belt moving, in comparison with the belt stopped. Sideforce reductions of 5.0, 6.3 and 13.3% were found at 15.0 degrees (ΔC_Y= -0.050, -0.063 and -0.133) with fixture of airdam 1, 2 and 6, respectively.

Figure 39(c): fixture of either side skirt on the model increased sideforce, greater increases in sideforce being obtained with the smaller side ground clearance. The increase obtained at 15.0 degrees with side skirt 1 and 2 was 14.1 and 23.6% (ΔC_Y= 0.134 and 0.225), respectively.

Figure 39(d): these sideforce reductions were broadly slightly increased with the belt moving in comparison with the belt stopped. Sideforce increases of 16.8 and 23.4% were obtained at 15.0 degrees (ΔC_Y= 0.168 and 0.234) with fixture of side skirt 1 and 2, respectively. With the stopped belt, fitting both airdam 2 and side skirt 2 resulted in very little change of sideforce up to 15.0 degrees yaw, however, a near linear rise of sideforce (similar to side skirt 1) was obtained with the belt moving. Hence at 10.0 degrees, with the

belt stopped only a 2.5% (ΔC_Y= 0.015) sideforce increase was measured, whilst a 13.3% (ΔC_Y= 0.084) increase was obtained with the belt moving.

(iii) Yawing moment

Figure 40(a): fixture of any airdam on the model reduced the yawing moment. Although fixture of airdam 2 or 6 produced very similar yawing moment reductions at 2.5 and 10.0 degrees (ΔC_N differences of 0.001 and 0.002, respectively), generally greater yawing moment reductions were obtained with smaller front ground clearances. The coefficient reductions obtained at 15.0 degrees with airdam 1, 2 and 6 being -0.030, -0.041 and -0.088, respectively. However, considering the baseline model's yawing moment coefficient of -0.053 at 15.0 degrees, fixture of either three airdams can be seen to have a substantial effect (56.6, 77.4 and 166.0% with airdam 1, 2 and 6, respectively) on the model's yawing moment characteristics.

Figure 40(b): the general reduction of yawing moment with smaller front ground clearances was slightly increased (except for airdams 1 and 2 at 10.0 degrees) and more clearly defined (a difference of ΔC_N obtained between airdams 2 and 6, at 2.5 and 15.0 degrees) with the belt moving, in comparison with the belt stopped. Yawing moment coefficient reductions of -0.040, -0.058 and -0.090 were obtained at 15.0 degrees with fixture of airdam 1, 2 and 6, respectively, which are very substantial compared with the baseline model's coefficient of -0.056.

Figure 40(c): fixture of either side skirt increased the model's yawing moment, although smaller increases (except at 5.0 degrees) were obtained with the smaller side ground clearance. Similar to the fixing of airdams on the model, the yawing moment changes with side skirt fixture were very significant (for example, at 15.0 degrees yawing moment increases of 45.3 and 22.6% were obtained with fixture of side skirt 1 and 2, respectively).

Figure 40(d): these yawing moment increases were broadly decreased with the belt moving in comparison with the belt stopped. Negligible differences were found at 2.5 and 10.0 degrees between either side skirt (ΔC_N difference of 0.001), while opposing trends were observed at 5.0 and 15.0 degrees. With belt motion fitting both airdam 2 and side skirt 2 resulted in a near steady decrease of yawing

moment coefficient, ranging from a minimum -0.013 (at 10.0 degrees) to a maximum -0.030 (at 15.0 degrees). However, with the stopped belt a near linear variation of ΔC_N was obtained, ranging from 0.006 at 2.5 degrees, to -0.028 at 15.0 degrees.

(iv) Rolling moment

The changes of rolling moment with the fixture of the 'add-on' devices were very similar to those of sideforce, the main differences from (ii) being as follows.

Figure 41(a): fixture of airdam 2 resulted in slightly larger rolling moment reductions than airdam 6 at 2.5 degrees (29.3% in comparison with 21.3%) and 5.0 degrees (30.1% in comparison with 25.3%). The rolling moment reductions obtained at 15.0 degrees with airdam 1, 2 and 6 were 4.5, 7.2 and 13.0% (ΔC_R= -0.021, -0.034 and -0.061), respectively.

Figure 41(b): with belt motion, fixture of airdam 2 reduced the rolling moment slightly more than airdam 6 only at 2.5 degrees (21.8% in comparison with 19.2%). Rolling moment reductions of 4.6, 6.0 and 16.4% were observed at 15.0 degrees (ΔC_R= -0.023, -0.030 and -0.082) with fixture of airdam 1, 2 and 6, respectively. The reductions obtained with airdam 1 and 6 being slightly greater than those with the belt stopped only at 15.0 degrees.

Figure 41(c): the rolling moment increase obtained at 15.0 degrees with side skirt 1 and 2 was 9.8 and 16.8% (ΔC_R= 0.046 and 0.079), respectively.

Figure 41(d): the rolling moment increase at 15.0 degrees with fixture of side skirt 2 was slightly less than the stopped belt value, increases obtained with side skirt 1 and 2 being 12.0 and 14.8% (ΔC_R= 0.060 and 0.074), respectively. At 10.0 degrees, fitting both airdam 2 and side skirt 2 simultaneously resulted in a 4.2% rolling moment increase (ΔC_R= 0.021), while with the belt stopped a 1.7% decrease (ΔC_R= -0.008) was obtained.

5.4.4 Effect of Ground Motion

Whereas in 5.4.3 the effectiveness of 'add-on' devices was established with and without belt motion (and thus the absence and presence of a ground plane boundary layer). This section will examine

the sensitivity of each individual model configuration to ground motion. The results, presented graphically in Figures 42, 43 and 44, plot the incremental force and moment coefficients from the belt stopped values to the belt moving values.

(i) Drag

Belt motion at zero degrees yaw decreased the baseline model's drag by 1.3% (ΔC_D= -0.009), and increased the drag with both airdam 2 and side skirt 2 simultaneously fitted by 1.4% (ΔC_D= 0.009). Yawing the baseline model increased the drag decrease up to 2.2% (ΔC_D= -0.016) at 5.0 degrees and thereafter the drag decrease fell to 0.4% and 0.2% at 10.0 and 15.0 degrees (ΔC_D= -0.003 and -0.002), respectively. Whilst for the airdam and skirted model increased drag values of 2.9 and 3.5% were obtained at 10.0 and 15.0 degrees (ΔC_D= 0.022 and 0.031), respectively.

With individual airdams fitted (Figure 43) the effect of belt motion on the drag was very unpredictable throughout the yaw range, the greatest sensitivity being a 1.8% increase with airdam 1 at 10.0 degrees yaw (ΔC_D= 0.014). However, at zero degrees yaw, the drag with either airdam 1 or 2 fitted did not change with belt motion and even with airdam 6 fitted only a slight 0.3% increase of drag (ΔC_D= -0.002) was measured. For side skirts 1 and 2 drag reductions of 1.3 and 1.9% (ΔC_D= -0.009 and -0.013), respectively, with belt motion at zero degrees yaw, broadly reduced with increasing yaw, until drag increases of 0.5% and 2.5% were obtained at 15.0 degrees (ΔC_D= 0.004 and 0.021, respectively).

(ii) Sideforce

For the baseline model, belt motion increased the sideforce coefficient throughout the yaw range. Fixture of airdams or side skirts increasing the coefficient change by similar amounts. Surprisingly, airdam 2 (at all yaw angles) and side skirt 1 (at 10.0 and 15.0 degrees) gave larger sideforce coefficient increases than airdam 6 and side skirt 2, respectively. In comparison with the other configurations, with airdam 2 and side skirt 2 fitted a significantly larger sideforce coefficient increase was found only at 10.0 degrees (ΔC_Y= 0.098).

The near linear sideforce coefficient increase with belt motion over the yaw range for the baseline model was equivalent to a gradual increase from the configuration's original (stopped belt) sideforce characteristics, a 5.0% increase of sideforce (ΔC_Y= 0.048) being obtained at 15.0 degrees. However, the largest sideforce increase obtained with belt motion was not found at 15.0 degrees for any of the other configurations. In fact the lowest sideforce increase generally occurred at the higher yaw angles for either of the three airdams. The largest sideforce increase, at which angle it occurred and the average of the sideforce increases at 2.5, 5.0, 10.0 and 15.0 degrees are presented in Table 27 (below).

Baseline	max.sideforce = 5.0%	(15.0 deg.)	ave.= 3.8%
Airdam 1	10.1%	(5.0 deg.)	ave.= 7.3%
Airdam 2	26.1%	(5.0 deg.)	ave.= 15.1%
Airdam 6	14.4%	(2.5 deg.)	ave.= 10.9%
Side Skirt 1	8.8%	(10.0 deg.)	ave.= 7.0%
Side Skirt 2	7.8%	(10.0 deg.)	ave.= 6.7%
Airdam 2 & Side skirt 2	15.8%	(10.0 deg.)	ave.= 10.5%

Table 27

(iii) Yawing moment

Yawing moments decreased with belt motion (except at 2.5 degrees for the baseline, airdam 1 and side skirt 1 configurations). The increase of yawing moment coefficient at 2.5 degrees (ΔC_N= 0.002) for the side skirt 2 configuration, however, altered to give coefficient reductions which increased up to 15.0 degrees (ΔC_N= -0.016) . Additionally, with side skirt 1 fitted instead of side skirt 2, a larger yawing moment coefficient reduction was obtained at the intermediate yaw angles. With both airdam 2 and side skirt 2 fitted the reduction of yawing moment coefficient at 2.5 degrees yaw (ΔC_N= -0.021) was reduced to -0.005 at 15.0 degrees.

Similar to the yawing moment results reported in 5.4.3 the yawing moment changes with belt motion had a substantial effect on each configuration's original (stopped belt) yawing moment characteristics. For example, the above changes of yawing moment coefficient for the airdam and skirted model were equivalent to a

140.0 and 6.2% increase of the yawing moment at 2.5 and 15.0 degrees, respectively.

(iv) Rolling moment

Rolling moments were found to increase with belt motion, the results being very similar to those of sideforce. The major difference from (ii) was found with airdam 6 fitted, with which the increase of rolling moment coefficient was less than that associated with airdam 1 at all yaw angles except 5.0 degrees (airdam 1 also had a larger coefficient increase than airdam 2 at 10.0 degrees). Additionally, the rolling moment coefficient increase with belt motion was found to reduce from 10.0 to 15.0 degrees for airdam 6 (0.019 to 0.008) and side skirt 2 (0.028 to 0.024).

The largest rolling moment increase from the configuration's original (stopped belt) characteristics, at which angle it occurred and the average of the rolling moment increases at 2.5, 5.0, 10.0 and 15.0 degrees are presented in Table 28 (below).

Baseline	max.rolling m.= 6.2%	(15.0 deg.)	ave.= 4.4%
Airdam 1	13.3%	(5.0 deg.)	ave.= 9.6%
Airdam 2	26.5%	(5.0 deg.)	ave.= 14.7%
Airdam 6	17.4%	(5.0 deg.)	ave.= 8.4%
Side Skirt 1	9.4%	(10.0 deg.)	ave.= 7.5%
Side Skirt 2	9.1%	(2.5 deg.)	ave.= 7.6%
Airdam 2 & Side skirt 2	15.3%	(10.0 deg.)	ave.= 8.9%

Table 28

5.4.5 Concluding Remarks

The primary aim of this final study was to present detailed and unique yawed force and moment measurements, indicating the sensitivity of a typical truck model to ground plane motion obtained from the yawed moving ground facility. Similarly to the study reported in 5.3, no attempt was made to detail the flow changes under the model, which caused the variation of measurements obtained.

Poor correlation of absolute and difference drag coefficients was found with the fixture of the same aerodynamic 'add-on' devices in

the 2.1m x 1.7m wind tunnel and the 3.5m x 2.6m wind tunnel. Significant differences between the wheel mounting used in each tunnel, however, was a likely source of the error. Therefore, further tests using the 1:6 scale model with the trailing arm rotating wheel assembly should be completed at zero yaw over the yawed moving ground facility, in order to provide data for a future comparison.

At high yaw angles, drag changes with fixture of any of the three airdams was only slightly altered with belt motion. However, at small yaw angles the performance of any of the three airdams was more dependent on belt motion. Generally, with the ground stopped, fixture of airdams gave rise to drag reductions, but with ground motion drag was found to increase. Even so, the small size of the airdam related drag reductions at zero yaw and the large drag increases at non-zero yaw would indicate that the airdams were not representative of those results reported by previous investigators. This was probably caused by the model's lack of realistic under-cab detail (for example, no cooling flow) and the airdams' simple shape.

The drag reductions with either side skirt altered little with belt motion. Also, whether the belt was stopped or moving bore little effect on the sideforce, yawing moment and rolling moment changes obtained with fixture of either airdams or side skirts. However, changes obtained with the moving belt, especially with fixture of any of the three airdams, were seen to be more clearly defined (a result of boundary layer removal) and large differences were found in the results obtained with the fixture of both airdam and side skirt simultaneously. This latter finding indicated that the force and moment coefficients were more sensitive to ground plane changes when the front and sides of the model were extended towards the ground.

Rolling moment coefficient characteristics generally resembled those of sideforce, except the changes with belt motion for individual configurations were not exactly similar at the higher yaw angles.

Sideforce (and thus rolling moment) coefficients increased with belt motion, which, because of larger ground plane boundary layers associated with the stopped belt, corresponded to a reduction of dynamic pressure acting on the lower portion of the vehicle.

Changes of yawing moment coefficient with either addition of 'add-on' devices, or ground motion, were very substantial in comparison to the configuration's original characteristics, changes in excess of 100% not being uncommon.

CHAPTER 6
CONCLUSIONS AND RECOMMENDATIONS

6.1 INTRODUCTION

Conclusions drawn from the work completed may be separated into two distinct categories, those relating to the experimental operation of the wind tunnel facilities (6.1), and those of direct research interest (6.2). Using these conclusions and experience amassed during the research programme, recommendations are made for possible future research topics arising from the present work and on the facilities required for the wind tunnel testing of commercial vehicle models.

6.2 EXPERIMENTAL CONCLUSIONS

The main experimental conclusions from the present research programme are as follows.

(i) The overhead mechanical balance in the 2.1m x 1.7m wind tunnel is excellent for tests on road vehicle models. Its sensitivity and repeatability have contributed to the University's success in this field of research.

(ii) A three component strain gauge dynamometer was recently built. When the dynamometer was mounted within a yawed model in the 2.1m x 1.7m wind tunnel, yawed drag forces were evaluated which correlated closely with measurements made in other establishments. Additionally, measurements of sideforce, yawing and rolling moments were obtained from the dynamometer.

(iii) The overhead balance in the 3.5m x 2.6m wind tunnel is of very limited use for vehicle tests, lacking sensitivity and repeatability. Further work continues with a direct drag measurement load cell positioned within the mounting strut of the model.

(iv) Velocity deficits 10mm above the moving ground installation in the 2.1m x 1.7m wind tunnel were found to be within 6% of freestream. However, the construction of a new front suction box, with greater design consideration given to the boundary layer removal, would significantly improve the velocity distribution obtained above the belt. Additionally, improvements of the crude belt suction lay-out, incorporating sophisticated control of suction, would probably enable belt speeds in excess of 30m/s to be attained.

(v) A new 5.3m x 2.4m moving ground in the 3.5m x 2.6m wind tunnel has been modified and developed, with currently a maximum operating speed of 26m/s*. Future work to reduce belt lift, by improved belt suction, should enable speeds of 30m/s to be attained. This new moving ground is one of the largest currently being used for road vehicle testing.

*May 1986

(vi) The existing 2.0m x 1.1m moving ground from the 2.1m x 1.7m wind tunnel has been installed in the 3.5m x 2.6m wind tunnel. This has allowed tests on a 1:6 scale truck model in which both the model

and moving ground have been yawed up to 15 degrees. Boundary layer traverses carried out at 26m/s during October 1985, showed that velocity deficits (10mm above belt) within 4% of freestream were achieved over most of the belt, thus meeting the required performance objectives. It is believed that this technique has not been used before for road vehicle testing.

(vii) The development of suitable techniques enabling the measurement of aerodynamic forces on models with wheels rotating on the ground has been illustrated.

(viii) Poor correlation of absolute and difference drag coefficients was found using the same model in the 2.1m x 1.7m and 3.5m x 2.6m wind tunnels. Differences in the wheel mountings used in each tunnel was a likely major source of error.

(ix) A comprehensive library of micro-computer programs, facilitating the automatic sampling and analysis of wind tunnel balance forces and 'scani-valve' pressure outputs has been written and used successfully.

6.3 RESEARCH CONCLUSIONS

Conclusions reached from the work reported in Chapters 4 and 5 are comprehensively detailed in each respective chapter.

As a prelude to these two main avenues of research, tests using a semi-detailed 1:6 scale rigid truck model in the 2.1m x 1.7m wind tunnel were completed. The preliminary study detailed the effect of crosswind, when the model (with fixed wheels) was yawed relative to the wind and moving belt. Trends observed in the measured aerodynamic forces throughout a yaw range of 0 to 20.2 degrees were presented and examined with the assistance of flow visualization.

Additionally, the effect of Reynolds number, transition fixing, flow turbulence, ground clearance and ground plane boundary layer were studied. The model's drag, being the most important parameter for commercial vehicles, was found only to be drastically altered with the presence of the turbulence generating grid (24% increase) and fixture of wire transition on the yawed model (5% decrease at 20.2 degrees). The model's lift was also found to be sensitive to transition fixing, changes of ground clearance and ground plane boundary layer. However, the effect of different transition types was found to vary, on both lift and drag.

6.4 RECOMMENDATIONS

6.4.1 1:8 Scale Idealized Rigid Truck Model

Results reported using the 1:8 scale idealized truck model only considered the experimental findings at zero yaw. However, other areas of research were planned which were to include the study of model yaw and a comparison with theory.

Because the model has edge radii which would give totally different flow regimes, this would enable a full range of experimental data (surface static pressure measurements) from this basic model, to be compared with those predicted by Computational Fluid Dynamics (for example C.H.A.M. Pheonics-84). Regions of correct flow simulation and the limitations of a current C.F.D. method could be found, in preparation for the publication of a comprehensive set of experimental results for future comparisons.

Future work should also attempt to broaden understanding of the flow field around the model. Testing using the 'china-clay' technique (Refs. 25 & 29) would establish the nature of the boundary layer over the model, which if associated with transition fixing, could provide a more detailed study on the effect of transition. Also measurements of the flow stagnation and separation from surface static pressures would provide a quantitive insight into the postulated causes of the drag reductions and variations of lift, obtained with cab and container rounding.

Finally, using C.F.D. techniques Paul and LaFond(28) have shown that sharper non-circular edges can be designed which provide good aerodynamic performance without sacrificing internal volume. Thus, in addition to the above studies, the 1:8 scale model could be adapted to experimentally explore the effect of non-circular edge rounding.

6.4.2 Transition

The limited studies of transition reported in Chapters 3 and 4 posed more questions than were quantatively answered. Future work should attempt to assess the possibility, and thus the type and location of transition needed, to simulate boundary layer behaviour typical of that at full-scale.

6.4.3 Commercial Vehicle Wind Tunnel Tesing

In considering the wind tunnel testing of a commercial vehicle, an engineer must take several factors into account. Three such factors, which may dictate the facility eventually used, are as follows.

(i) Ground plane

Changes of the ground plane boundary layer (or more specifically, stopped-moving ground belt, and with-without upstream suction) have shown that a typical, current truck design was not affected at zero and non-zero yaw in such a manner as to substantially affect any aerodynamic vehicle development. Investigations studying the parallel phenomenon of wheel rotation also produced similar conclusions. Reduction of the tunnel floor boundary layer, by upstream suction, being an adequate ground plane simulation.

(ii) Reynolds number

All Reynolds number tests attempted during the present research, although completed using a small range of dynamic pressures, did not indicate any notable trends. However, previous investigators have asserted the presence of Reynolds number effects, especially when assessing the flow field around a vehicle body curvature. The forebody aerodynamic behaviour of current commercial vehicles is highly dependent on the cab-container geometry, and therefore the cab's leading edge. It is a necessity to correctly simulate the cab-container flow interference in the wind tunnel, which can only be achieved by full-scale Reynolds numbers or perhaps the correct use of transition.

(iii) Yaw Angle

Results presented in this report and by other authors, have shown that in yaw the zero yaw flow field around a commercial vehicle quickly breaks down and other flow fields proliferate. For this reason commercial vehicle aerodynamists often account for the probable effect of crosswinds, by making use of 'wind-averaged' coefficients. However, yawed wind tunnel tests are not a true simulation of crosswinds. The smooth, uniform flow in the wind tunnel not being the gusty, sheared flow present in real life: and it is in this context that the results obtained with flow turbulence should be considered.

Therefore, another area of commercial vehicle aerodynamics which presents itself as a worthwhile field of study is the understanding and wind tunnel simulation of surface wind characteristics, in particular their effect on yawed trucks.

REFERENCES

1. ALLAN,J.W., BURGIN,K. and LILLEY,G.M.(1977)'On water spray generation by road vehicles and methods for its control', Contract Report for the Department of the Environment, Transport and Road Research Laboratory, Crowthorne, Berks.

2. ALLAN,J.W.(1980)'Aerodynamic drag and pressure measurements on a simplified tractor-trailer model', Proc.4th Colloquium on Industrial Aerodynamics (Aachen).

3. ALLAN,J.W. and LILLEY,G.M.(1983)'The reduction of water spray from heavy road vehicles', Int. J. of Vehicle Design, Technological Advances in Vehicle Design Series, SP3, Impact of Aerodynamics on Vehicle Design, pp. 270-307.

4. CARR,G.W.(1968)'The aerodynamics of basic shapes for road vehicles, Part 1 (Simple rectangular bodies)', Motor Industry Research Association (M.I.R.A.), Report No.1968/2.

5. COGOTTI,A.(1983)'Aerodynamic characteristics of car wheels', Int. J. of Vehicle Design, Technological Advances in Vehicle Design Series, SP3, Impact of Aerodynamics on Vehicle Design, pp. 173-196.

6. COOPER,K.R.(1976)'A wind tunnel investigation into the fuel savings available from the aerodynamic drag reduction of trucks', Natl. Res. Counc.(Canada), Dept. Mech. Eng./ Natl. Aeronaut. Establ., Q. Bull. 1976/3.

7. COOPER,K.R. and CAMPBELL,W.F.(1980)'An examination of the effects of wind turbulence on the aerodynamic drag of vehicles', Proc.4th Colloquium on Industrial Aerodynamics (Aachen).

8. COOPER,K.R., MASON,W.T.Jr. and BETTES,W.H.(1982)'Correlation experience with the S.A.E. wind tunnel test procedure for trucks and buses', S.A.E. Paper 820375.

9. COOPER,K.R.(1984)'The wind tunnel simulation of surface vehicles', J. Wind Eng. and Ind. Aero., 17(1984), pp. 167-198.

10. COOPER,K.R.(1985)'The effect of front-edge rounding and rear-edge shaping on the aerodynamic drag of bluff vehicles in ground proximity', S.A.E. Paper 850288.

11. COOPER,K.R., GERHARDT,H.J., WHITBREAD,R., GARRY,K.P. and CARR,G.W.(1985)'A comparison of aerodynamic drag measurements on model trucks in closed-jet and open-jet wind tunnels', Proc 6th Colloquium on Industrial Aerodynamics (Aachen).

12. COWPERTHWAITE,N.A.(1985)'An investigation of the effect of rear body pitch on the aerodynamic characteristics of a simplified tractor-trailer model', Proc 6th Colloquium on Industrial Aerodynamics (Aachen).

13. EGLE,S., HERZUM,N., HOFELE,G. and KONITZER,H.(1982)'Wind tunnel for aerodynamic research', S.A.E. Paper 820372.

14. FACKRELL,J.E. and HARVEY,J.K.(1973)'The flow field and pressure distribution of an isolated road wheel', Advances in Road Vehicle Aerodynamics, B.H.R.A. Fluid Engineering, Paper 10, pp. 155-165.

15. FACKRELL,J.E. and HARVEY,J.K.(1974)'The aerodynamics of an isolated road wheel', Proc. 2nd A.I.A.A. Symp. Aerodynamics of Sports and Competition Autos., Los Angelos, pp. 119-125.

16. GEORGE,A.R.(1979)'Aerodynamics of simple bluff bodies including effects of body shape, ground proximity and pitch', A.S.M.E. Symposium on Aerodynamics of Transportation, Niagara Falls.

17. GILHAUS,A.(1980)'The influence of cab shape on air drag of trucks', Proc.4th Colloquium on Industrial Aerodynamics (Aachen).

18. GILHAUS,A.(1984)'Aerodynamics of heavy commercial vehicles', Vehicle Aerodynamics, von Karman Institute for Fluid Mechanics, Short Course 1984-01.

19. GUTTERIDGE,L.(1984)'Tunnel to tunnel correlation with 1:12 and 1:6 scale truck models', Leyland Vehicles Limited, Preston, England.(Restricted).

20. HUCHO,W.H., JANSSEN,L.J. and EMMEIMANN,H.J.(1976)'The optimization of body details - A method for reducing the aerodynamic drag of road vehicles', S.A.E. Paper 760185.

21. HURST,D.W.(1982)'Some aspects of the aerodynamics of bluff bodies in proximity of the ground', Ph.D. Thesis, Department of Aeronautics and Astronautics, University of Southampton.

22. KANGAS,T.(1979)'The use of small scale wind tunnel data in the design of cab-over-engine tractor/trailer combinations', S.A.E. Paper 790767.

23. KELLY,K.B., PROVENCHER,L.G. and SCHENKEL,F.K.(1982)'The General Motors Engineering Staff Aerodynamics Laboratory - A full-scale automotive wind tunnel', S.A.E. Paper 820371.

24. KRAMER,C., GERHARDT,H.J. and HELLING,J.(1982)'Wind tunnel tests on bluff bodies regarding truck aerodynamics', Int. Symp. on Vehicle Aerodynamics. Organised by Volkswagenwerk AG-Research Division, Wolfsburg.

25. MOIR,I.R.M.(1986)'Recent experience in the R.A.E. 5-metre wind tunnel of a china clay method for indicating boundary layer transition', The Aeronautical Journal, Vol. 90, No. 891, Jan. 1986, pp. 6-9.

26. NEWELL,P.G.(1983)'An experimental investigation into the aerodynamics of a racing sports car, involving the design, construction and calibration of a three component strain gauge dynamometer', B.Sc. Hons. Project, Department of Aeronautics and Astronautics, University of Southampton.

27. OSWALD,L.J. and BROWNE,A.L.(1981)'The airflow field around an operating tire and its effect on tire power loss', S.A.E. Paper 810166.

28. PAUL,J.C. and LAFOND,J.G.(1983)'Analysis and design of automobile forebodies using potential flow theory and a boundary layer separation criterion', S.A.E. Paper 830999.

29. POPE,A. and HARPER,J.J.(1966)'Low-speed wind tunnel testing', John Wiley and Sons, Inc., New York.

30. ROSHKO,A. and KOENIG,K.(1976)'Interaction effects on the drag of bluff bodies in tandem', in G.Sovran et al. (Eds.), Aerodynamic Drag Mechanisms of Bluff Bodies and Road Vehicles, General Motors, Detroit, Plenum Press, New York, 1978.

31. S.A.E. Wind Tunnel Test Procedure for Trucks and Buses, S.A.E. J1252 Oct79.

32. STAPLEFORD,W.R. and CARR,G.W.(1970)'Aerodynamic characteristics of exposed rotating wheels', Motor Industry Research Association (M.I.R.A.), Report No.1970/2.

33. STAPLEFORD,W.R. and CARR,G.W.(1971)'A further study of the simulation problem in wind tunnel tests of road vehicles', Motor Industry Research Association (M.I.R.A.), Report No.1971/6.

34. STOLLERY,J. and GARRY,K.P.(1983)'Techniques for reducing commercial vehicle aerodynamic drag', Int. J. of Vehicle Design, Technological Advances in Vehicle Design Series, SP3, Impact of Aerodynamics on Vehicle Design, pp. 210-228.

BIBLIOGRAPHY

ADEY,P.C.(1985)'Rigid truck aerodynamics over a moving ground - preliminary report', A.A.S.U. Memorandum 85/20, Department of Aeronautics and Astronautics, University of Southampton.

ADEY,P.C.(1985)'Effect of wheel rotation and ground plane simulation on the aerodynamics of a rigid truck model', A.A.S.U. Memorandum 85/21, Department of Aeronautics and Astronautics, University of Southampton.

BARTH,R.(1966)'Effect of unsymmetrical wind incidence on aerodynamic forces acting on vehicle models and similar bodies', S.A.E. Paper 650136.

BEARMAN,P.W.(1979)'Bluff body flows applicable to vehicle aerodynamics', A.S.M.E. Symposium on Aerodynamics of Transportation, Niagara Falls.

BEAUVAIS,F.N., TIGNOR,S.C. and TURNER,T.R.(1968)'Problems of ground simulation in automotive aerodynamics', S.A.E. Paper 680121.

BERTA,C. and BONIS,B.(1980)'Experimental shape research of ideal aerodynamic characteristics for industrial vehicles', S.A.E. Paper 801402.

BRASSEUR,J.G.(1984)'The physics of ground effect', A.A.S.U. Memorandum 84/2, Department of Aeronautics and Astronautics, University of Southampton.

BUCKLEY,F.T.Jr. and SEKSCIENSKI,W.S.(1975)'Comparisons of effectiveness of commercially available devices for the reduction of aerodynamic drag on tractor-trailers', S.A.E. Paper 750704.

BUCKLEY,F.T.Jr., MARKS,C.H. and WALSTON,W.H.Jr.(1978)'A study of aerodynamic methods for improving truck fuel economy', Dept. of Mech. Eng., Maryland University.

BUCKLEY,F.T.Jr.(1985)'An improved over-the-road test method for determining the fuel savings benefit of a truck aerodynamic drag-reducing device', S.A.E. Paper 850285.

BURGIN.K., ADEY,P.C. and BEATHAM,J.P.(1985)'Wind tunnel tests on road vehicle models using a moving belt simulation of ground effect', Proc 6th Colloquium on Industrial Aerodynamics (Aachen).

COWPERTHWAITE,N.A.(1986)'The influence of simple add-on devices on the wake geometry of large articulated road vehicles', Vehicle Aerodynamics, von Karman Institute for Fluid Mechanics, Lecture Series 1986-05.

DAVIES,P.O.A.L.(1961)'The new 7 x 5½ ft and 15 x 12 ft low speed wind tunnel at the University of Southampton', A.A.S.U. Report No. 202, Department of Aeronautics and Astronautics, University of Southampton.

DAVIES,P.O.A.L., DYKE,R.W. and MARCHAJ,C.A.(1962)'The wind tunnel balances in the large low speed tunnel at Southampton University', A.A.S.U. Report No. 208, Department of Aeronautics and Astronautics, University of Southampton.

DAVIS,W.R., ERYOU,N.D. and PATRY,J.C.(1977)'Operational road tests of truck aerodynamic drag reduction devices', S.A.E. Paper 770690.

FACKRELL,J.E.(1975)'The simulation and prediction of ground effect in car aerodynamics', I.C. Aero. Report 75-11, Imperial College, London.

GARRY,K.P. and STOLLERY,J.L.(1982)'Reducing the aerodynamic drag of commercial vehicles', Int. J. of Vehicle Design, Vol. 3, No. 2, pp. 160-170.

GARRY,K.P.(1985)'A review of commercial vehicle aerodynamic drag reduction techniques', Proc. Instn. Mech. Engrs, Vol. 199, No. D3, pp. 215-220.

GILHAUS,A.(1983)'Aerodynamics of a design study for a modern long-haul truck', Int. J. of Vehicle Design, Technological Advances in Vehicle Design Series, SP3, Impact of Aerodynamics on Vehicle Design, pp. 256-269.

GOTZ,H.(1984)'Present and future trends in automotive aerodynamics', Vehicle Aerodynamics, von Karman Institute for Fluid Mechanics, Short Course 1984-01.

GUTTERIDGE,L. and STAPLEFORD,W.R.(1982)'Drag reduction techniques applied to a range of truck configurations using 1:8 scale models', Int. Symp. on Vehicle Aerodynamics. Organised by Volkswagenwerk AG-Research Division, Wolfsburg.

HARRIS,H.T.(1980)'Fuel savings through aerodynamic drag reduction of trucks', The South African Mechanical Engineer, Vol. 30, pp. 214-220.

HOFFMANN,P.H., SAUNDERS,J.W. and WATKINS,S.(1984)'Wind tunnel tests of two truck models with various aerodynamic drag-reducing devices', Vehicle Aerodynamic Group Report WTR 1029, Dept. Mech. and Prod. Eng., Royal Melbourne Institute of Technology.

HOLMES,H.R.(1976)'Practical economic aspects of tractor-trailer aerodynamics', S.A.E. Paper 760103.

HUCHO,W.H., JANSSEN,L.J. and SCHWARTZ,G.(1975)'The wind tunnel's ground plane boundary layer - Its interference with the flow underneath cars', S.A.E. Paper 750066.

HURST,D.W., ALLAN,J.W. and BURGIN,K.(1983)'Pressure measurements on a full-scale tractor-trailer combination and comparison with data from wind-tunnel model tests', Int. J. of Vehicle Design, Technological Advances in Vehicle Design Series, SP3, Impact of Aerodynamics on Vehicle Design, pp. 471-479.

INGRAM,K.C.(1977)'Wind tunnel tests on scale models of heavy goods vehicles', Department of the Environment and Department of Transport, Transport and Road Research Laboratory (T.R.R.L.) Report SR 337, Crowthorne, Berks.

LISSAMAN,P.B.S.(1975)'Development of devices to reduce the aerodynamic resistance of trucks', S.A.E. Paper 750702

MARKS,C.H., BUCKLEY,F.T.Jr. and WALSTON,W.H.Jr.(1976)'An evaluation of the aerodynamic drag reductions produced by various cab roof fairings and a gap seal on tractor-trailer trucks', S.A.E. Paper 760105.

MARKS,C.H. and BUCKLEY,F.T.Jr.(1980)'The effect of tractor-trailer flow interaction on the drag and distribution of drag of tractor-trailer trucks', S.A.E. Paper 801403.

MASON,W.T. and SOVRAN,G.(1973)'Ground-plane effects on the aerodynamic characteristics of automobile models - An examination of wind tunnel test technique', Advances in Road Vehicle Aerodynamics, B.H.R.A. Fluid Engineering, Paper 17, pp. 291-309.

MASON,W.T.Jr.(1975)'Wind tunnel development of the dragfoiler - A system for reducing tractor-trailer aerodynamic drag', S.A.E. Paper 750705.

MONTOYA,L.C. and STEERS,L.L.(1974)'Aerodynamic drag reduction tests on a full-scale tractor-trailer combination with several add-on devices', N.A.S.A. TM X-5602B, Dec. 1974.

MUIRHEAD,V.U. and SALTZMAN,E.J.(1979)'Reduction of aerodynamic drag and fuel consumption for tractor-trailer vehicles', Journal of Energy, Vol. 3, No. 5, Sept.-Oct. 1979, pp.279-284.

MUIRHEAD,V.U.(1981)'An investigation of drag reduction for a standard truck with various modifications', N.A.S.A. C 163107, May 1981.

RAJAN,A.A.(1981)'Reduction of aerodynamic drag on tractor-trailer vehicles', M.Sc. Thesis, Department of Aeronautics and Fluid Mechanics, University of Glasgow.

SAUNDERS,J.W., WATKINS,S., HOFFMANN,P.H. and BUCKLEY,F.T.Jr.(1985)'Comparison of on-road and wind-tunnel tests for tractor-trailer aerodynamic devices, and fuel savings predictions', S.A.E. Paper 850286.

SERVAIS,R.A. and BAUER,P.T.(1975)'Aerodynamic devices can significantly reduce the fuel consumption of trucks: Experience with CECA designs', S.A.E. Paper 750707.

STEERS,L.L., MONTOYA,L.C. and SALTZMAN,E.J.(1975)'Aerodynamic drag reduction tests on a full-scale tractor-trailer combination and a representative box-shaped ground vehicle', S.A.E. Paper 750703.

TADGHIGHI,H.(1983)'Preliminary calibration of the Southampton University 3.5m x 2.6m wind tunnel', A.A.S.U. Memorandum 83/3, Department of Aeronautics and Astronautics, University of Southampton.

TURNER,T.R.(1967)'Wind-tunnel investigation of a 3/8-scale automotive model over a moving-belt ground plane', N.A.S.A. Tech. Note TN D-4229, November 1967.

WATKINS,S. and SAUNDERS,J.W.(1984)'Wind tunnel studies on the drag of tanker trucks and tanker road trains', Vehicle Aerodynamic Group Report WTR 1037, Dept. Mech. and Prod. Eng., Royal Melbourne Institute of Technology.

WILLIAMS,T. and JACKLIN,D.(1979)'Methods of evaluating the effect of aerodynamics on the fuel consumption of commercial vehicles', Department of the Environment and Department of Transport, Transport and Road Research Laboratory (T.R.R.L.) Report SR 481, Crowthorne, Berks.

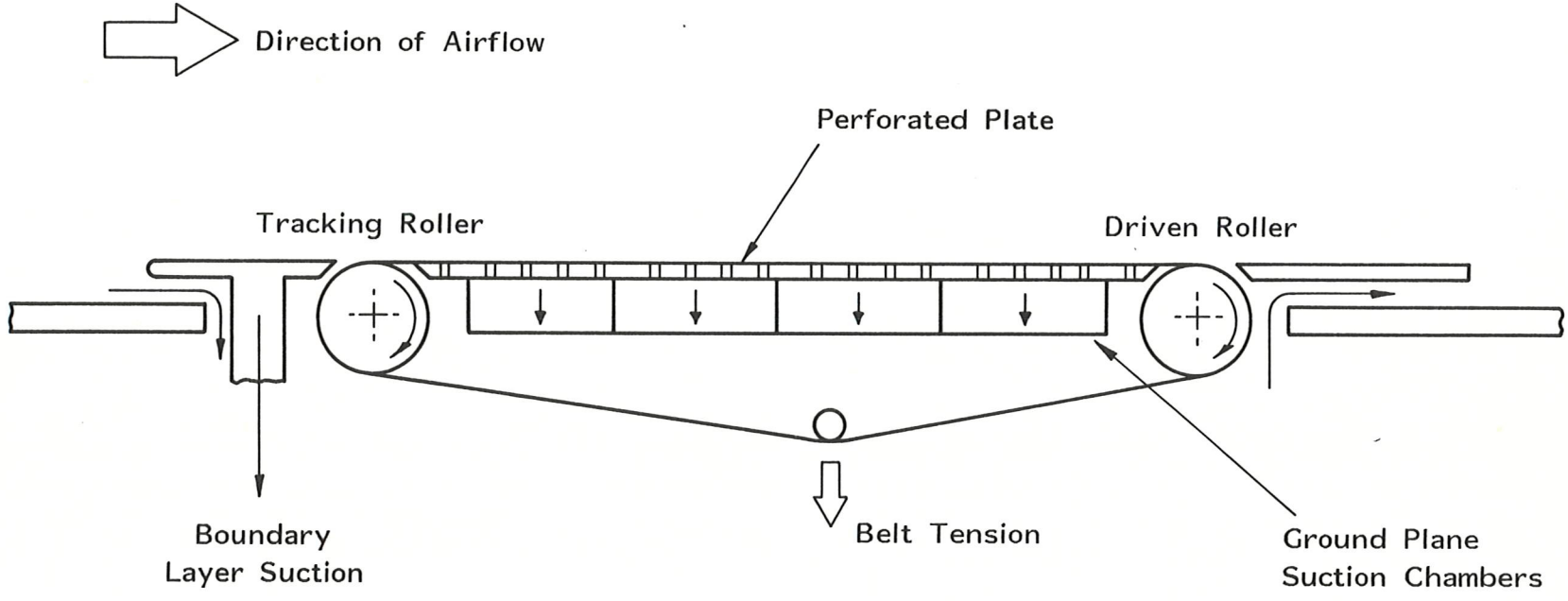

2.1m x 1.7m Wind Tunnel, Moving Ground Length = 2m and Width = 1.1m

3.5m x 2.6m Wind Tunnel, Moving Ground Length = 5.3m and Width = 2.4m

FIG. 1 SCHEMATIC LAYOUT OF MOVING GROUND PLANE.

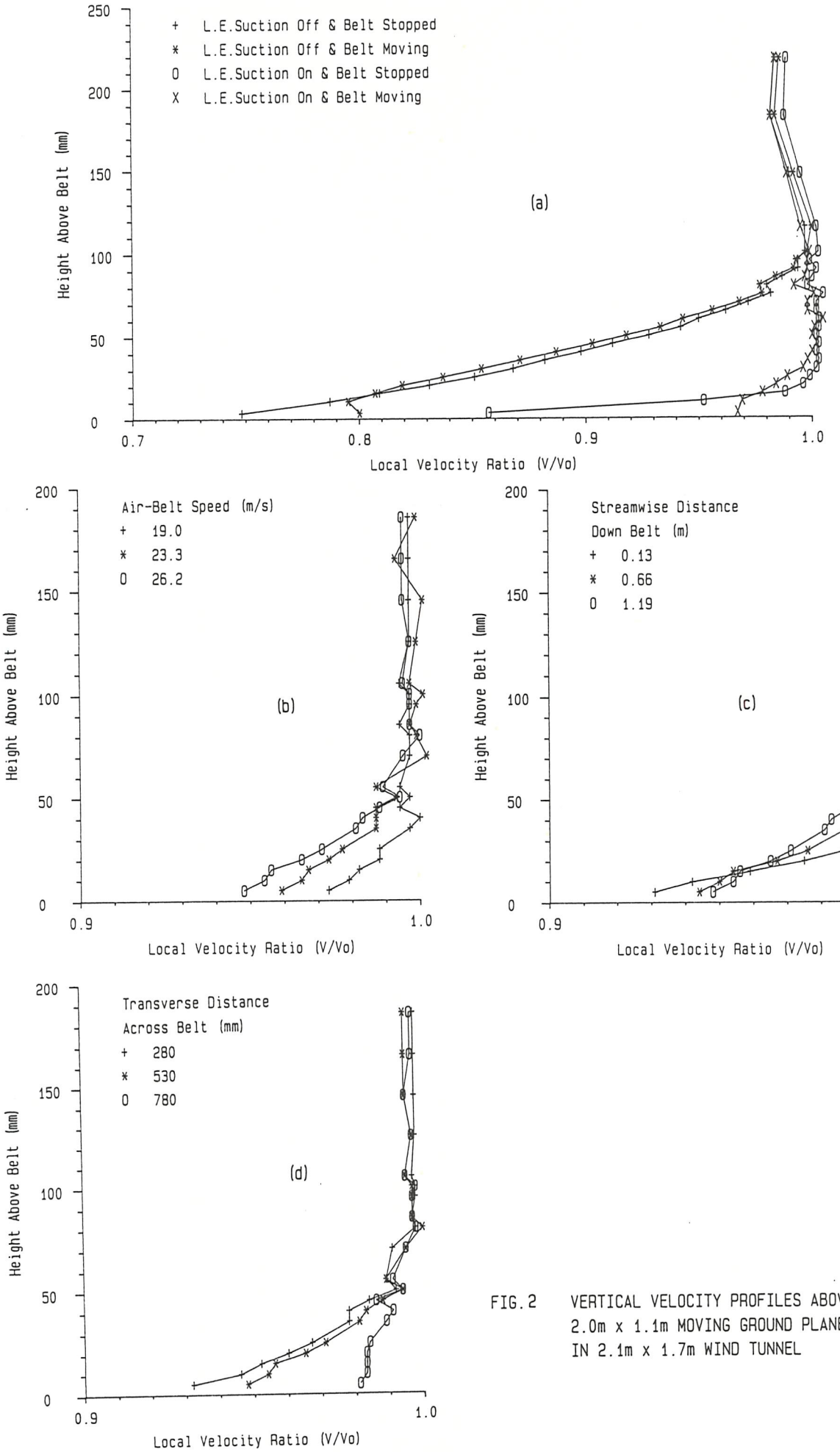

FIG. 2 VERTICAL VELOCITY PROFILES ABOVE 2.0m x 1.1m MOVING GROUND PLANE IN 2.1m x 1.7m WIND TUNNEL

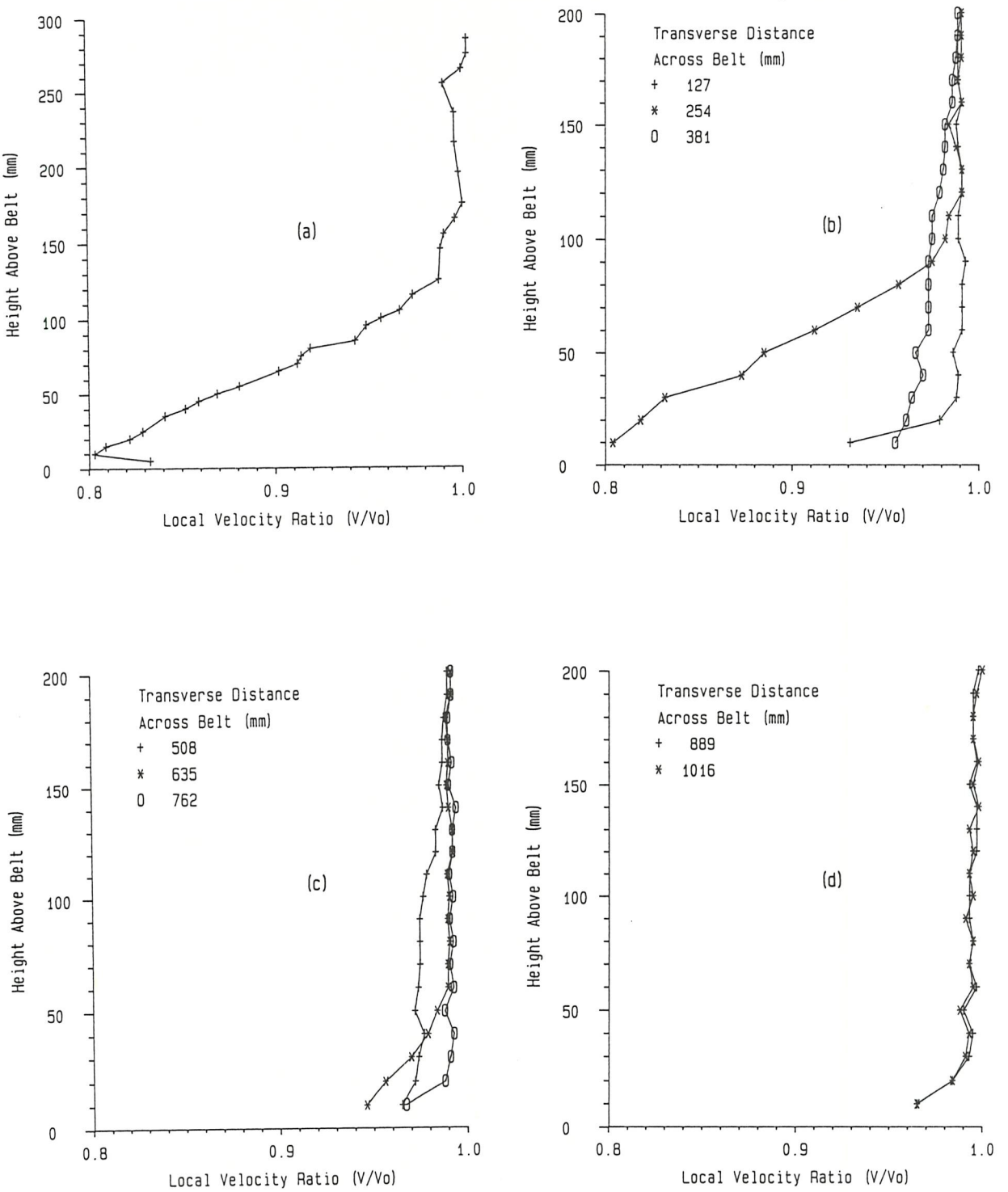

FIG. 3 VERTICAL VELOCITY PROFILES ABOVE YAWED 2.0m x 1.1m MOVING GROUND PLANE IN 3.5m x 2.6m WIND TUNNEL

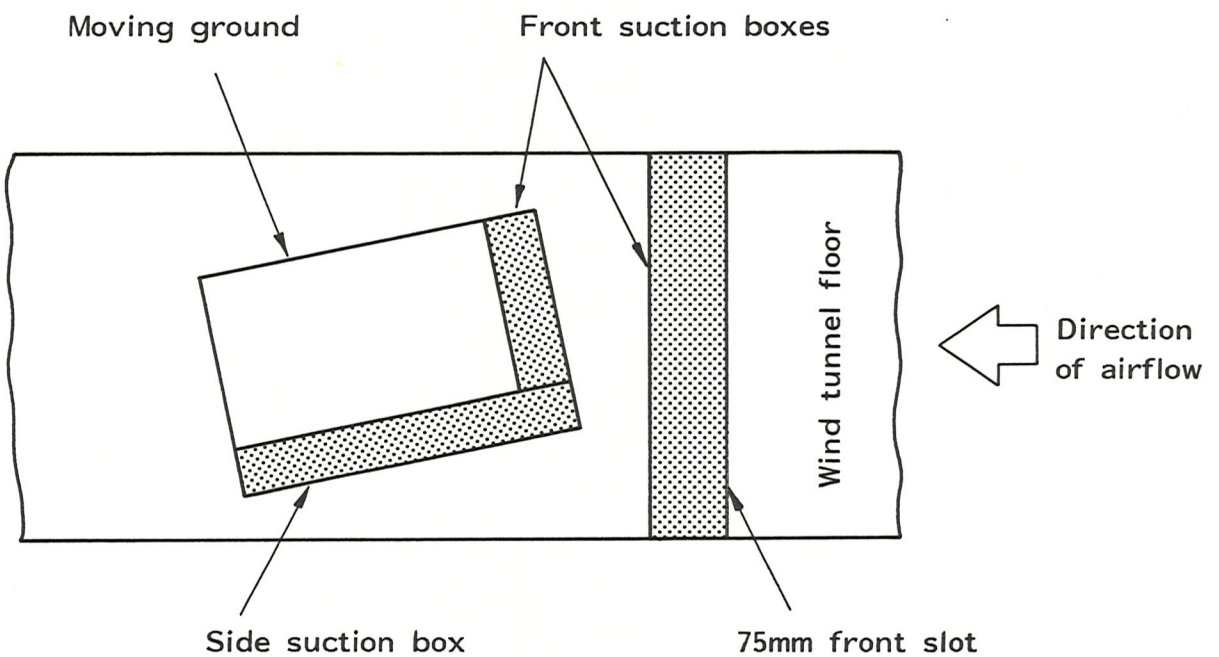

FIG. 4 SCHEMATIC PLAN VIEW OF YAWED MOVING GROUND PLANE.

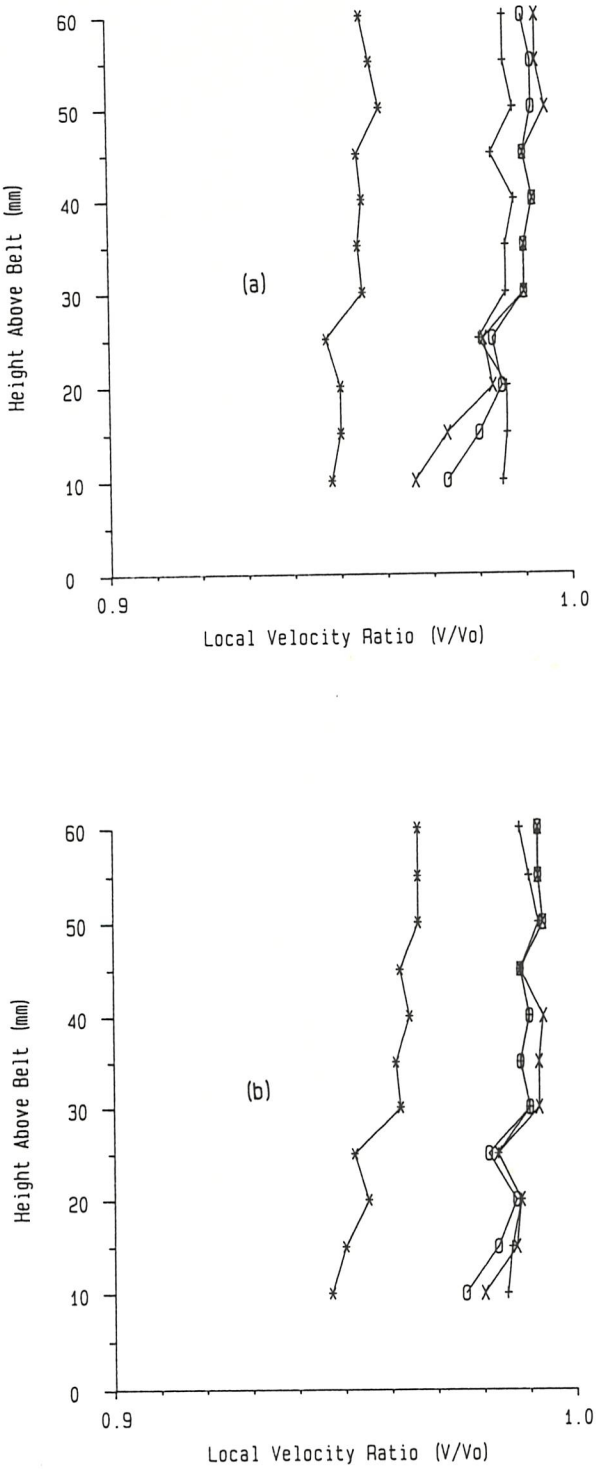

FIG. 5 VERTICAL VELOCITY PROFILES ABOVE YAWED 2.0m x 1.1m MOVING GROUND PLANE IN 3.5m x 2.6m WIND TUNNEL

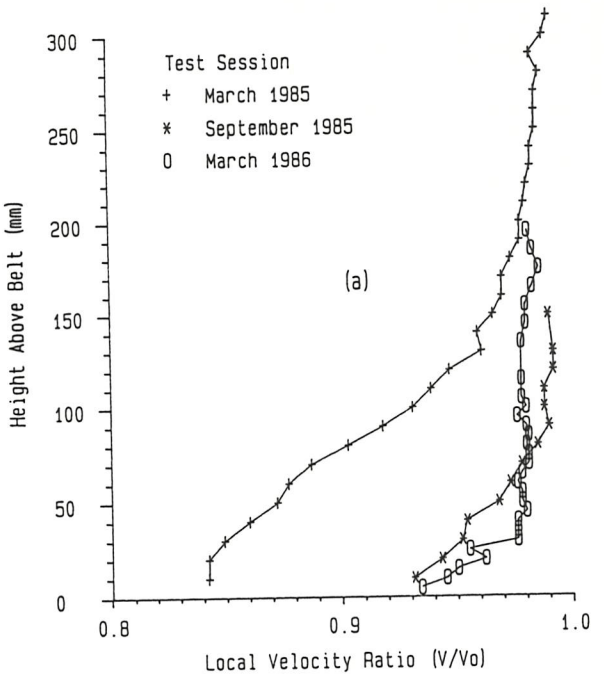

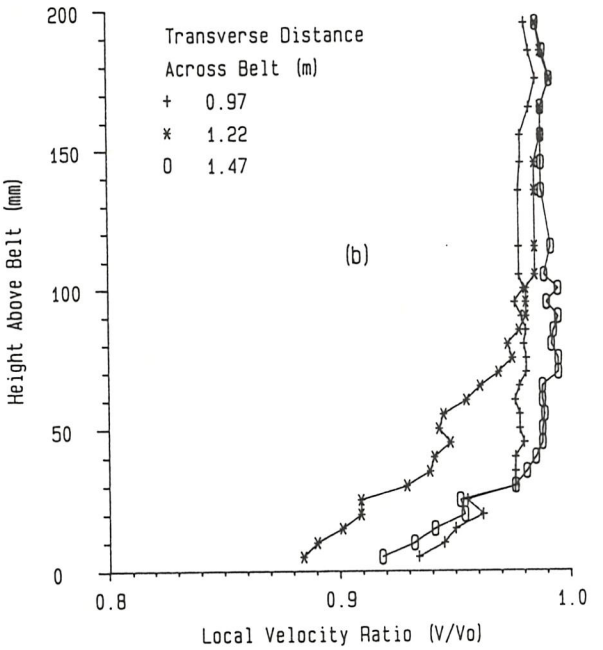

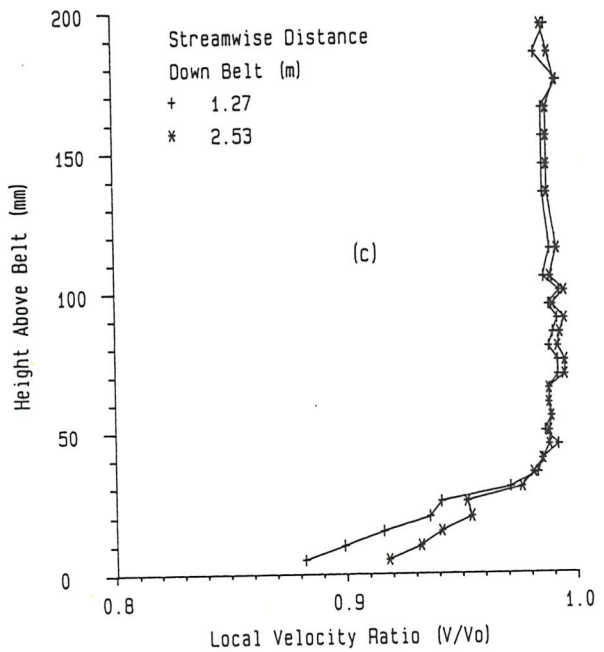

FIG. 6 VERTICAL VELOCITY PROFILES ABOVE 5.3m x 2.4m MOVING GROUND PLANE IN 3.5m x 2.6m WIND TUNNEL

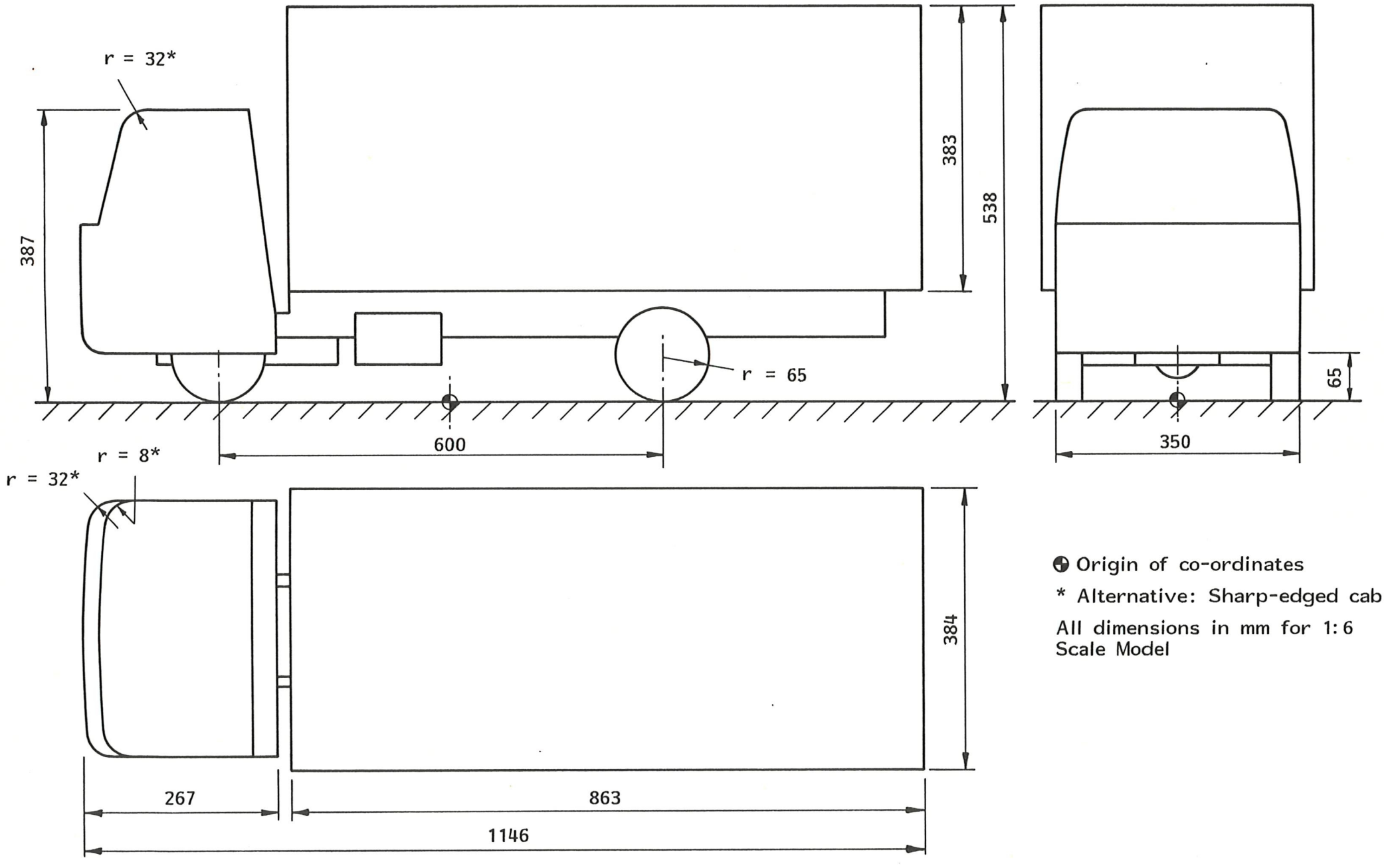

FIG. 7 PRINCIPLE DIMENSIONS OF 1:6 SCALE RIGID TRUCK MODEL

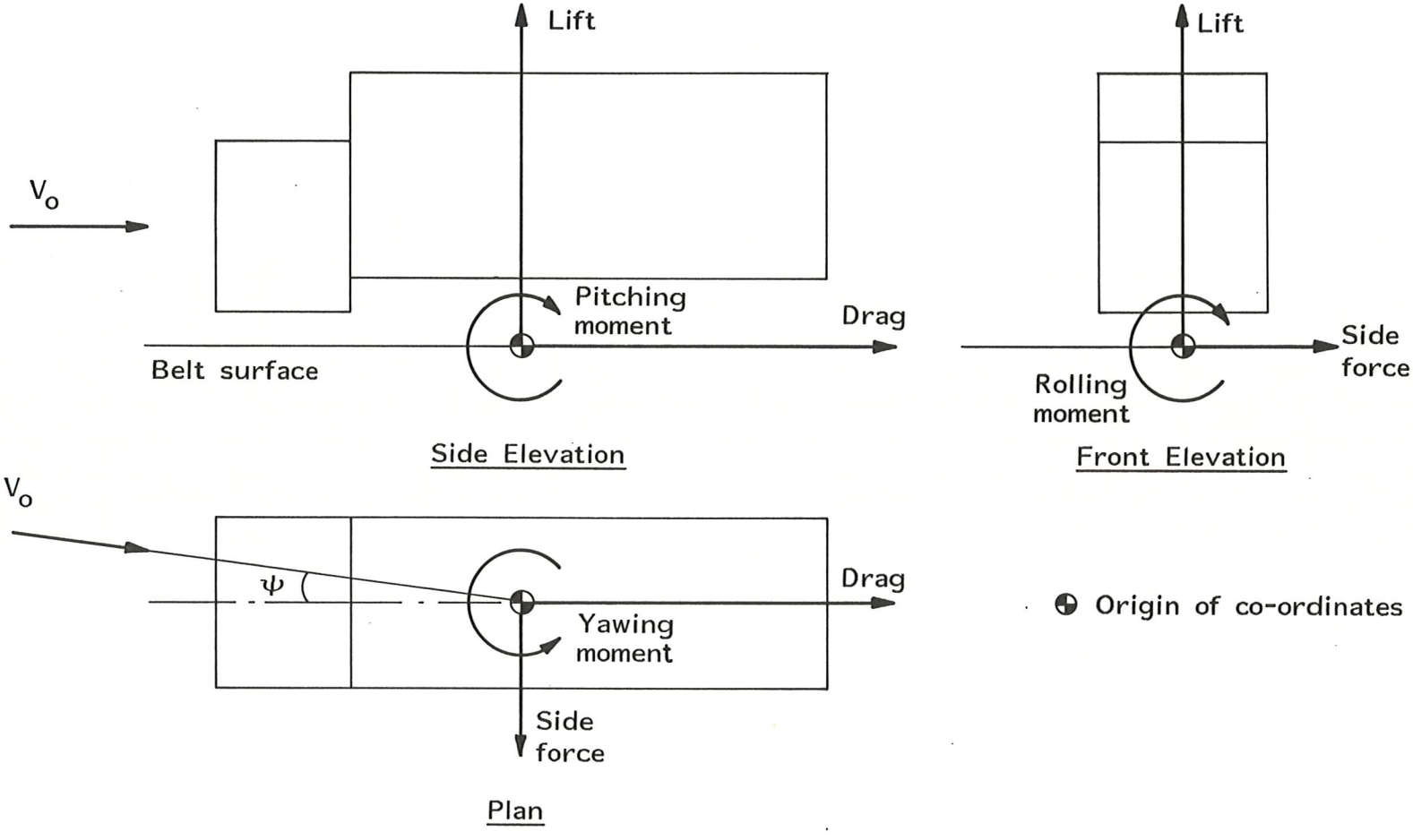

FIG. 8 BODY AXIS CO-ORDINATE SYSTEM

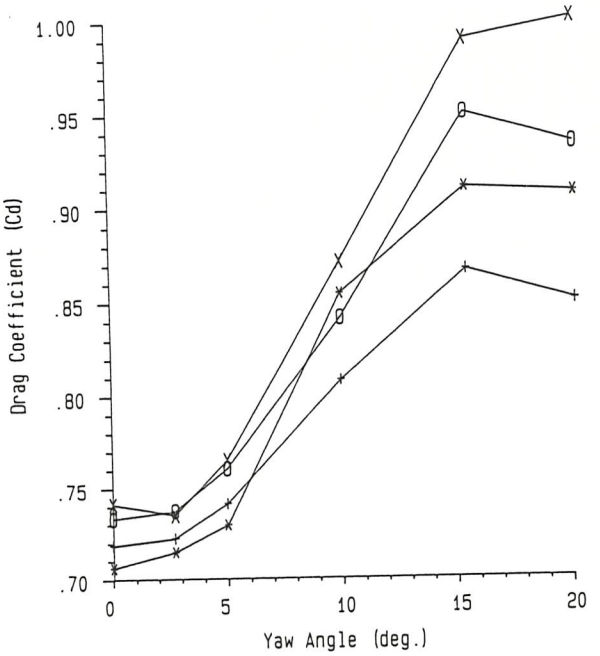

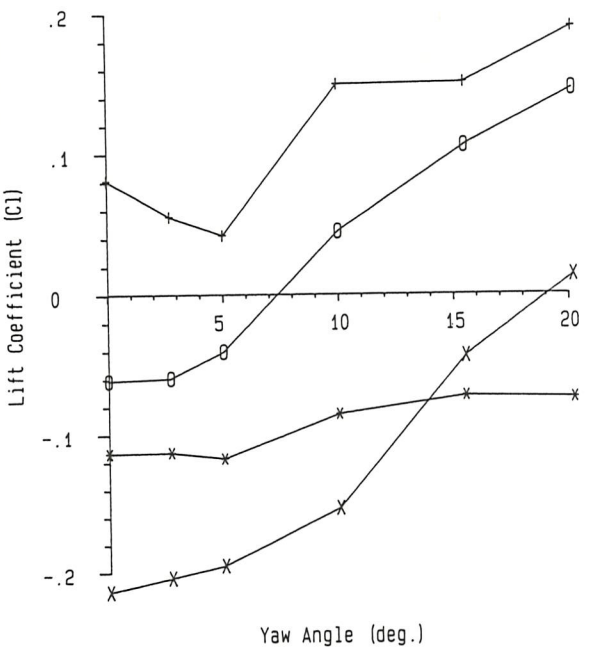

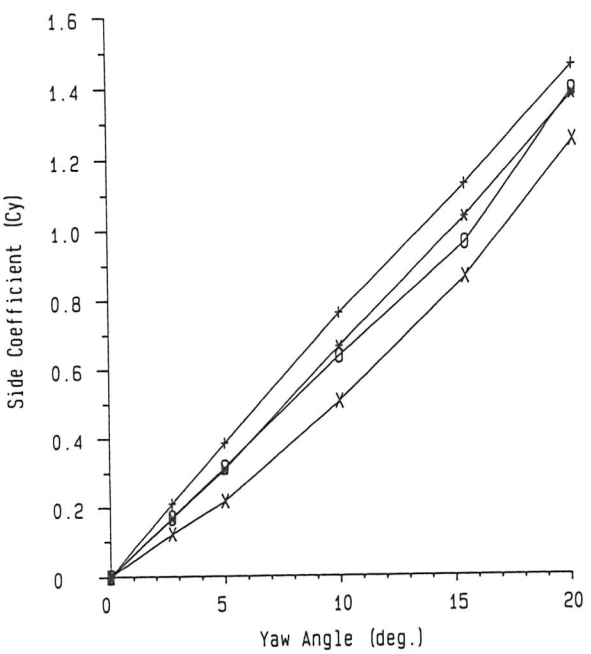

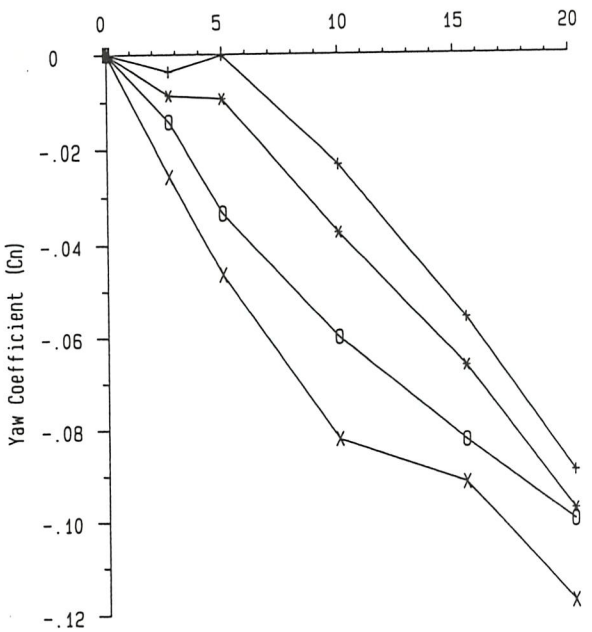

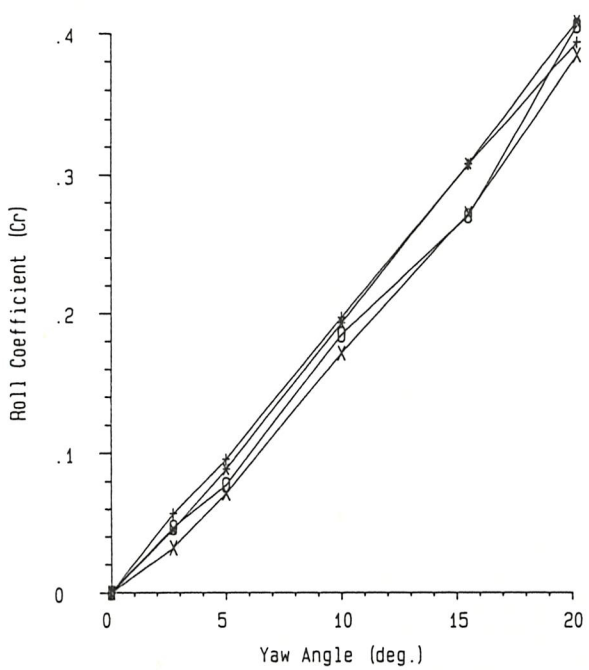

Cab Type
+ Round
* Round with Airdam
0 Square
X Square with Airdam

FIG. 9 EFFECT OF YAW ON 1:6 SCALE RIGID TRUCK MODEL IN 2.1m x 1.7m WIND TUNNEL

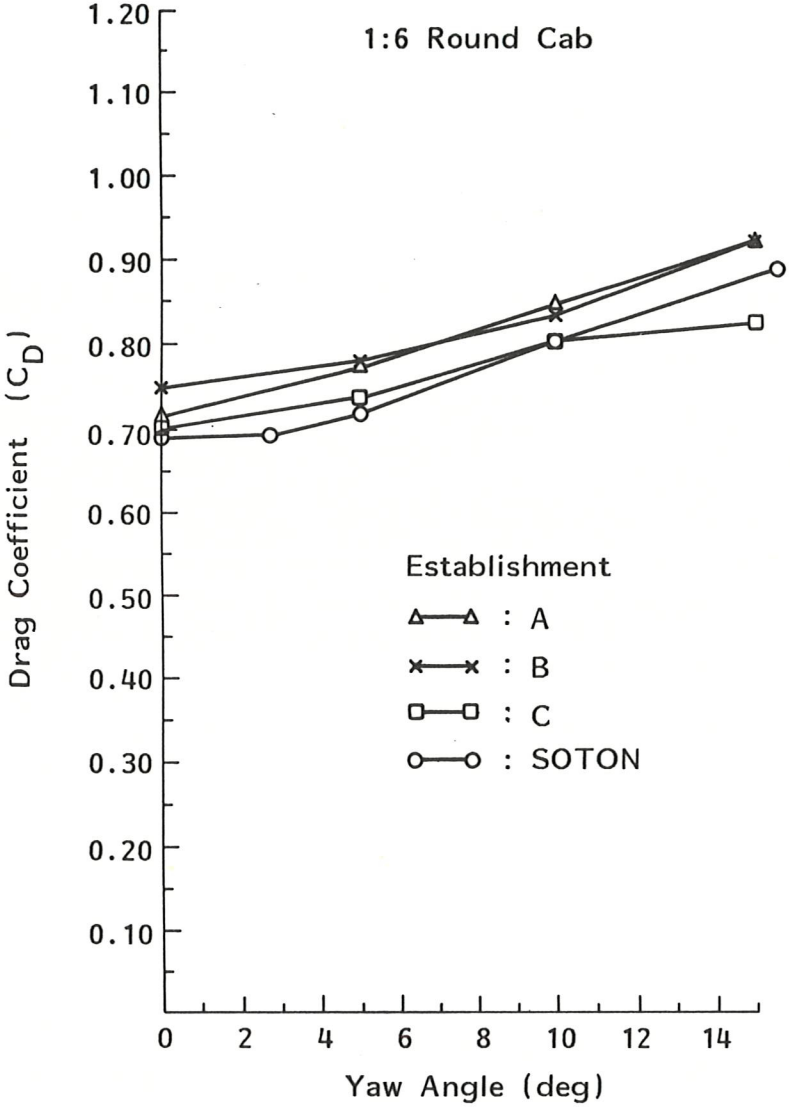

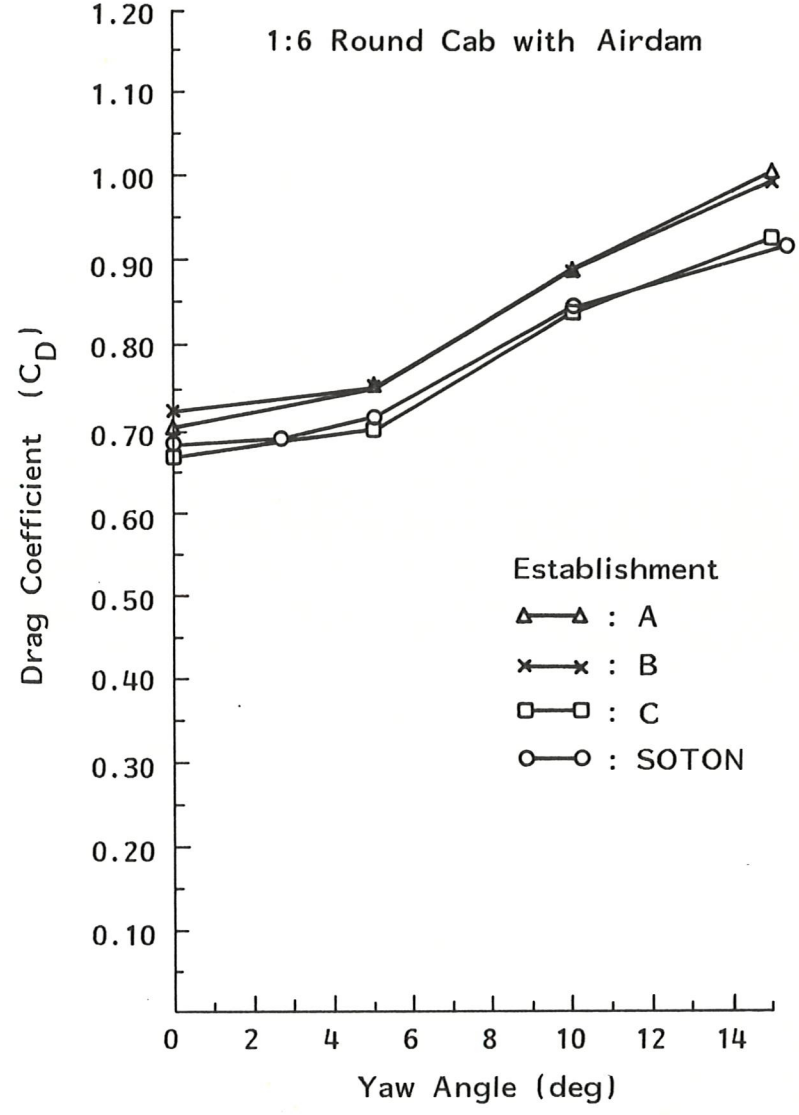

FIG. 10 DRAG COEFFICIENT VERSUS YAW ANGLE

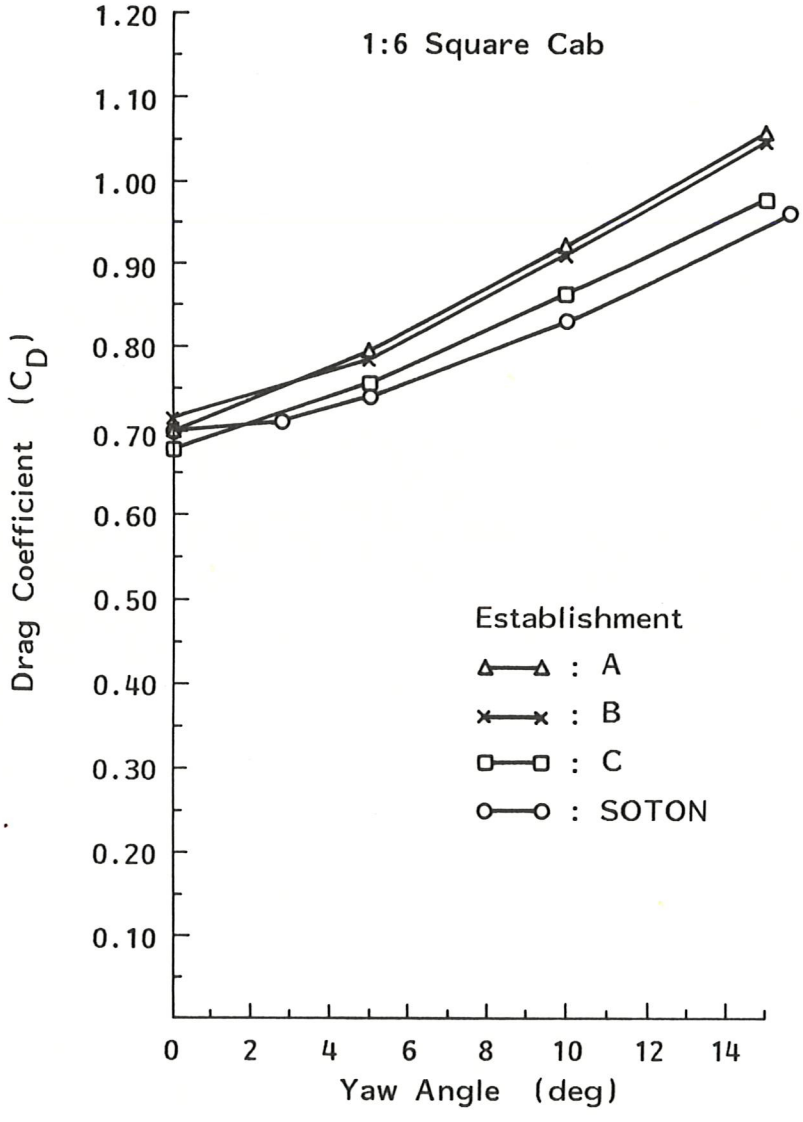

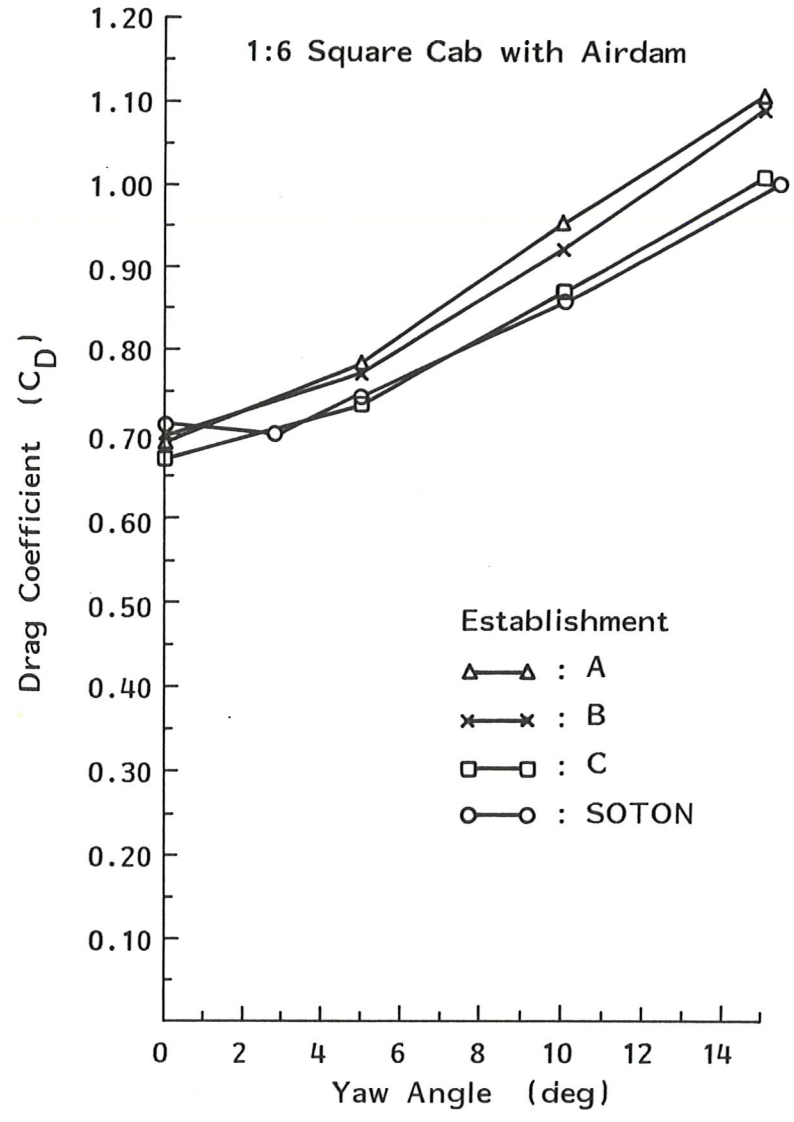

FIG. 11 DRAG COEFFICIENT VERSUS YAW ANGLE

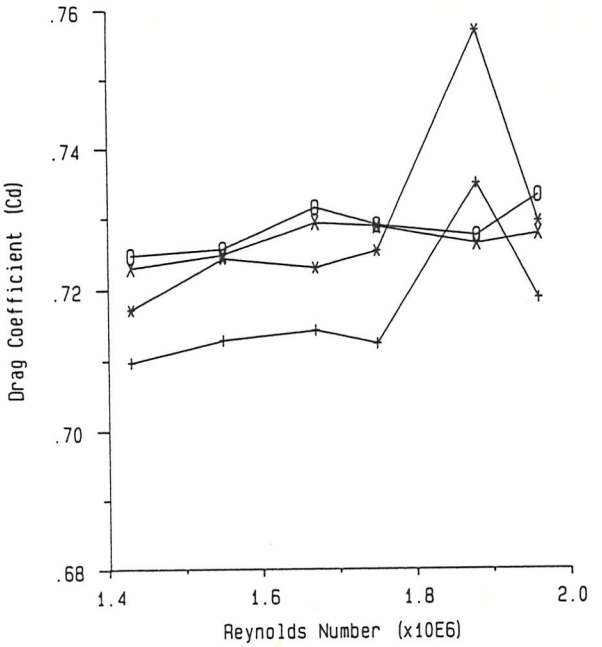

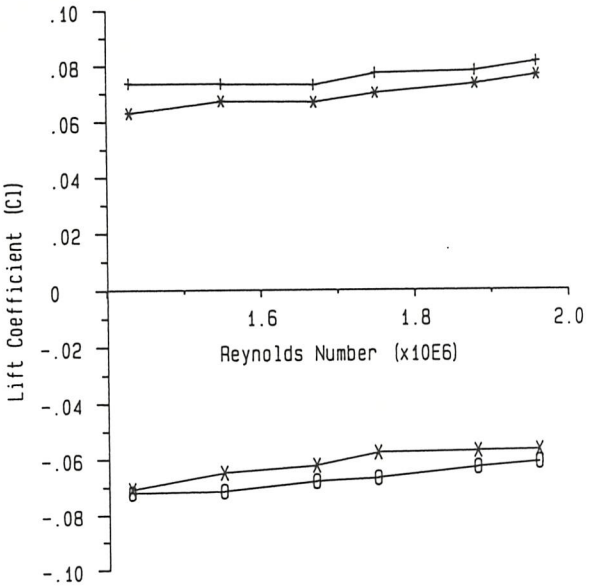

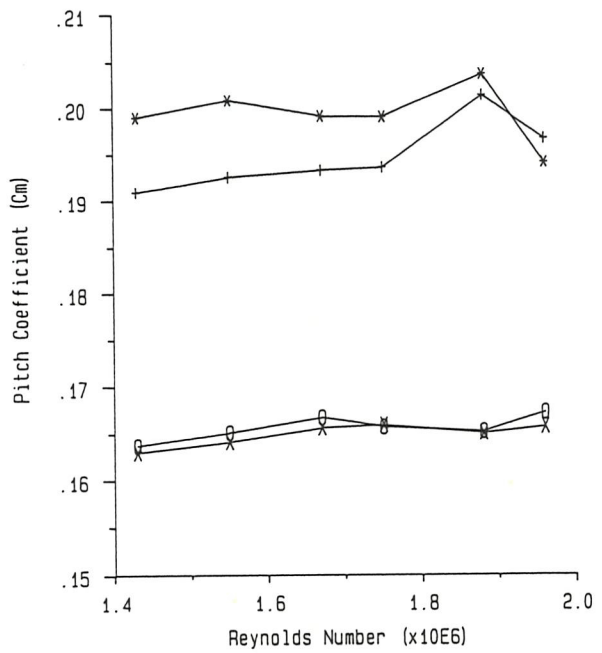

22 Gauge Wire Transition

\+ Transition Free, Round Cab

* Transition Fixed, Round Cab

0 Transition Free, Square Cab

X Transition Fixed, Square Cab

FIG. 12 EFFECT OF TRANSITION ON 1:6 SCALE RIGID TRUCK MODEL IN 2.1m x 1.7m WIND TUNNEL

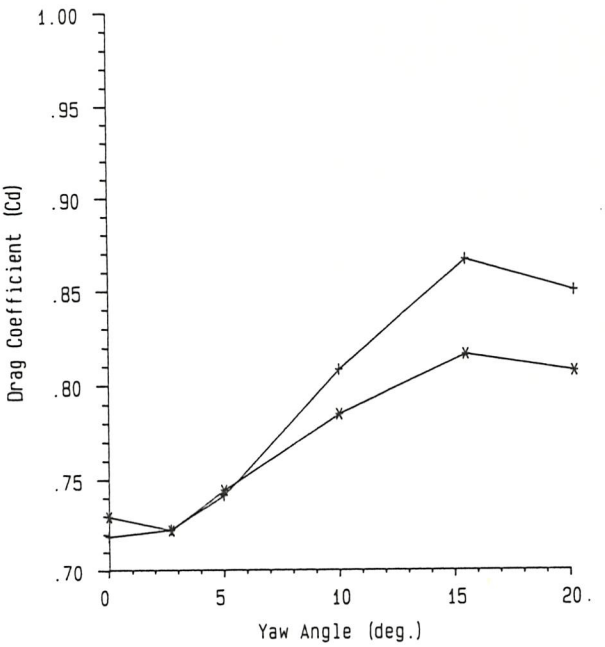

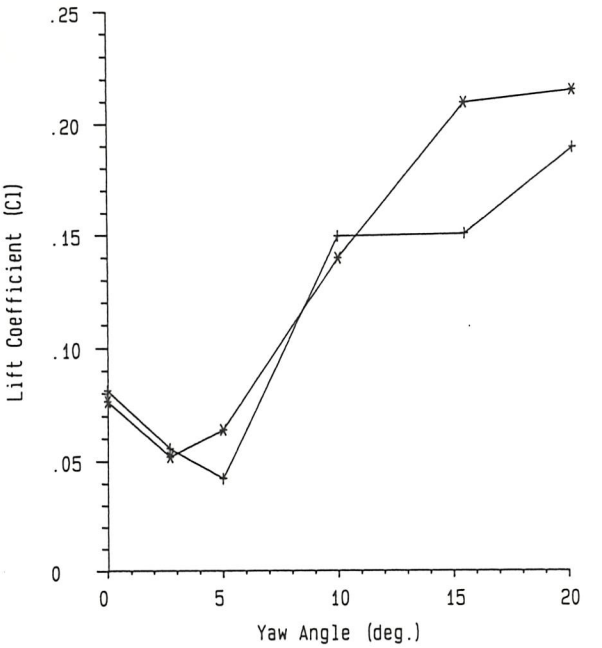

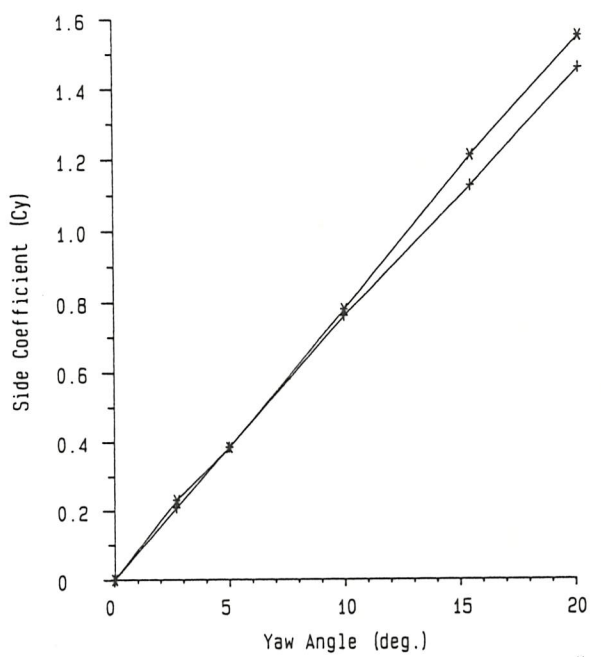

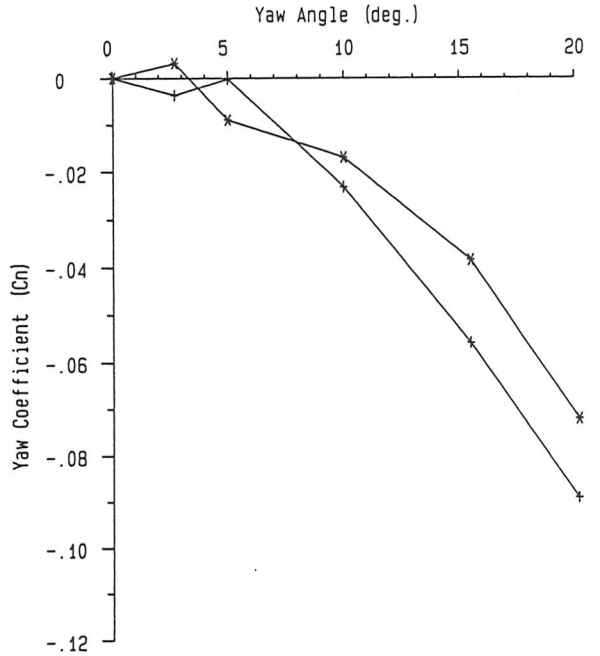

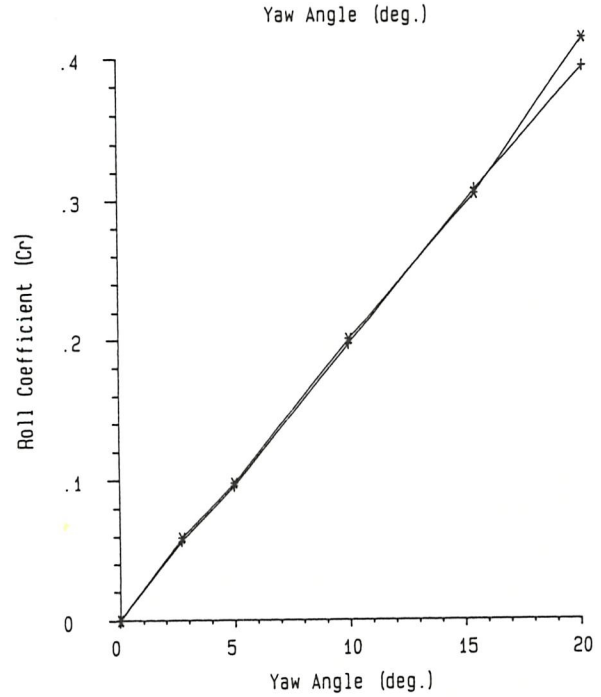

22 Gauge Wire Transition, Round Cab
\+ Transition Free
* Transition Fixed

FIG.13 EFFECT OF TRANSITION AT YAW ON 1:6 SCALE RIGID TRUCK MODEL IN 2.1m x 1.7m WIND TUNNEL

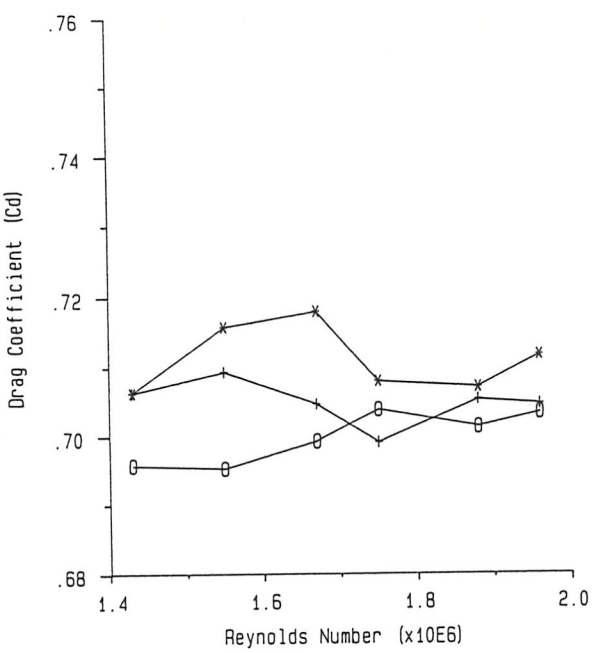

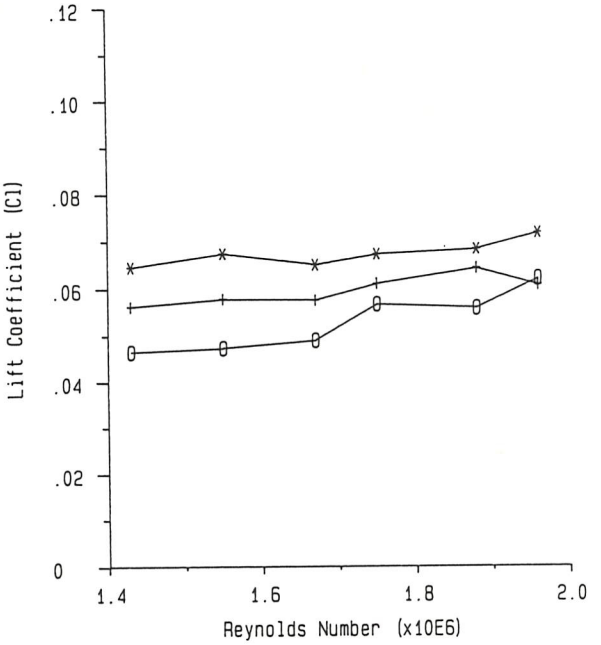

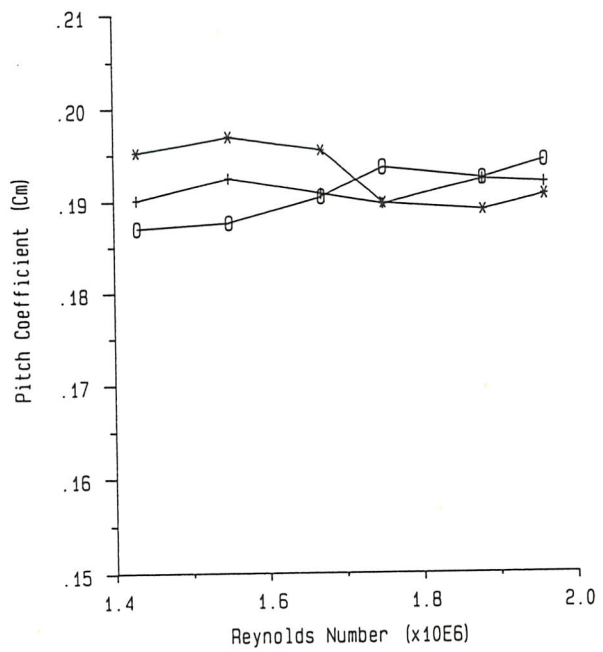

Round Cab

\+ Transition Free

* Transition Fixed, 18 Gauge Wire

0 Transition Fixed, 60 Carborundum

FIG. 14 EFFECT OF TRANSITION ON 1:6 SCALE RIGID TRUCK MODEL IN 2.1m x 1.7m WIND TUNNEL

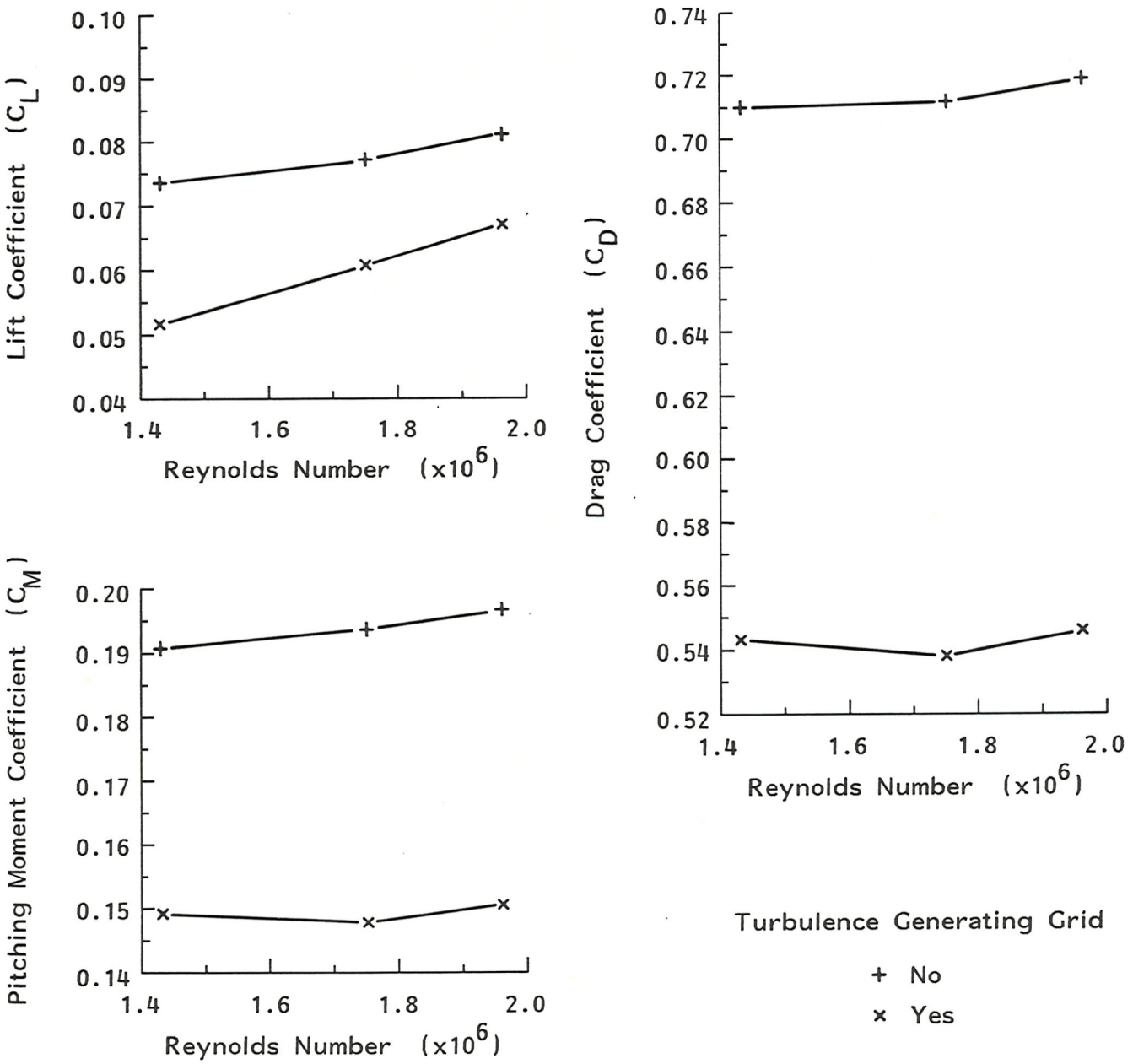

FIG. 15 EFFECT OF TURBULENCE GENERATING GRID FOR 1:6 RIGID TRUCK MODEL WITH ROUND CAB IN 2.1m x 1.7m WIND TUNNEL

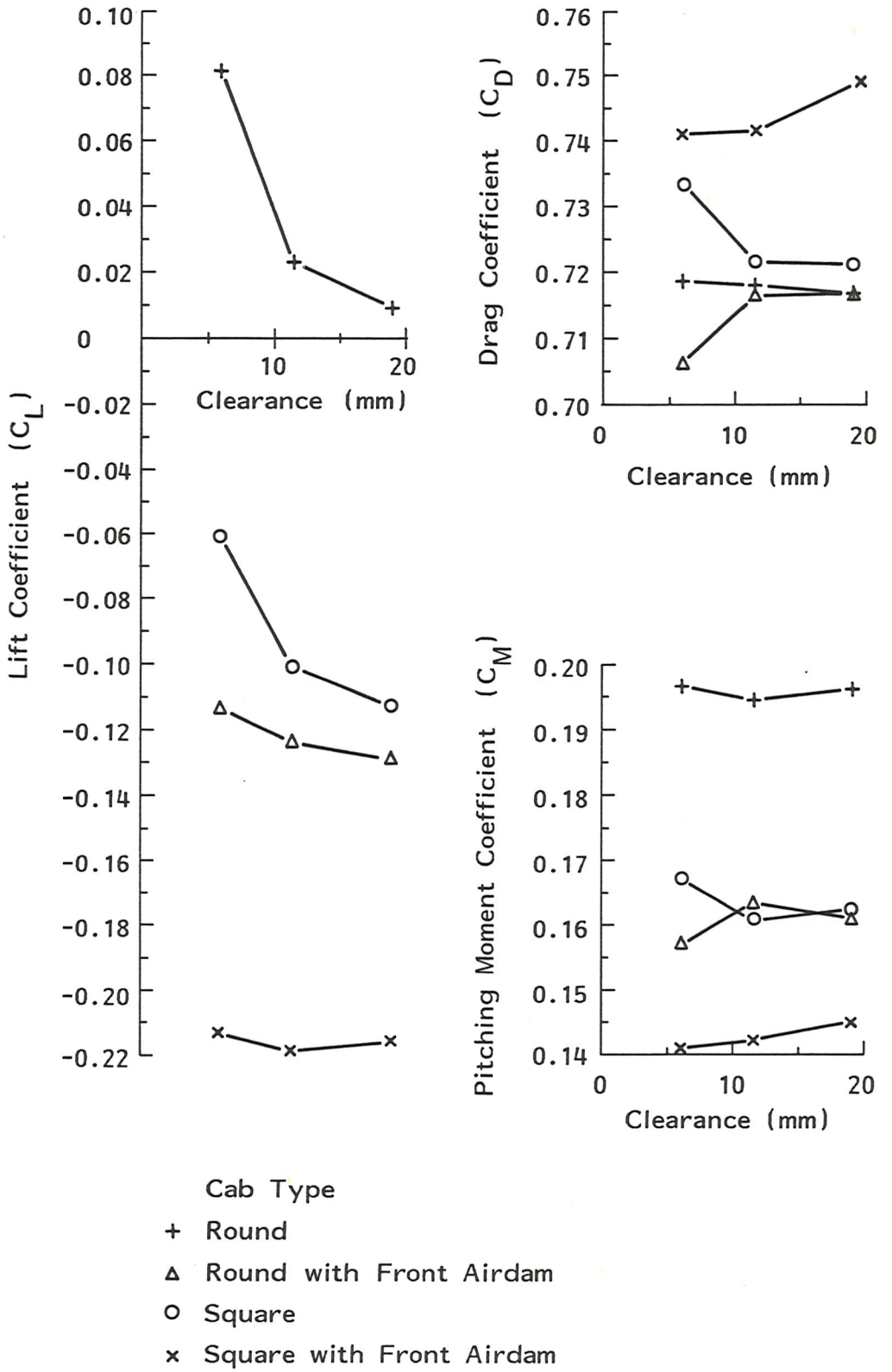

FIG. 16 EFFECT OF CLEARANCE UNDER WHEEL-FLATS FOR 1:6 RIGID TRUCK MODEL IN 2.1m x 1.7m WIND TUNNEL

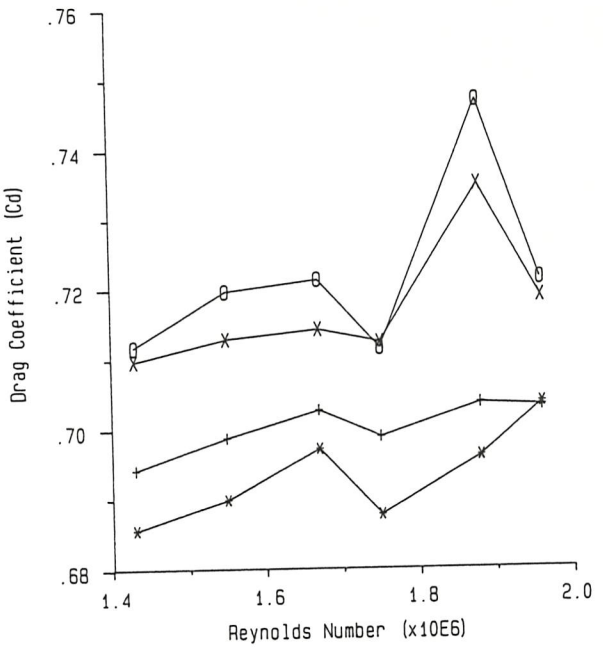

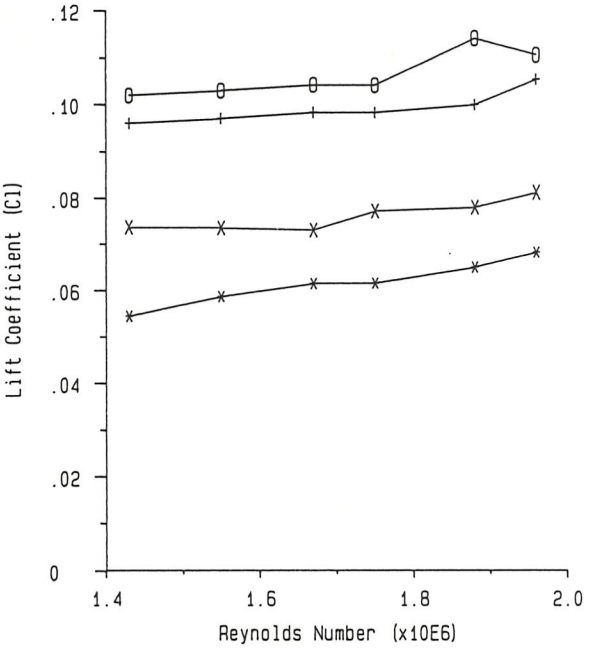

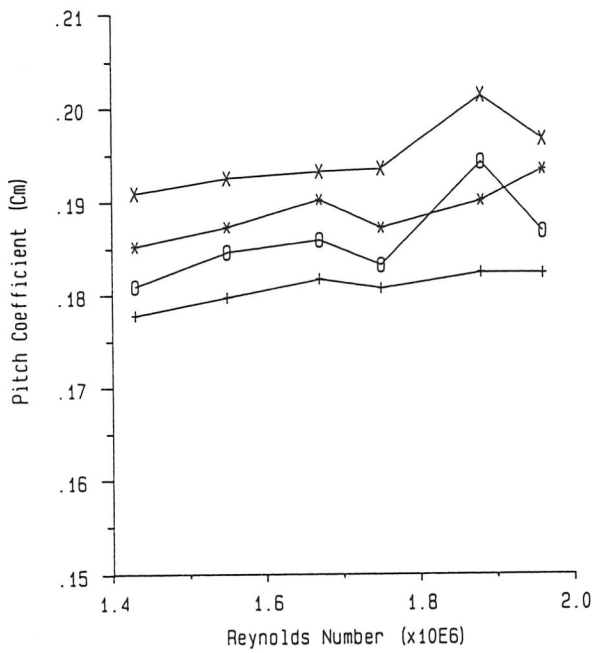

Round Cab

\+ L.E.Suction Off & Belt Stopped

* L.E.Suction Off & Belt Moving

0 L.E.Suction On & Belt Stopped

X L.E.Suction On & Belt Moving

FIG.17 EFFECT OF GROUND PLANE ON 1:6 SCALE RIGID TRUCK MODEL IN 2.1m x 1.7m WIND TUNNEL

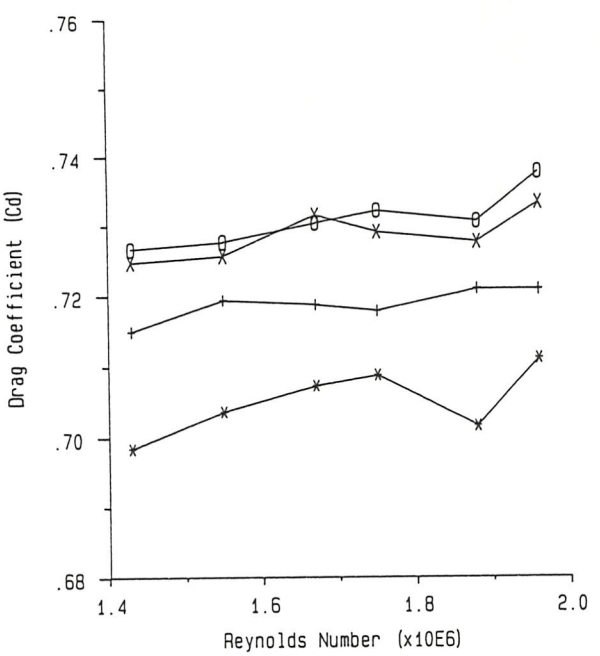

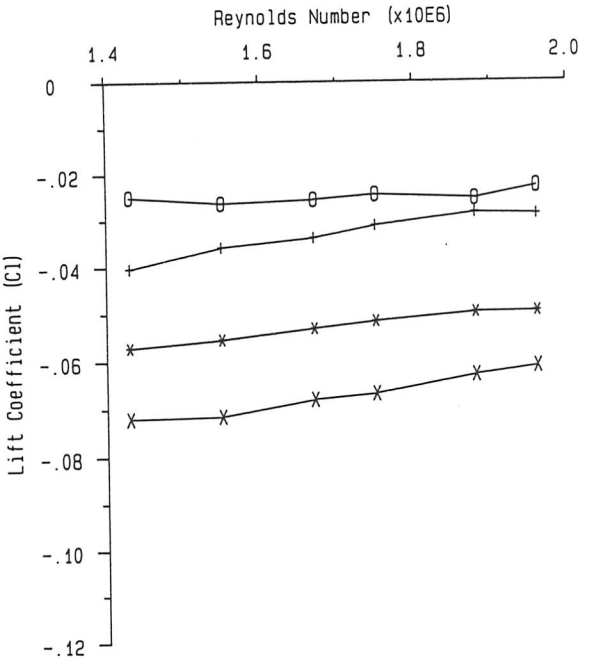

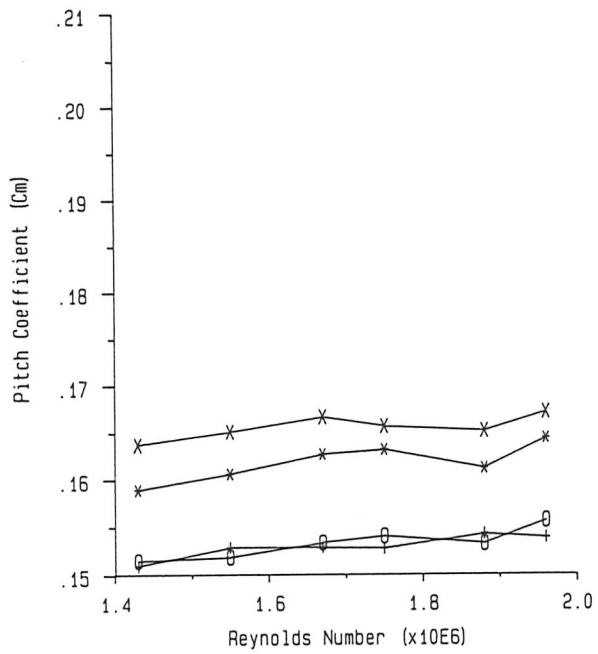

Square Cab

\+ L.E.Suction Off & Belt Stopped

* L.E.Suction Off & Belt Moving

0 L.E.Suction On & Belt Stopped

X L.E.Suction On & Belt Moving

FIG. 18 EFFECT OF GROUND PLANE ON 1:6 SCALE RIGID TRUCK MODEL IN 2.1m x 1.7m WIND TUNNEL

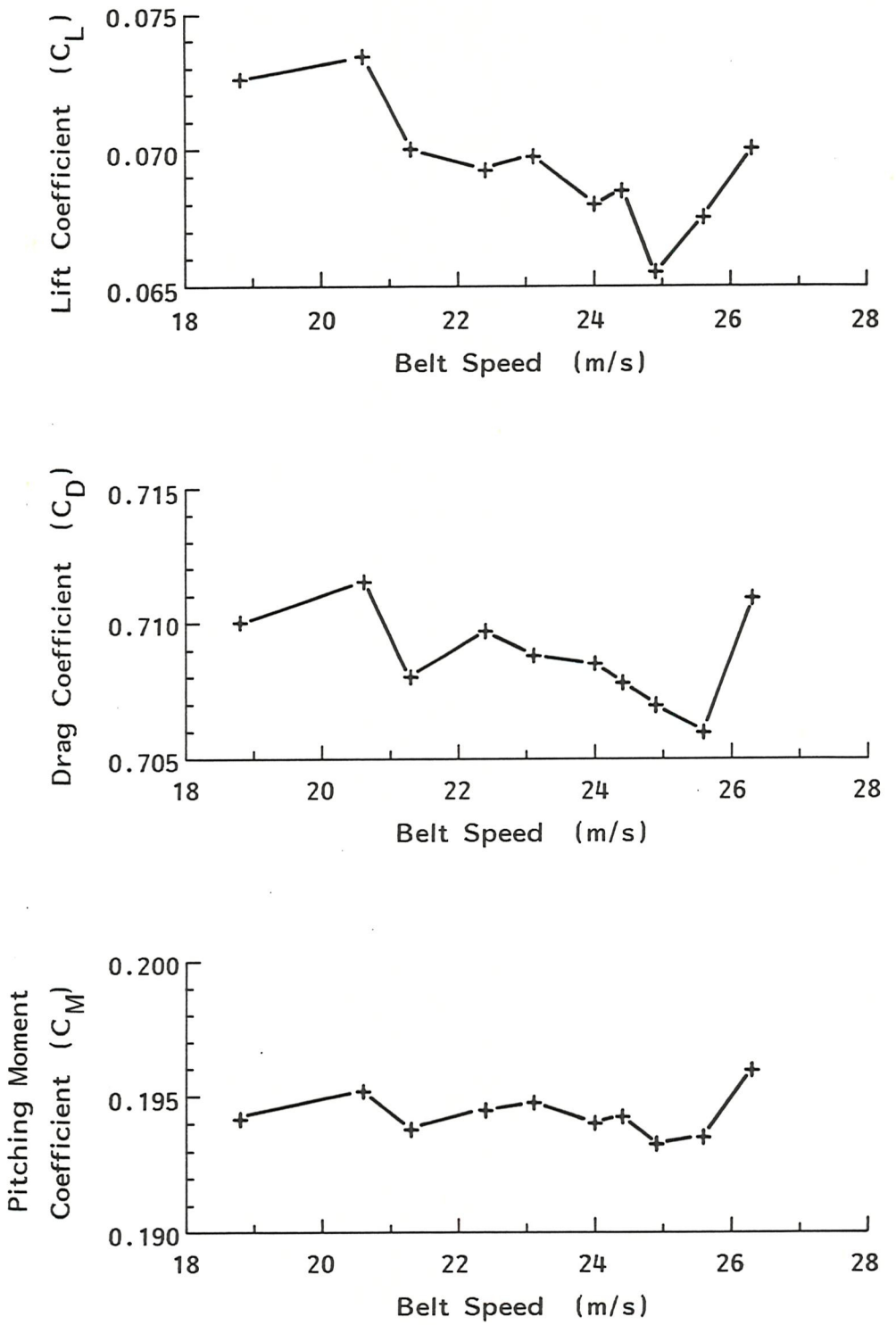

FIG. 19 EFFECT OF BELT SPEED FOR 1:6 RIGID TRUCK MODEL WITH ROUND CAB IN 2.1m x 1.7m WIND TUNNEL

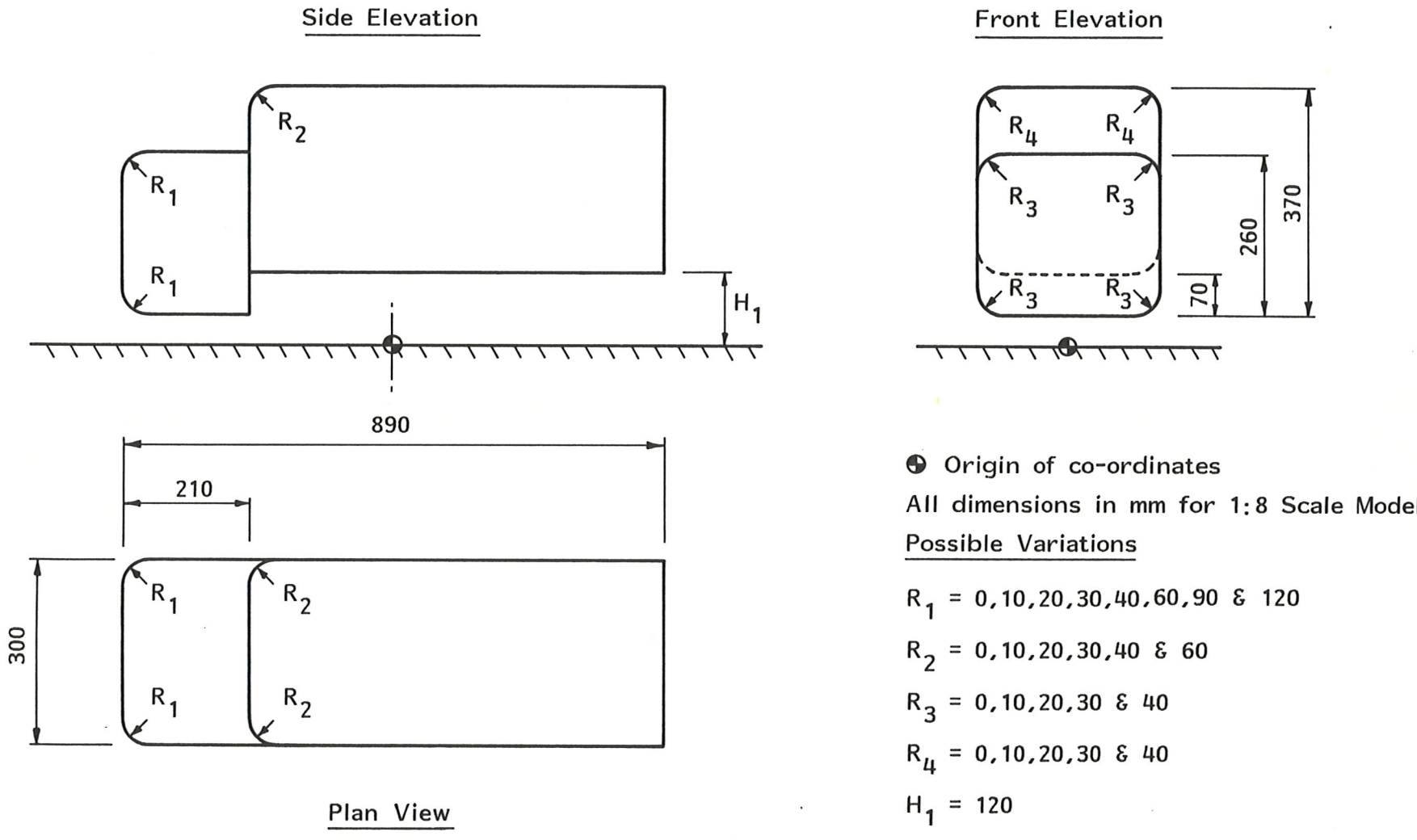

FIG. 20 PRINCIPLE DIMENSIONS AND VARIATIONS OF 1:8 SCALE IDEALIZED RIGID TRUCK MODEL

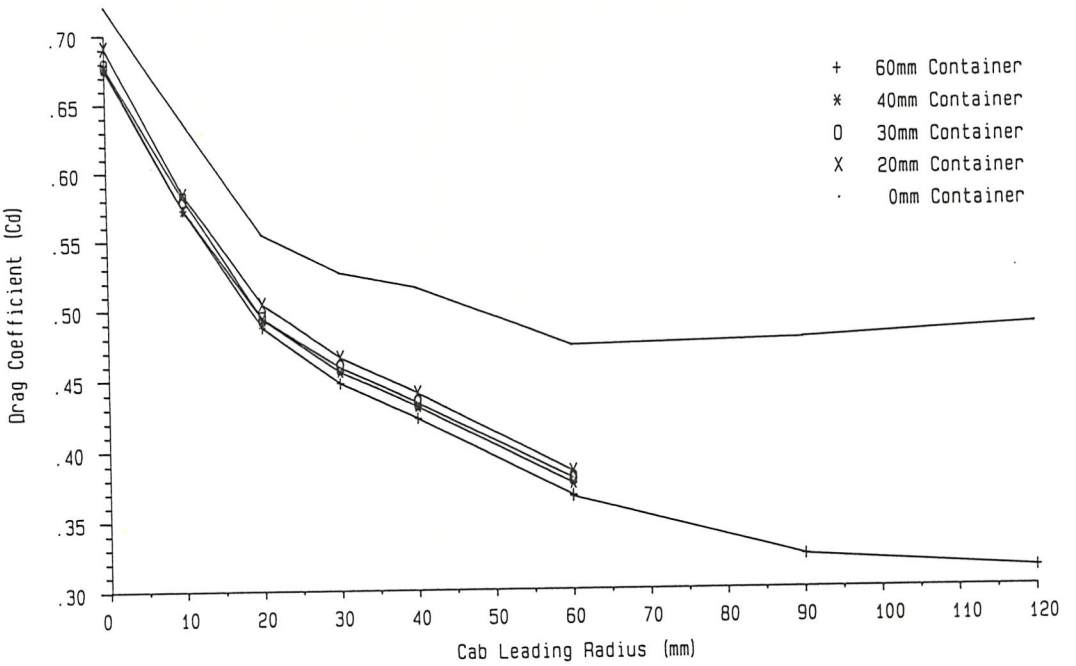

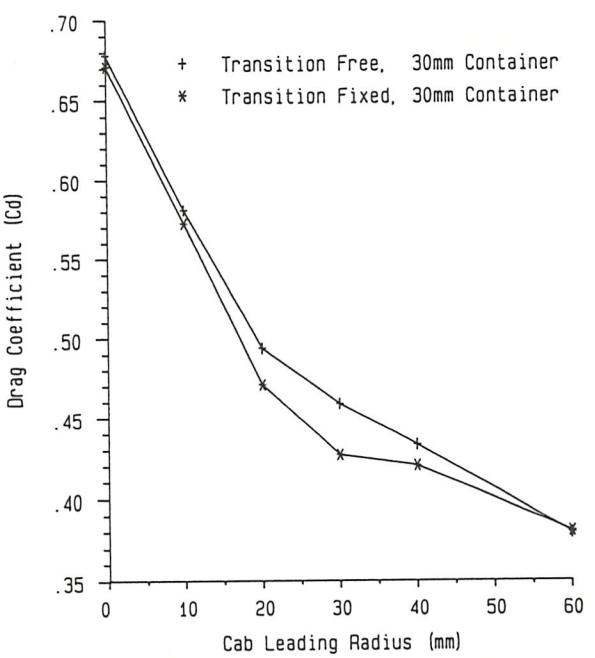

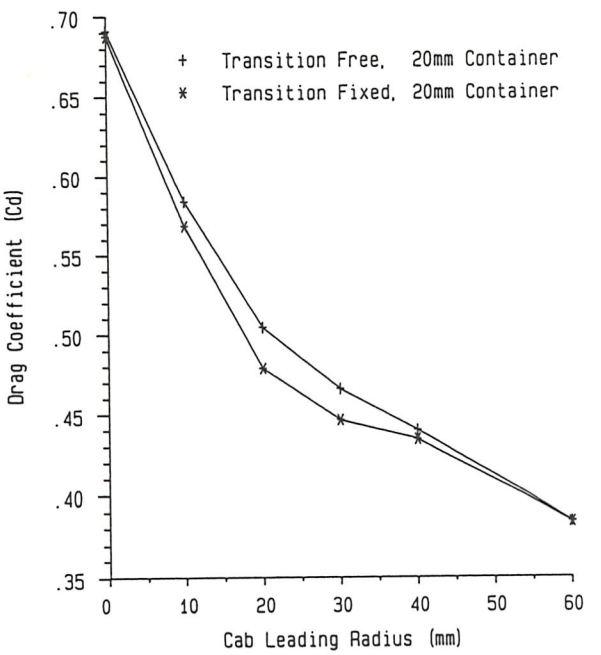

FIG. 21 DRAG RESULTS FOR 1:8 SCALE IDEALIZED RIGID TRUCK MODEL IN 2.1m x 1.7m WIND TUNNEL

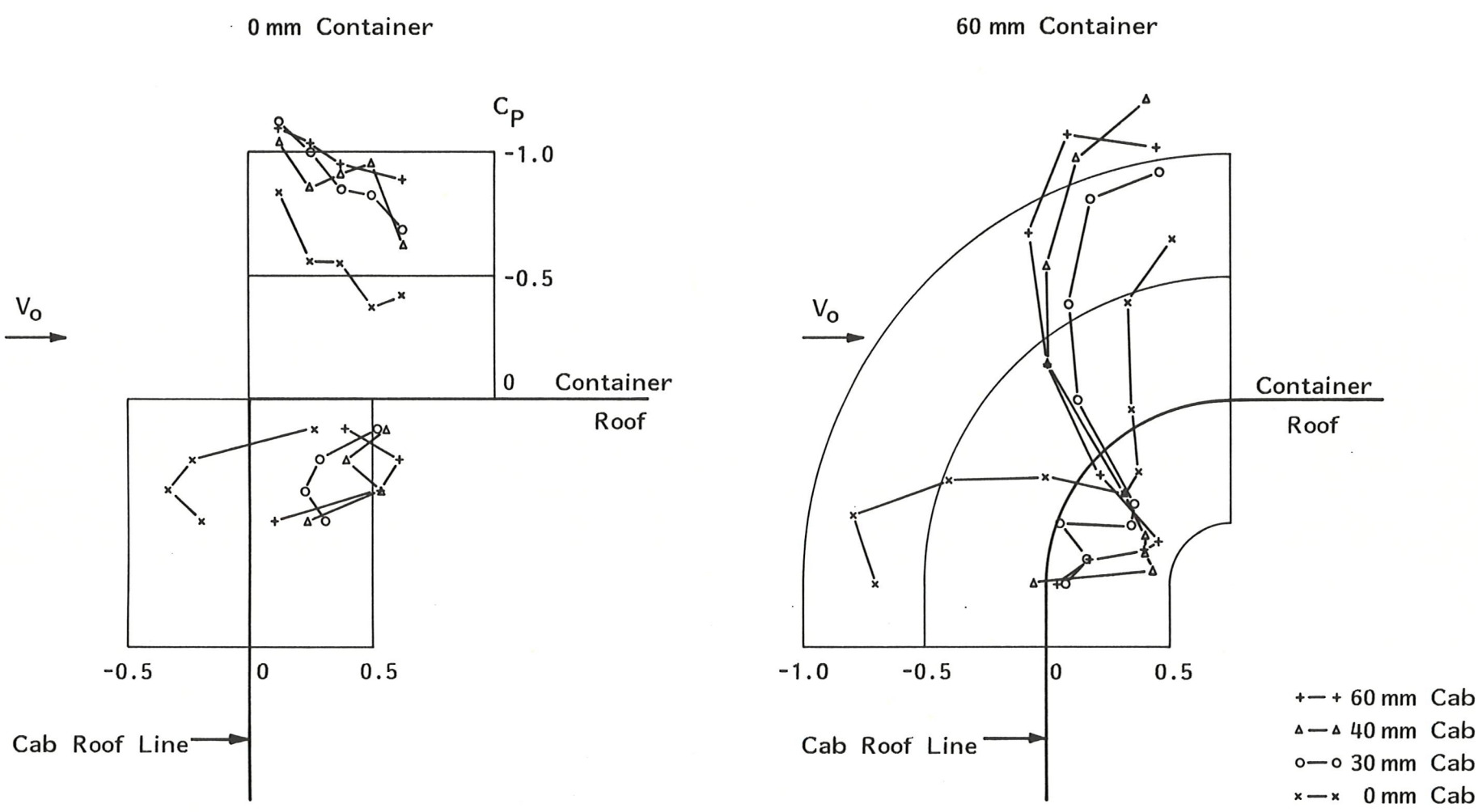

FIG. 22 SURFACE PRESSURE DISTRIBUTION AROUND CONTAINER LEADING EDGE

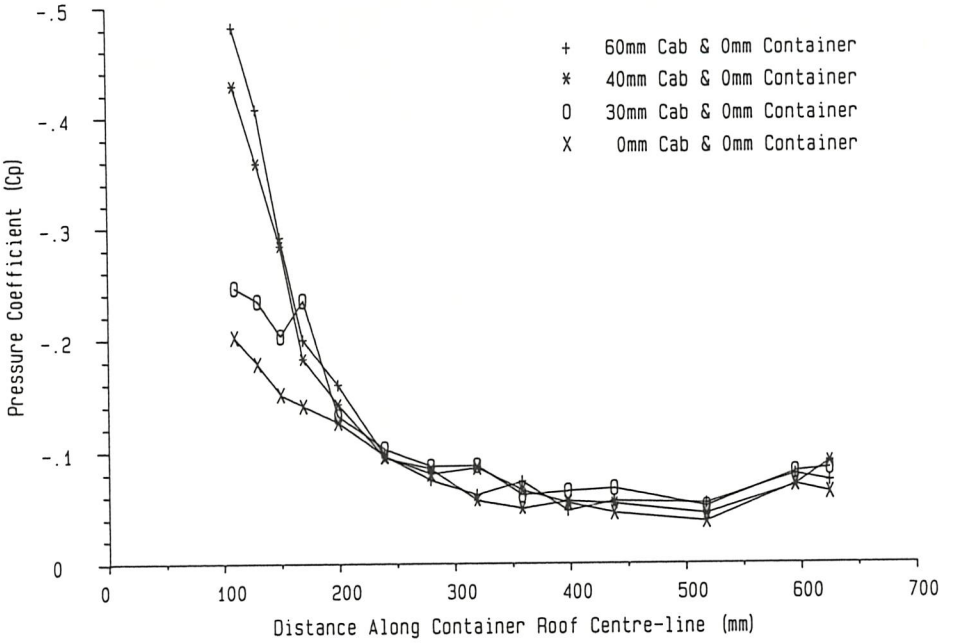

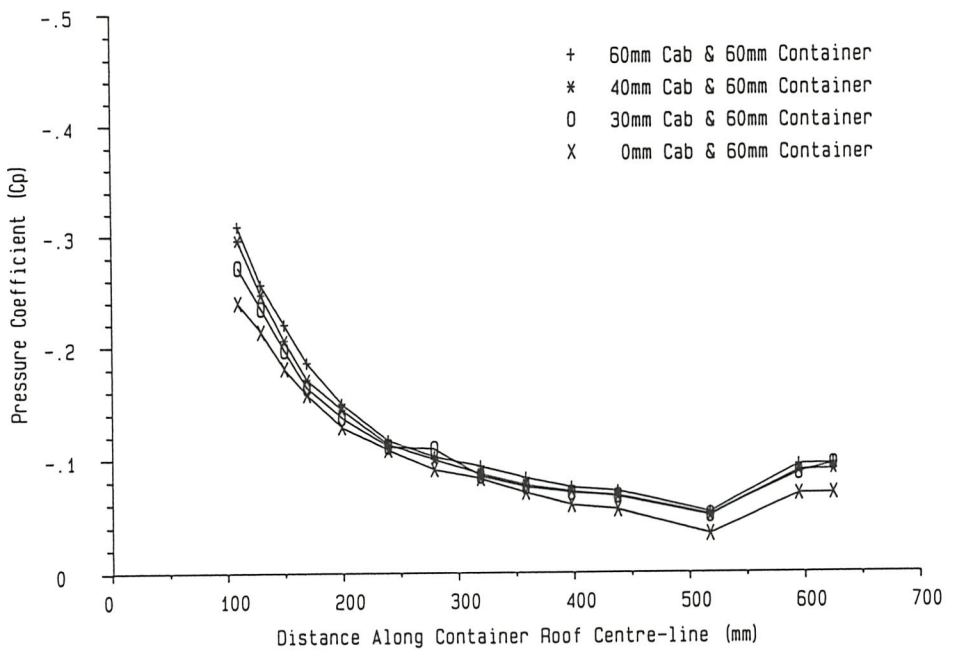

FIG. 23 CONTAINER UPPER SURFACE PRESSURE DISTRIBUTION ON 1:8 SCALE IDEALIZED RIGID TRUCK MODEL IN 2.1m x 1.7m WIND TUNNEL

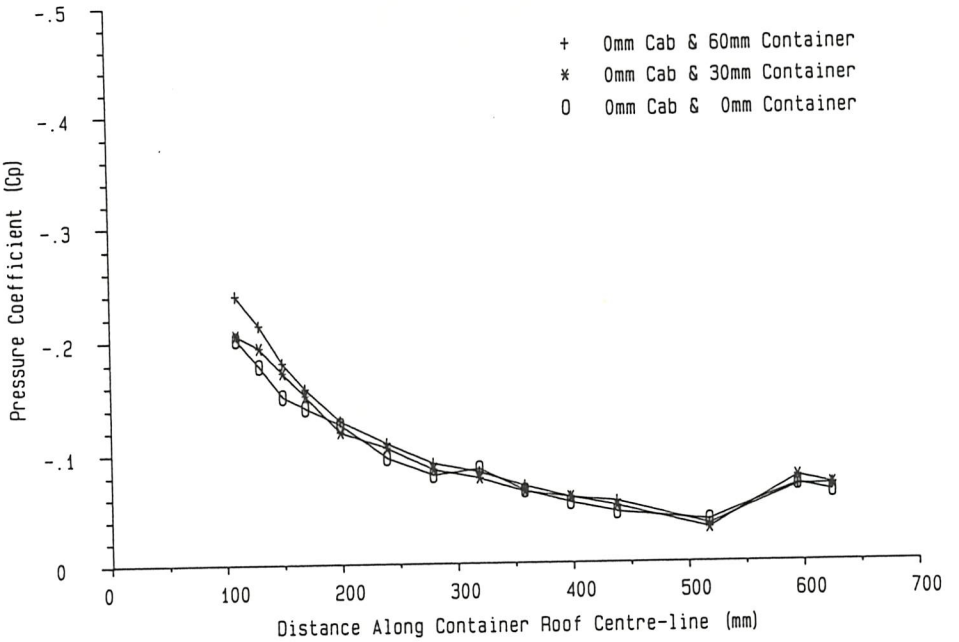

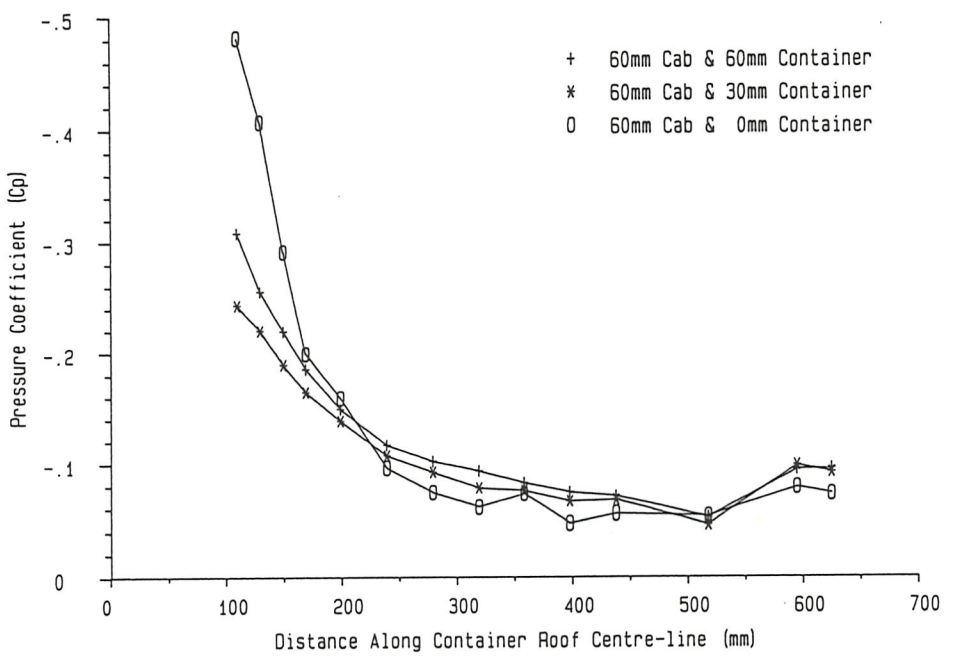

FIG. 24 CONTAINER UPPER SURFACE PRESSURE DISTRIBUTION ON 1:8 SCALE IDEALIZED RIGID TRUCK MODEL IN 2.1m x 1.7m WIND TUNNEL

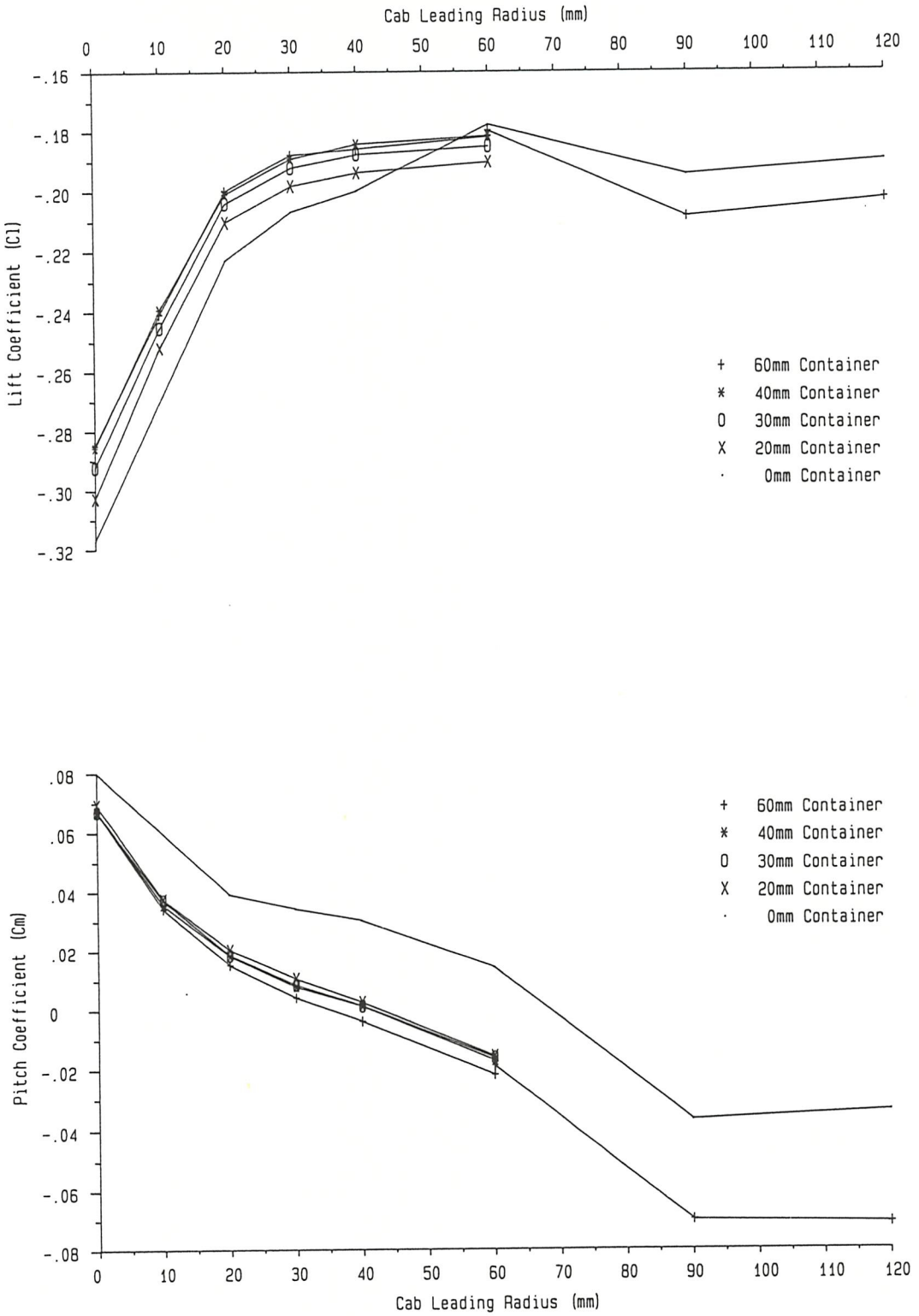

FIG. 25 LIFT AND PITCH RESULTS FOR 1:8 SCALE IDEALIZED RIGID TRUCK MODEL IN 2.1m x 1.7m WIND TUNNEL

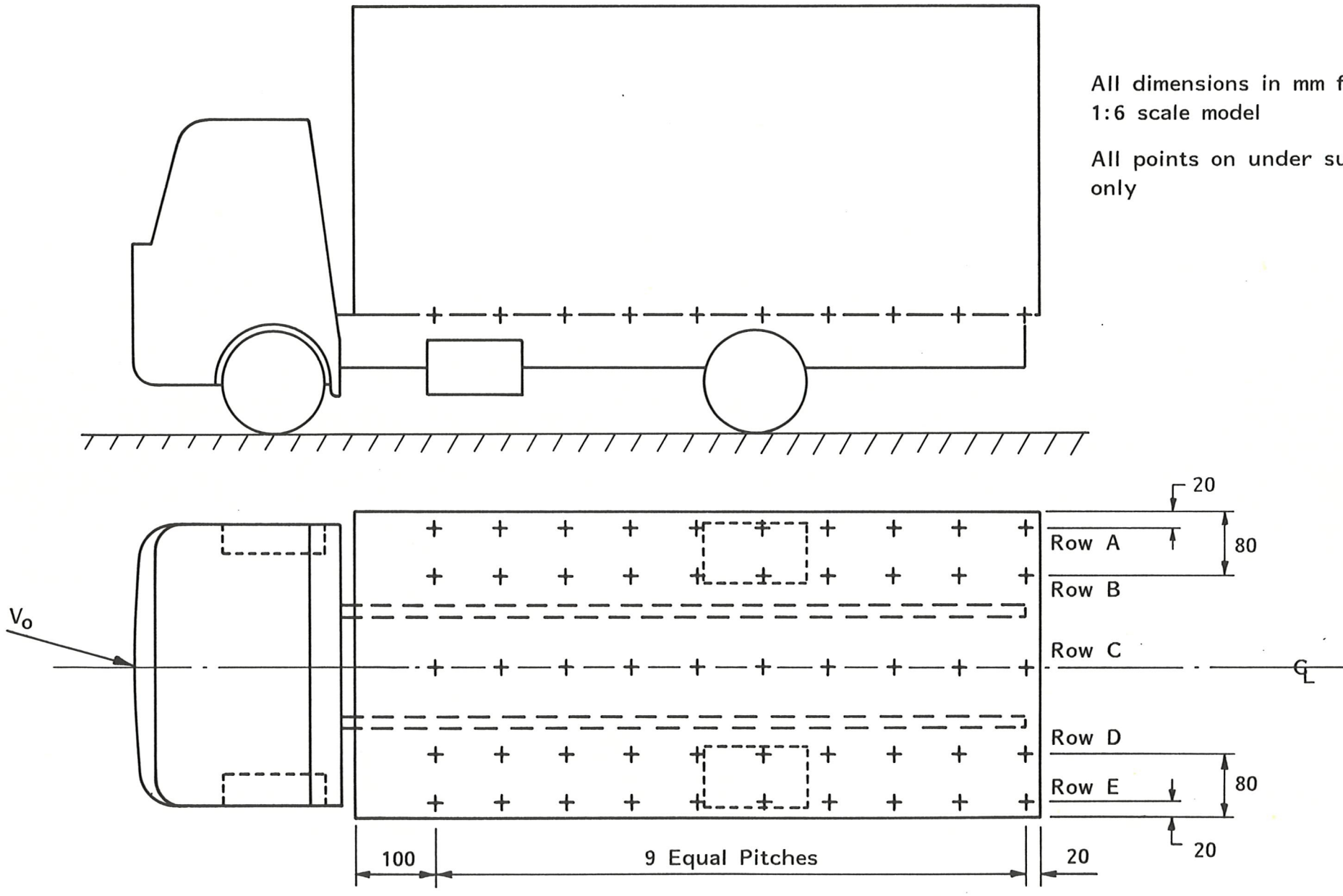

FIG. 26 PRESSURE PLOTTING DETAILS FOR 1:6 SCALE RIGID TRUCK MODEL

FIG.27

THE EFFECT OF WHEEL ROTATION ON CONTAINER LOWER SURFACE PRESSURE DISTRIBUTION
IN 3.5m x 2.6m WIND TUNNEL, MAY 85

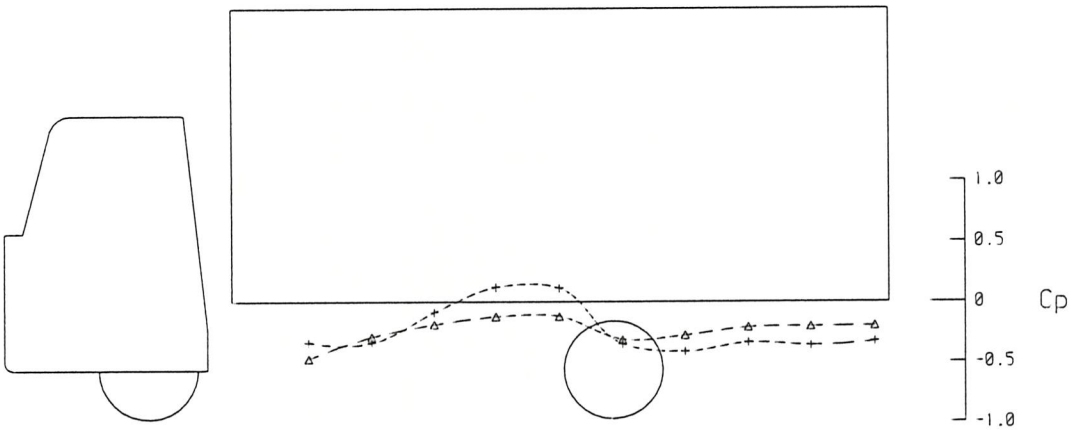

Loop A

Δ = Basic, Rotating wheels on non-yawed belt (model=0, MG=0)

\+ = Basic, Rotating wheels on yawed belt (model=15, MG=15)

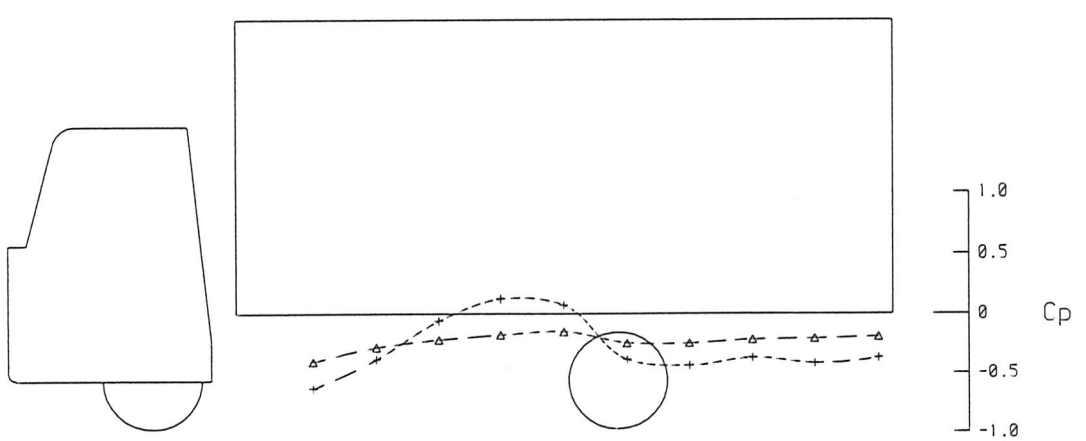

Loop A

Δ = Basic with airdam, Rotating wheels on non-yawed belt (model=0, MG=0)

\+ = Basic with airdam, Rotating wheels on yawed belt (model=15, MG=15)

FIG.28

THE EFFECT OF WHEEL ROTATION ON CONTAINER LOWER SURFACE PRESSURE DISTRIBUTION
IN 3.5m x 2.6m WIND TUNNEL, MAY 85

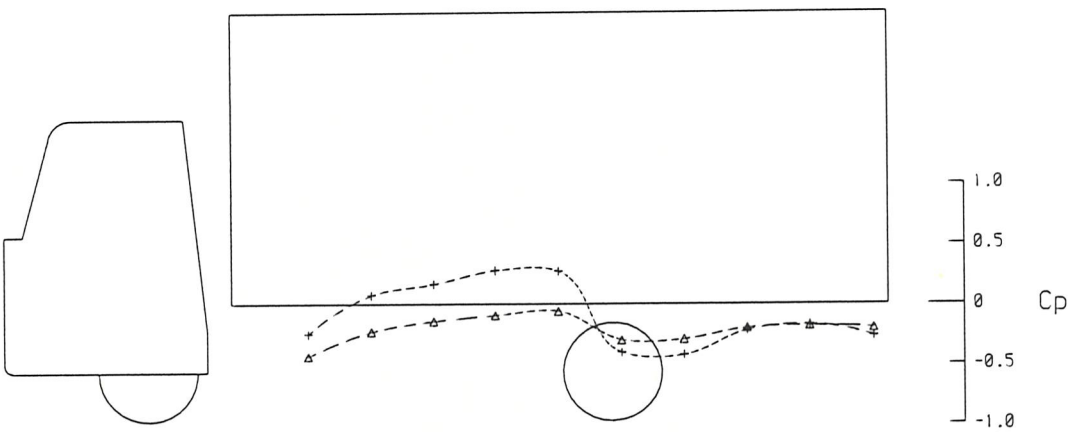

Loop B

Δ = Basic, Rotating wheels on non-yawed belt (model=0, MG=0)

\+ = Basic, Rotating wheels on yawed belt (model=15, MG=15)

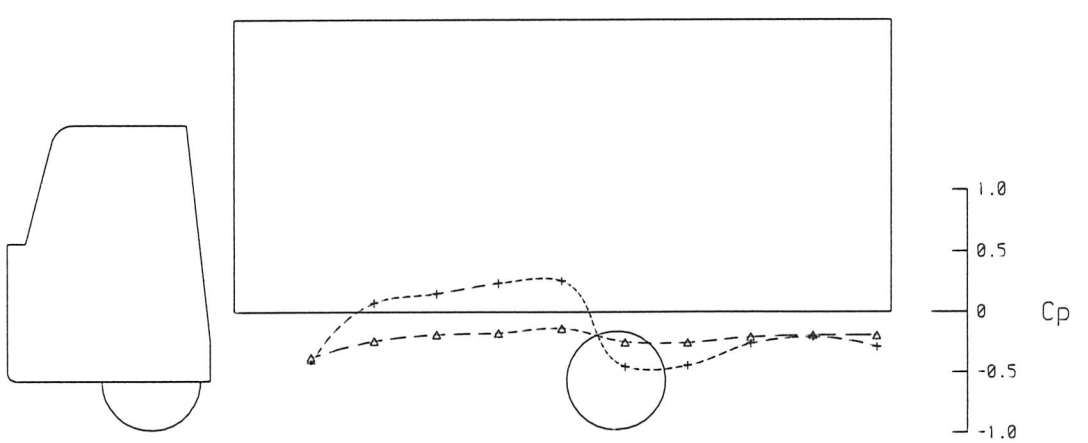

Loop B

Δ = Basic with airdam, Rotating wheels on non-yawed belt (model=0, MG=0)

\+ = Basic with airdam, Rotating wheels on yawed belt (model=15, MG=15)

FIG.29

THE EFFECT OF WHEEL ROTATION ON CONTAINER LOWER SURFACE PRESSURE DISTRIBUTION IN 3.5m x 2.6m WIND TUNNEL, MAY 85

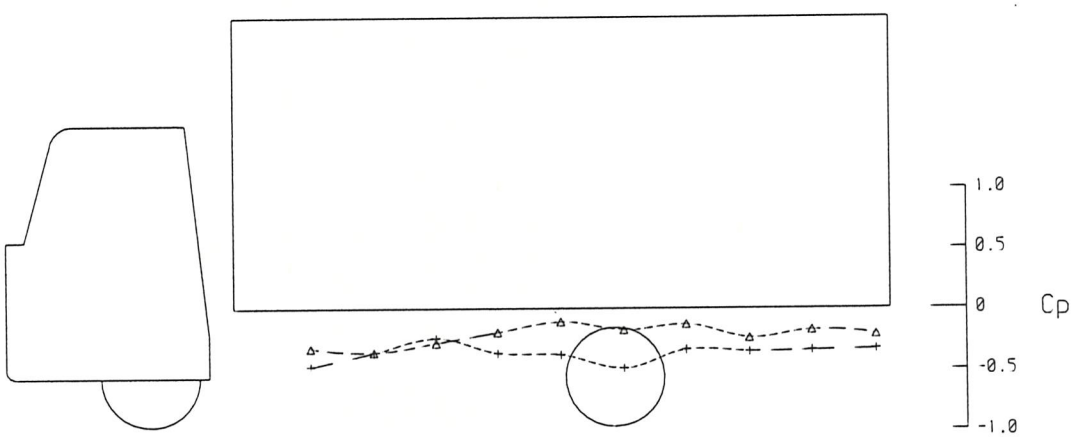

Loop C

△ = Basic, Rotating wheels on non-yawed belt (model=0, MG=0)

\+ = Basic, Rotating wheels on yawed belt (model=15, MG=15)

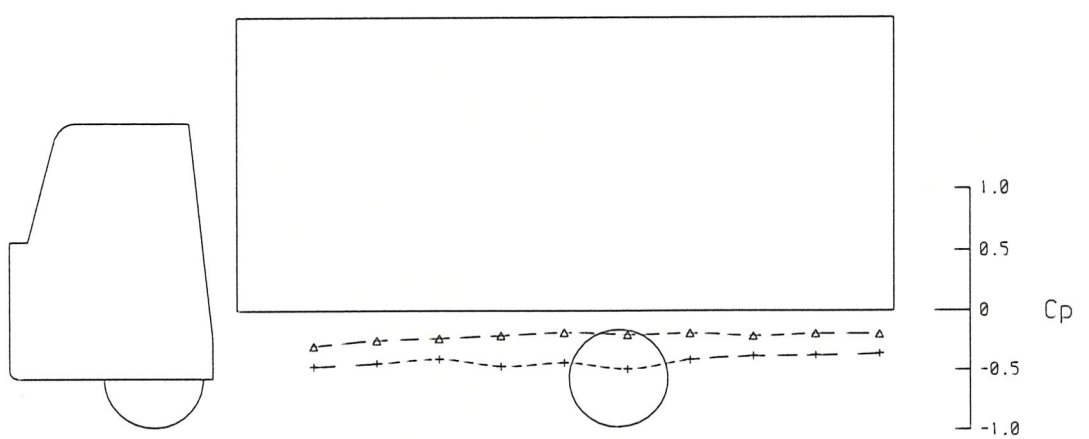

Loop C

△ = Basic with airdam, Rotating wheels on non-yawed belt (model=0, MG=0)

\+ = Basic with airdam, Rotating wheels on yawed belt (model=15, MG=15)

FIG.30

THE EFFECT OF WHEEL ROTATION ON CONTAINER LOWER SURFACE PRESSURE DISTRIBUTION IN 3.5m x 2.6m WIND TUNNEL, MAY 85

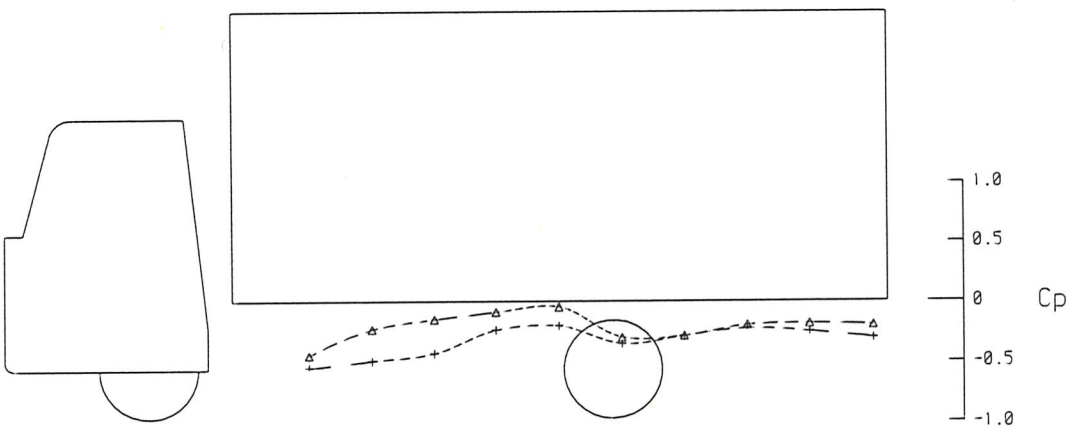

Loop D

Δ = Basic, Rotating wheels on non-yawed belt (model=0, MG=0)

\+ = Basic, Rotating wheels on yawed belt (model=15, MG=15)

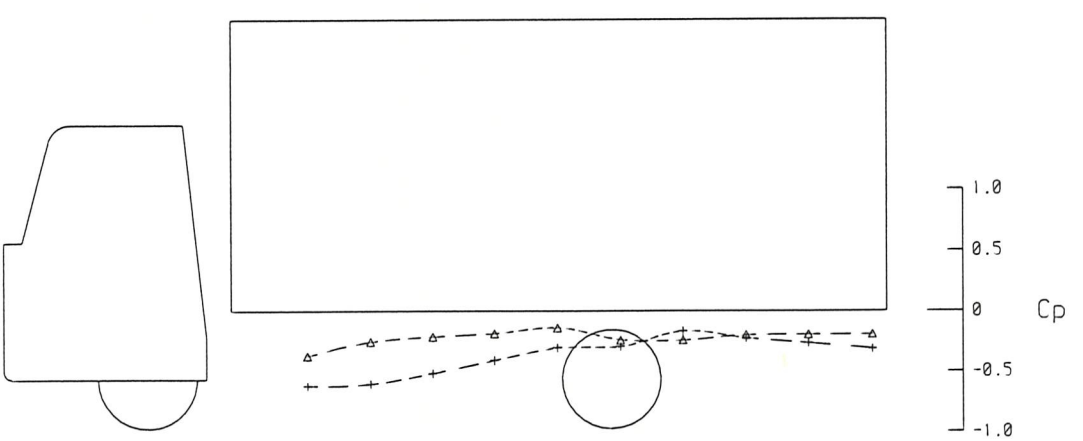

Loop D

Δ = Basic with airdam, Rotating wheels on non-yawed belt (model=0, MG=0)

\+ = Basic with airdam, Rotating wheels on yawed belt (model=15, MG=15)

FIG.31

THE EFFECT OF WHEEL ROTATION ON CONTAINER LOWER SURFACE PRESSURE DISTRIBUTION
IN 3.5m x 2.6m WIND TUNNEL,MAY 85

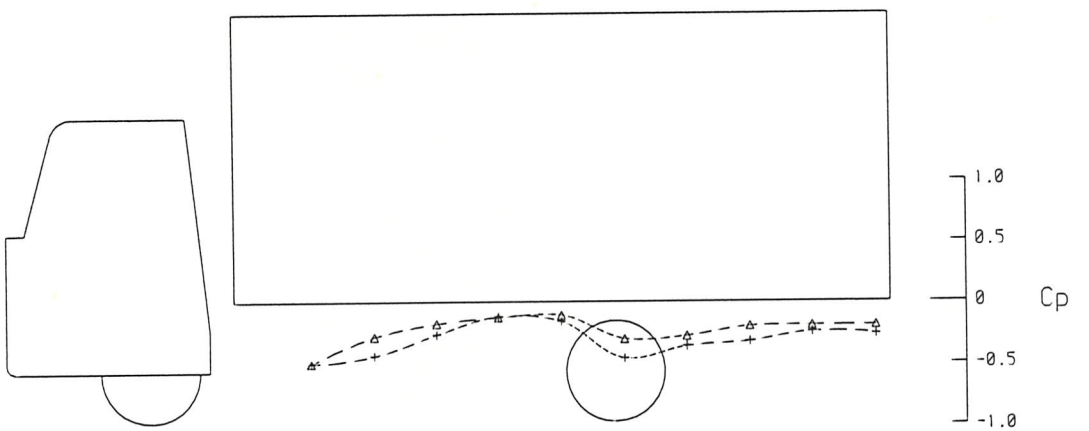

Loop E

Δ = Basic,Rotating wheels on non-yawed belt(model=0,MG=0)

+ = Basic,Rotating wheels on yawed belt(model=15,MG=15)

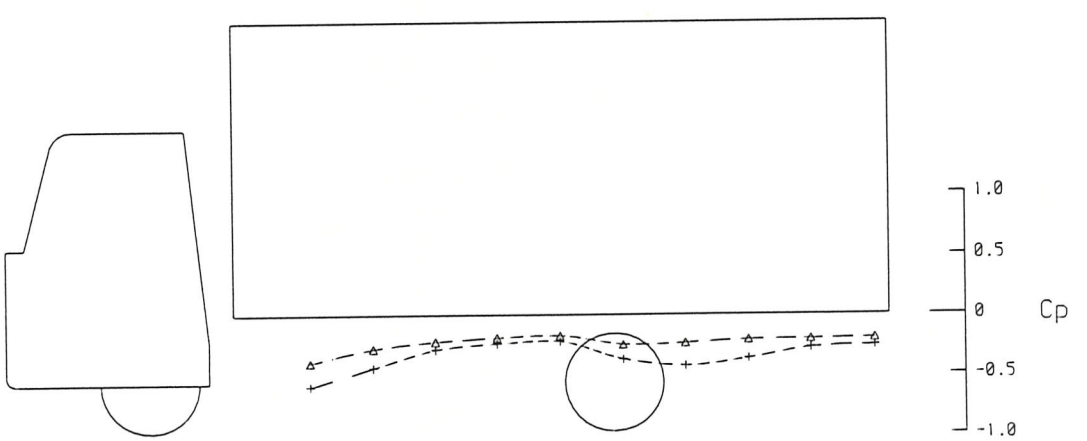

Loop E

Δ = Basic with airdam,Rotating wheels on non-yawed belt(model=0,MG=0)

+ = Basic with airdam,Rotating wheels on yawed belt(model=15,MG=15)

FIG.32

THE EFFECT OF WHEEL ROTATION ON CONTAINER LOWER SURFACE PRESSURE DISTRIBUTION
IN 3.5m x 2.6m WIND TUNNEL, MAY 85

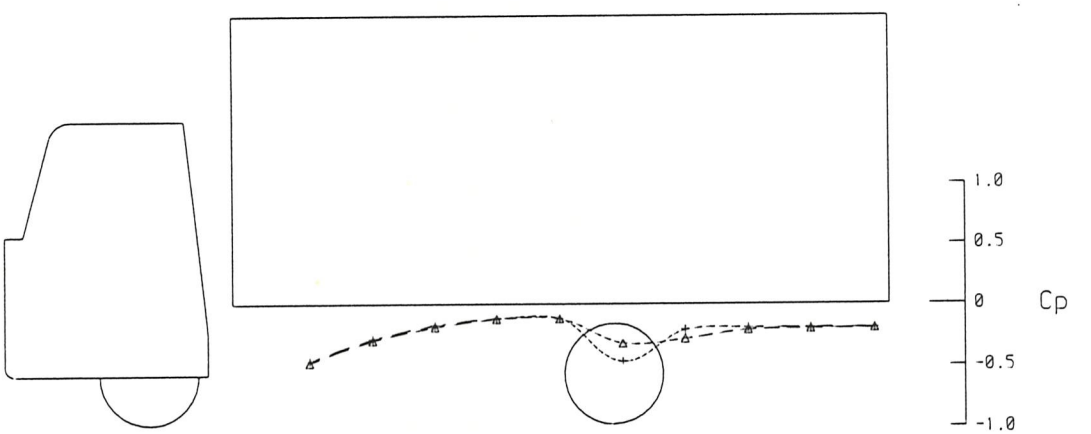

Loop A

Δ = Basic, Rotating wheels on non-yawed belt (model=0, MG=0)

+ = Basic, Fixed wheels over non-yawed belt (model=0, MG=0)

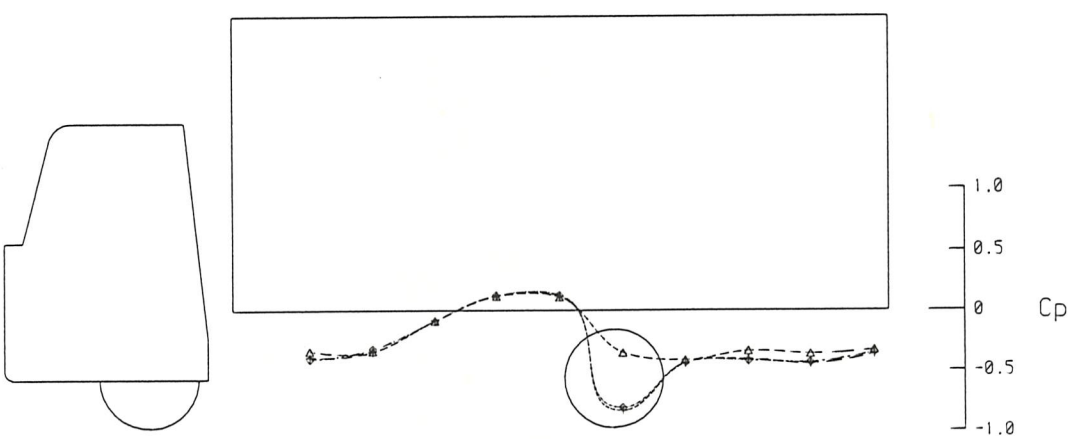

Loop A

Δ = Basic, Rotating wheels on yawed belt (model=15, MG=15)

+ = Basic, Fixed wheels over yawed belt (model=15, MG=15)

◇ = Basic, Fixed wheels over non-yawed belt (model=15, MG=0)

FIG.33

THE EFFECT OF WHEEL ROTATION ON CONTAINER LOWER SURFACE PRESSURE DISTRIBUTION IN 3.5m x 2.6m WIND TUNNEL, MAY 85

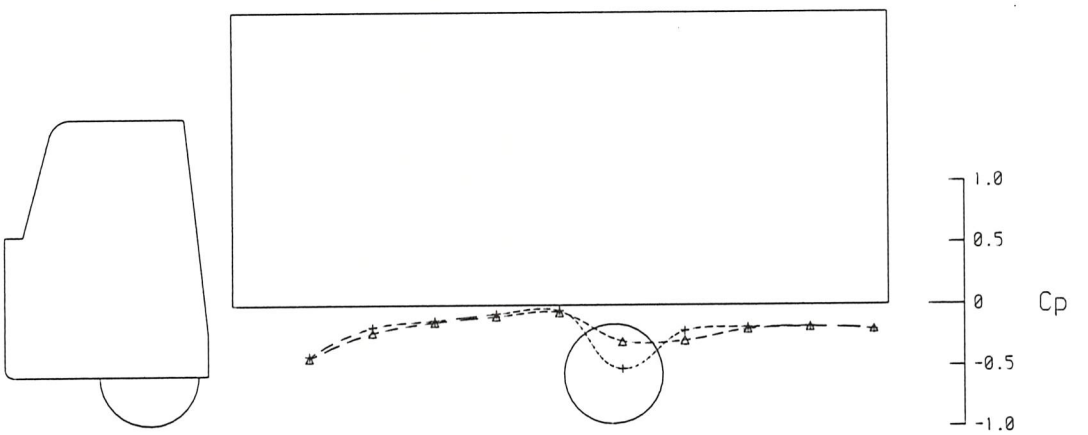

Loop B

△ = Basic, Rotating wheels on non-yawed belt (model=0, MG=0)

+ = Basic, Fixed wheels over non-yawed belt (model=0, MG=0)

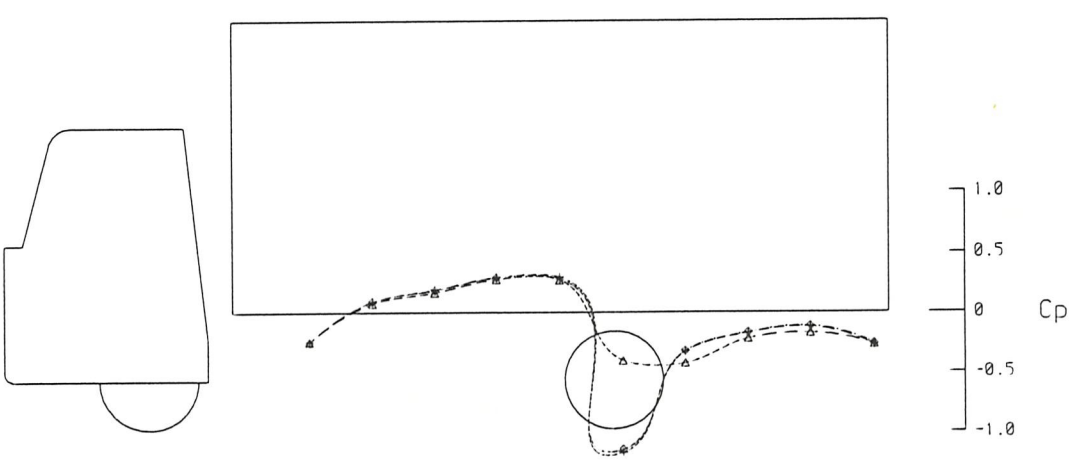

Loop B

△ = Basic, Rotating wheels on yawed belt (model=15, MG=15)

+ = Basic, Fixed wheels over yawed belt (model=15, MG=15)

◇ = Basic, Fixed wheels over non-yawed belt (model=15, MG=0)

FIG.34

THE EFFECT OF WHEEL ROTATION ON CONTAINER LOWER SURFACE PRESSURE DISTRIBUTION
IN 3.5m x 2.6m WIND TUNNEL, MAY 85

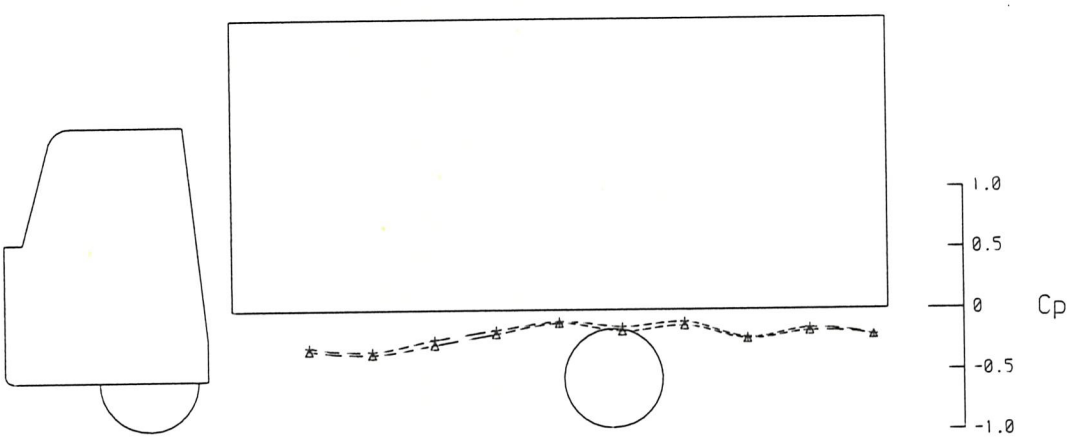

Loop C

Δ = Basic, Rotating wheels on non-yawed belt(model=0, MG=0)

+ = Basic, Fixed wheels over non-yawed belt(model=0, MG=0)

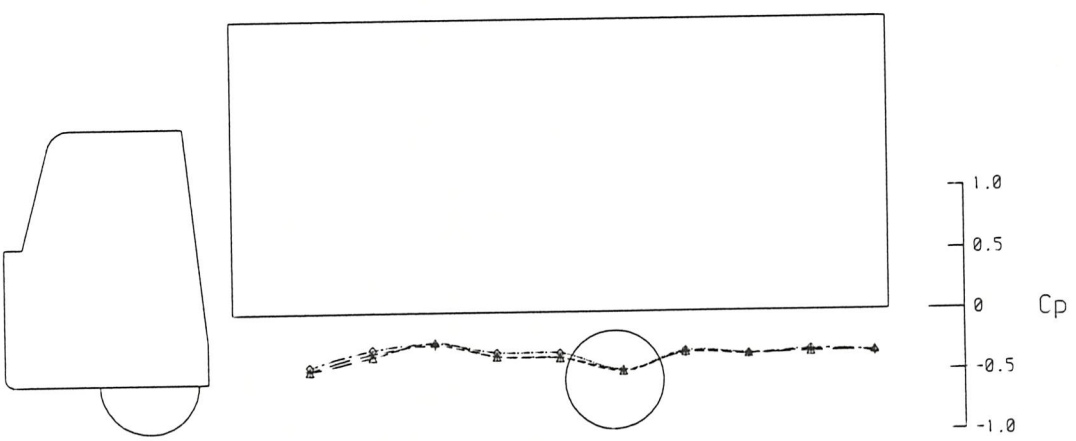

Loop C

Δ = Basic, Rotating wheels on yawed belt(model=15, MG=15)

+ = Basic, Fixed wheels over yawed belt(model=15, MG=15)

◇ = Basic, Fixed wheels over non-yawed belt(model=15, MG=0)

FIG.35

THE EFFECT OF WHEEL ROTATION ON CONTAINER LOWER SURFACE PRESSURE DISTRIBUTION IN 3.5m x 2.6m WIND TUNNEL, MAY 85

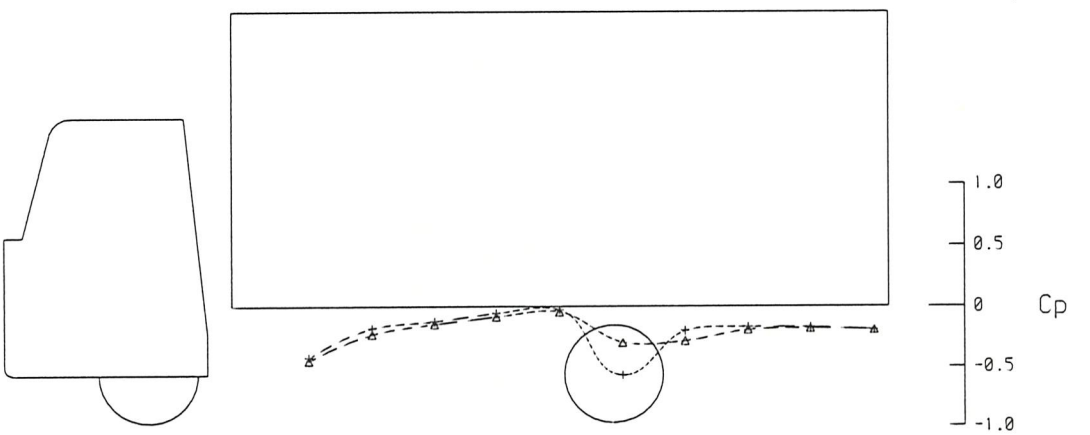

Loop D

Δ = Basic, Rotating wheels on non-yawed belt(model=0, MG=0)

+ = Basic, Fixed wheels over non-yawed belt(model=0, MG=0)

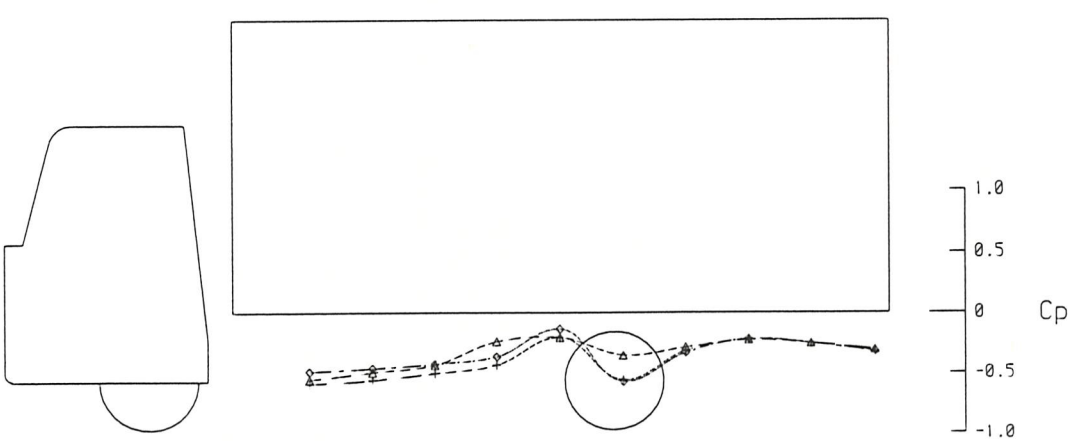

Loop D

Δ = Basic, Rotating wheels on yawed belt(model=15, MG=15)

+ = Basic, Fixed wheels over yawed belt(model=15, MG=15)

◇ = Basic, Fixed wheels over non-yawed belt(model=15, MG=0)

FIG.36

THE EFFECT OF WHEEL ROTATION ON CONTAINER LOWER SURFACE PRESSURE DISTRIBUTION
IN 3.5m x 2.6m WIND TUNNEL,MAY 85

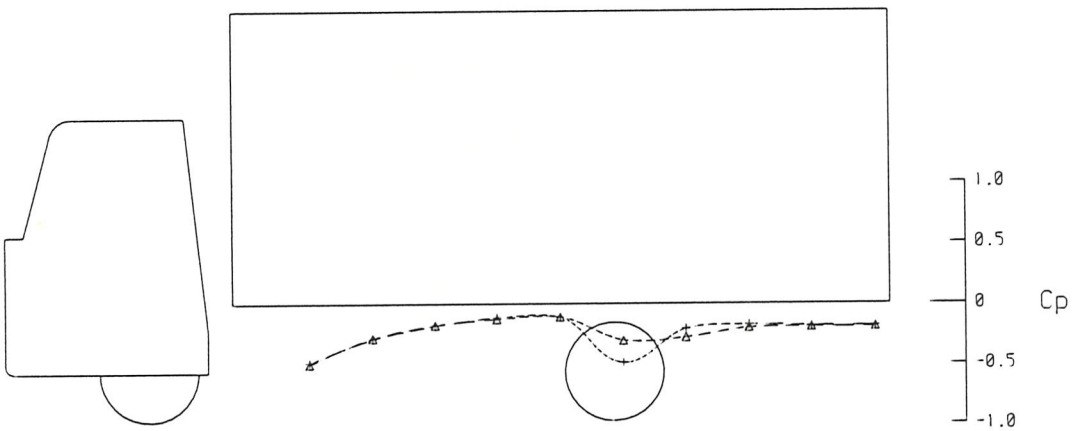

Loop E

Δ = Basic,Rotating wheels on non-yawed belt(model=0,MG=0)

+ = Basic,Fixed wheels over non-yawed belt(model=0,MG=0)

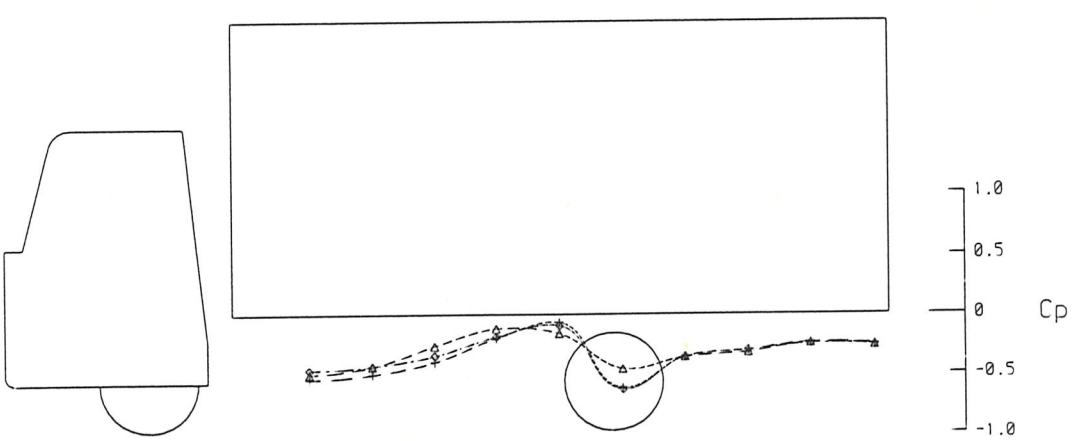

Loop E

Δ = Basic,Rotating wheels on yawed belt(model=15,MG=15)

+ = Basic,Fixed wheels over yawed belt(model=15,MG=15)

◇ = Basic,Fixed wheels over non-yawed belt(model=15,MG=0)

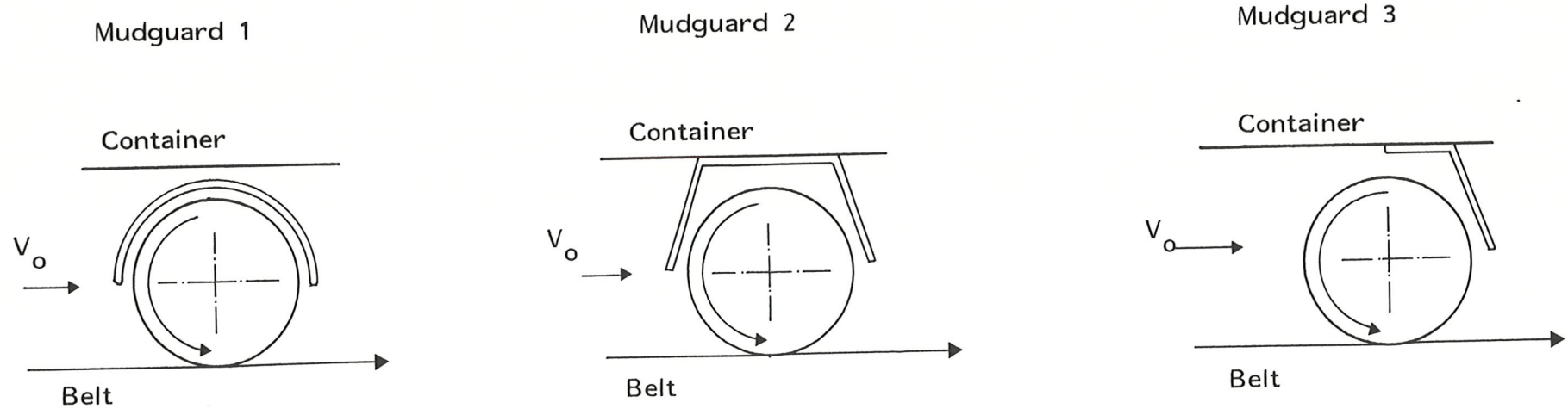

FIG. 37 TYPES OF REAR WHEEL MUDGUARDS FOR 1:6 SCALE RIGID TRUCK MODEL

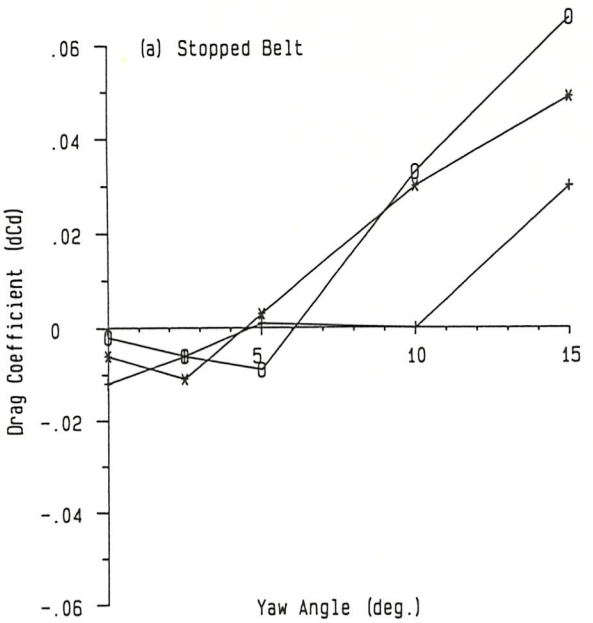

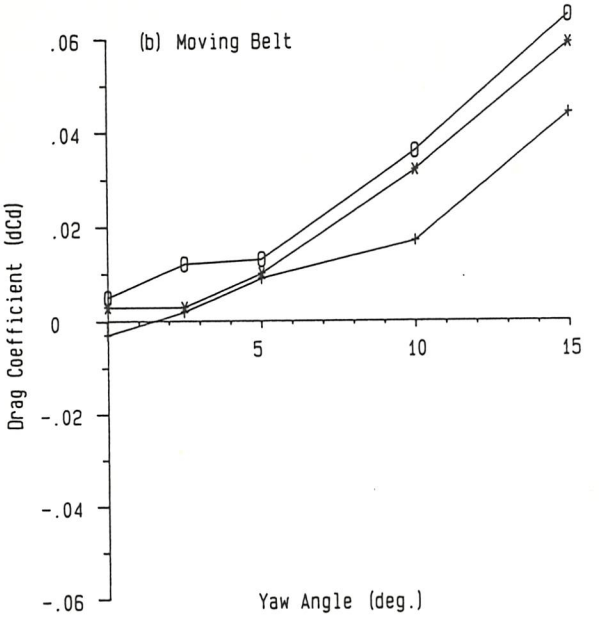

Device Fitted
+ Airdam (1)
* Airdam (2)
0 Airdam (6)

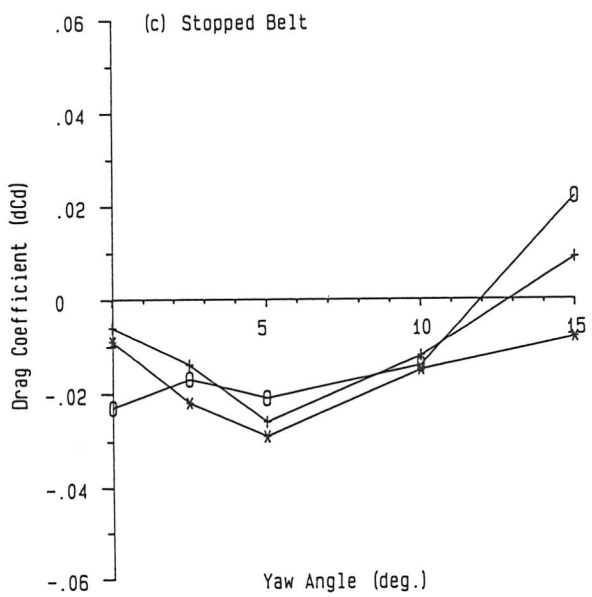

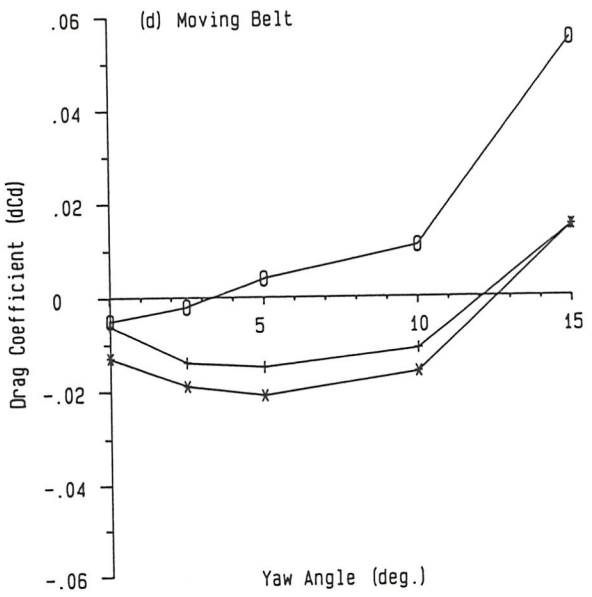

Device Fitted
+ Side Skirt (1)
* Side Skirt (2)
0 Airdam (2) & Side Skirt (2)

FIG. 38 EFFECT OF GROUND MOTION ON DRAG CHANGES WITH FIXTURE OF "ADD-ON" DEVICES FOR 1:6 SCALE RIGID TRUCK MODEL IN 3.5m x 2.6m WIND TUNNEL

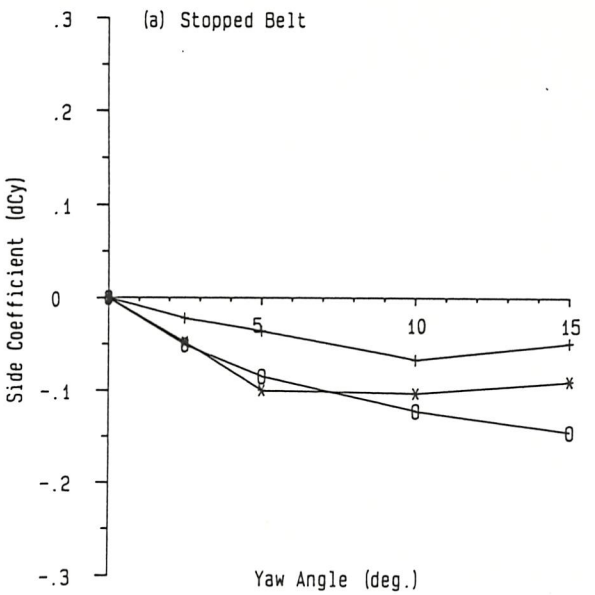

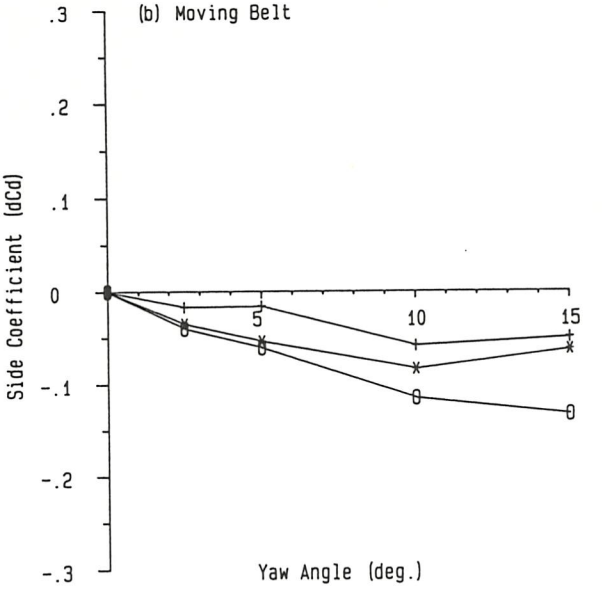

Device Fitted
+ Airdam (1)
* Airdam (2)
0 Airdam (6)

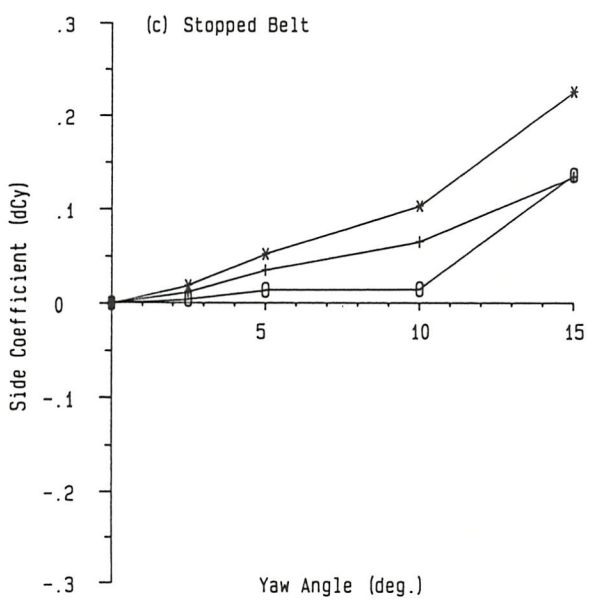

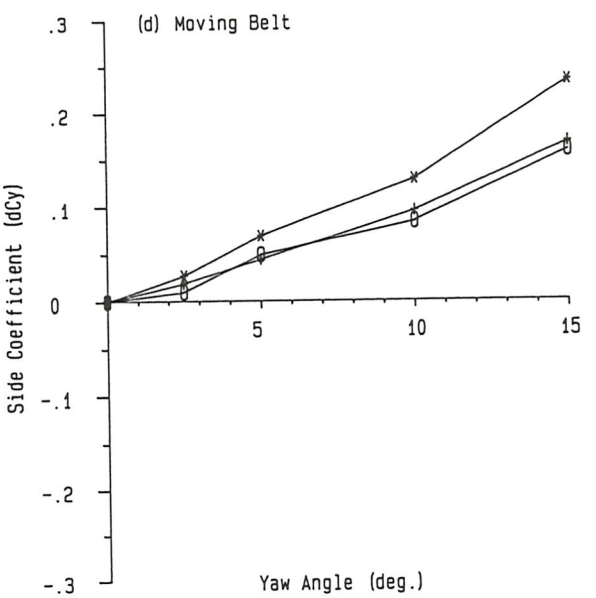

Device Fitted
+ Side Skirt (1)
* Side Skirt (2)
0 Airdam (2) & Side Skirt (2)

FIG. 39 EFFECT OF GROUND MOTION ON SIDE F. CHANGES WITH FIXTURE OF "ADD-ON" DEVICES FOR 1:6 SCALE RIGID TRUCK MODEL IN 3.5m x 2.6m WIND TUNNEL

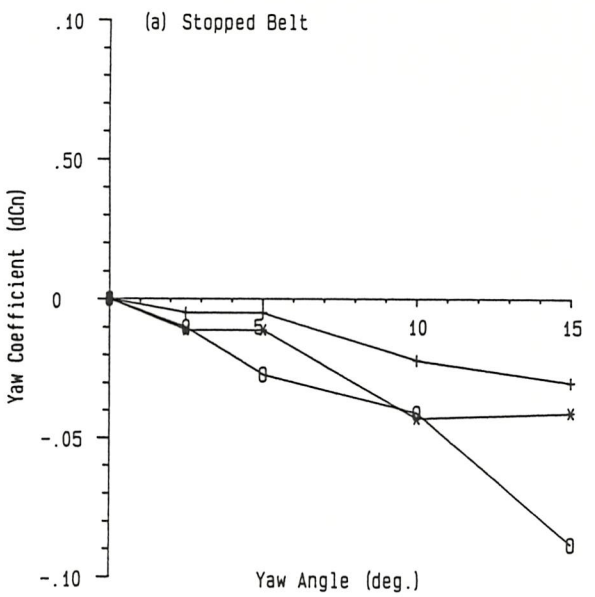

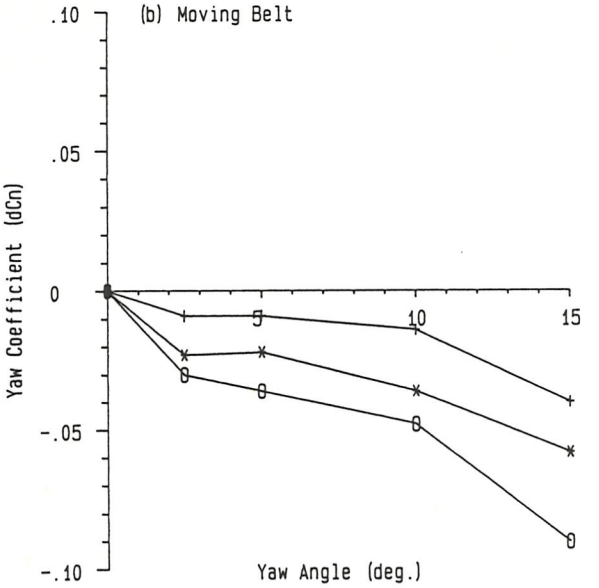

Device Fitted
+ Airdam (1)
* Airdam (2)
0 Airdam (6)

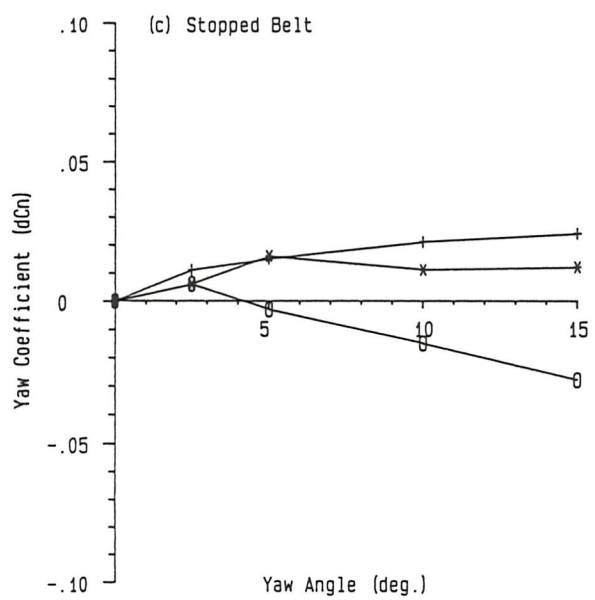

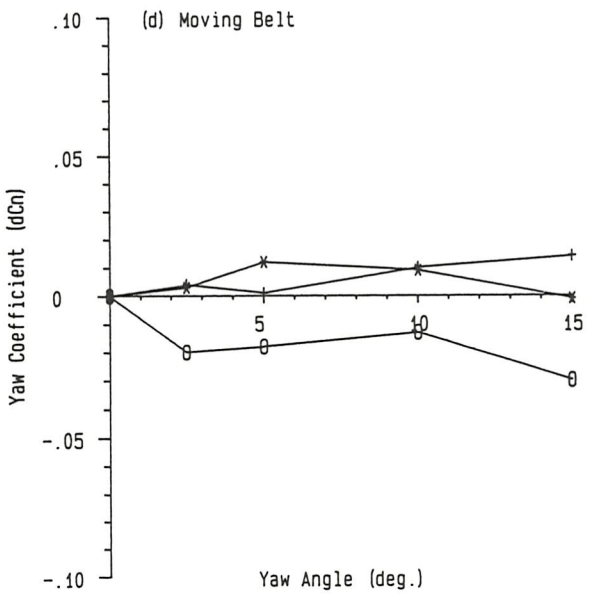

Device Fitted
+ Side Skirt (1)
* Side Skirt (2)
0 Airdam (2) & Side Skirt (2)

FIG. 40 EFFECT OF GROUND MOTION ON YAWING M. CHANGES WITH FIXTURE OF "ADD-ON" DEVICES FOR 1:6 SCALE RIGID TRUCK MODEL IN 3.5m x 2.6m WIND TUNNEL

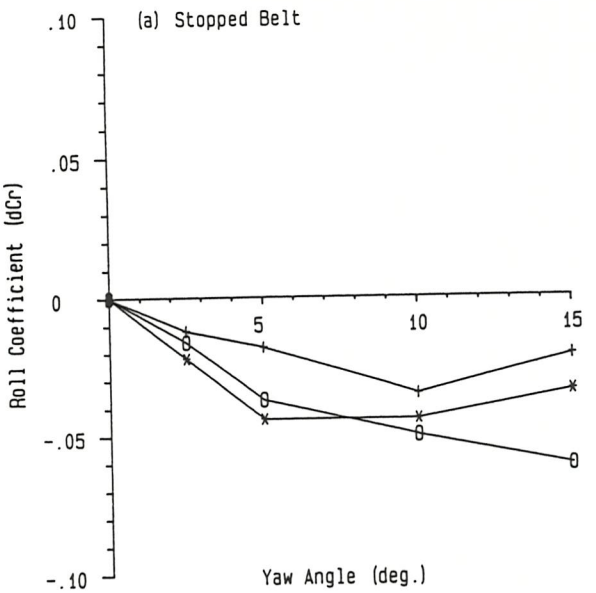

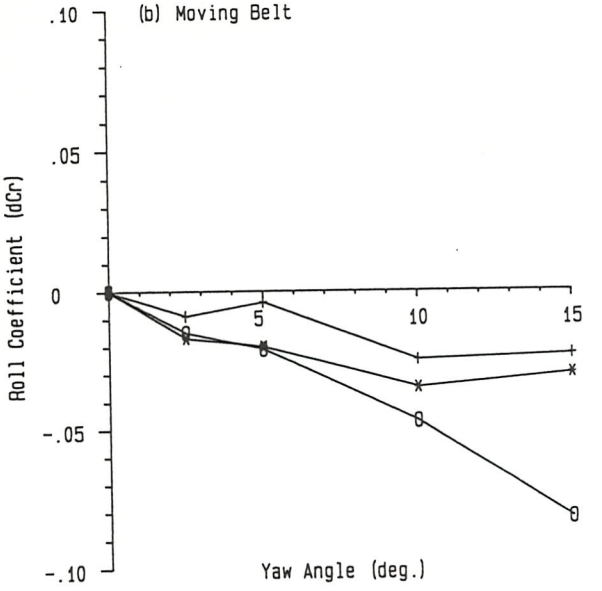

Device Fitted
+ Airdam (1)
* Airdam (2)
0 Airdam (6)

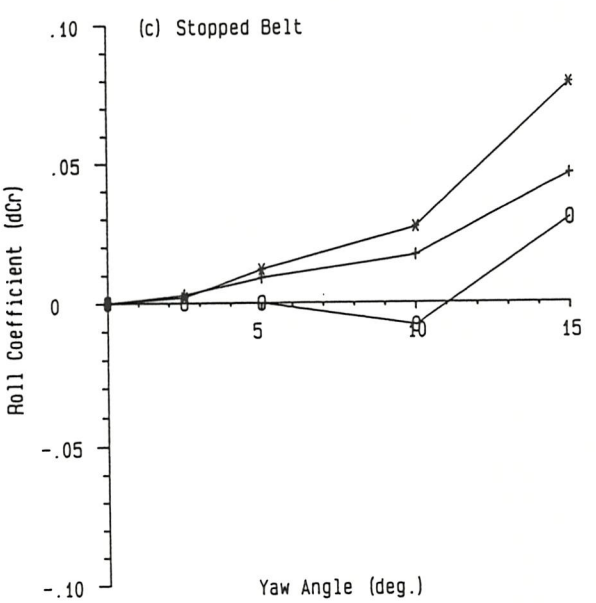

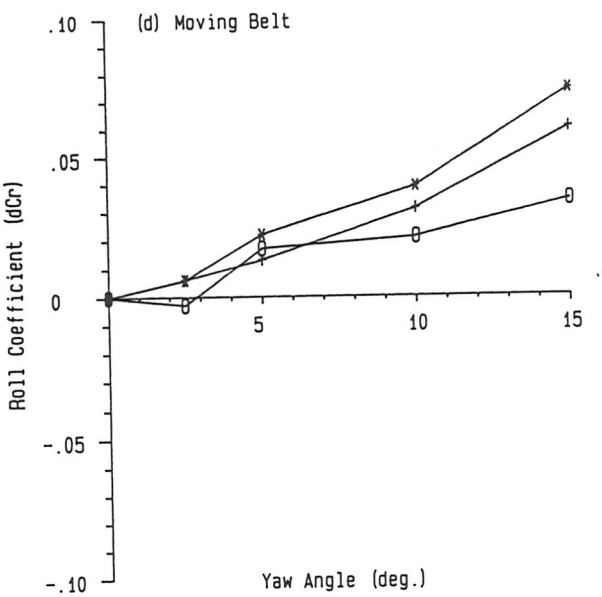

Device Fitted
+ Side Skirt (1)
* Side Skirt (2)
0 Airdam (2) & Side Skirt (2)

FIG. 41 EFFECT OF GROUND MOTION ON ROLLING M. CHANGES WITH FIXTURE OF "ADD-ON" DEVICES FOR 1:6 SCALE RIGID TRUCK MODEL IN 3.5m x 2.6m WIND TUNNEL

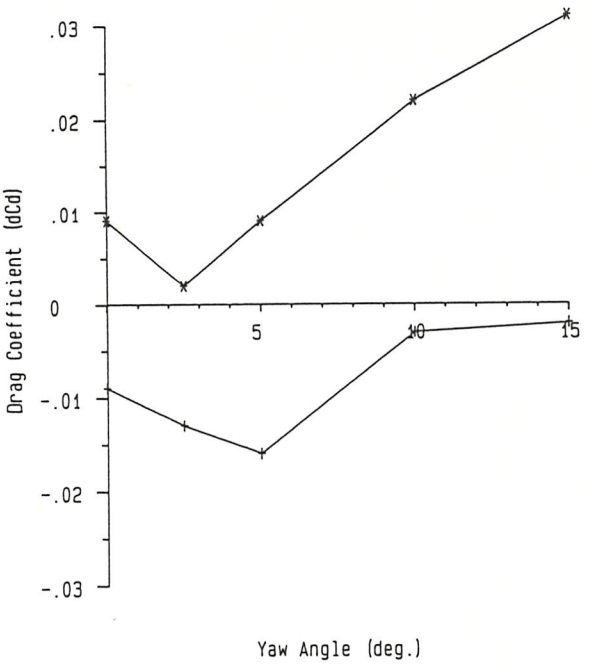

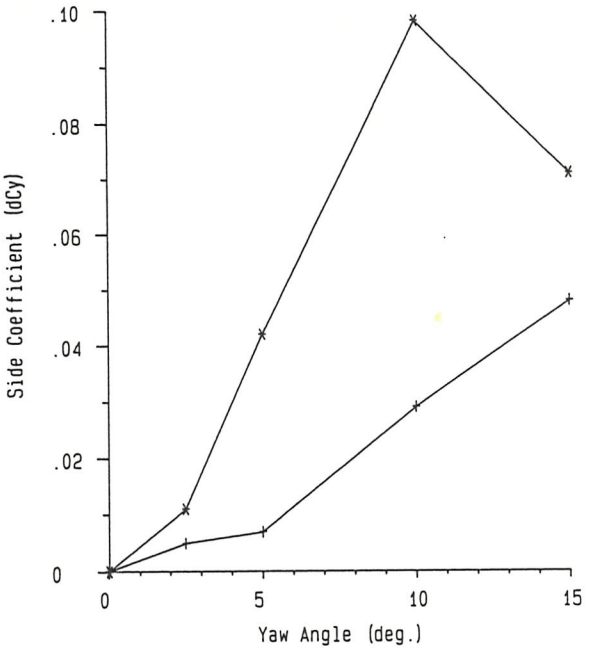

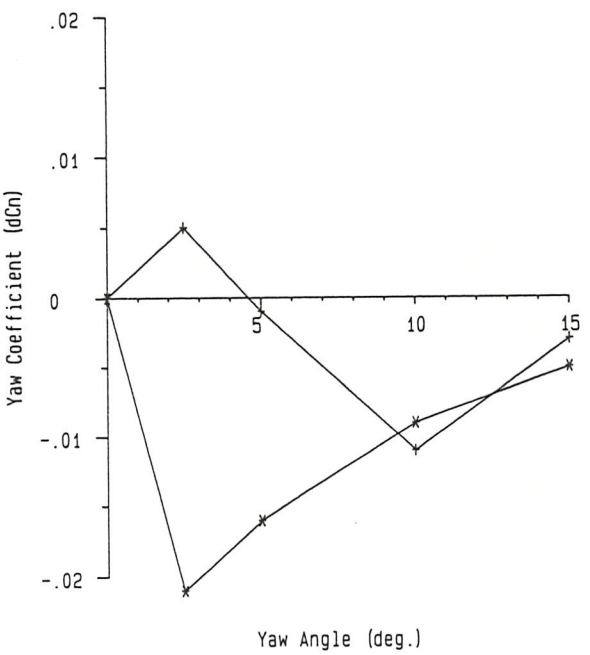

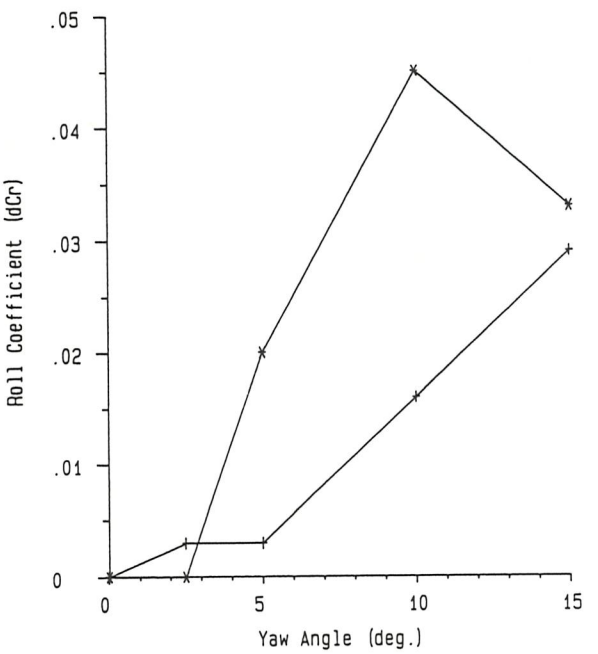

Model Configuration

\+ Baseline

* Baseline with Airdam (2) & Side-Skirt (2)

FIG. 42 EFFECT OF GROUND MOTION FOR 1:6 SCALE RIGID TRUCK MODEL IN 3.5m x 2.6m WIND TUNNEL

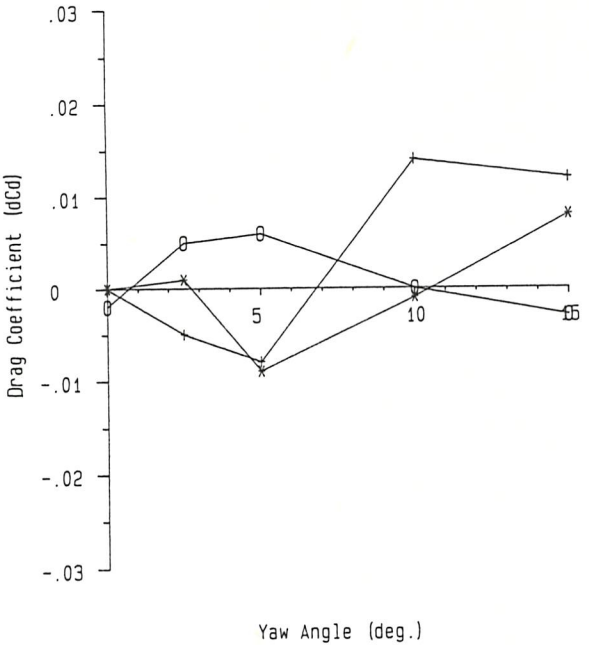

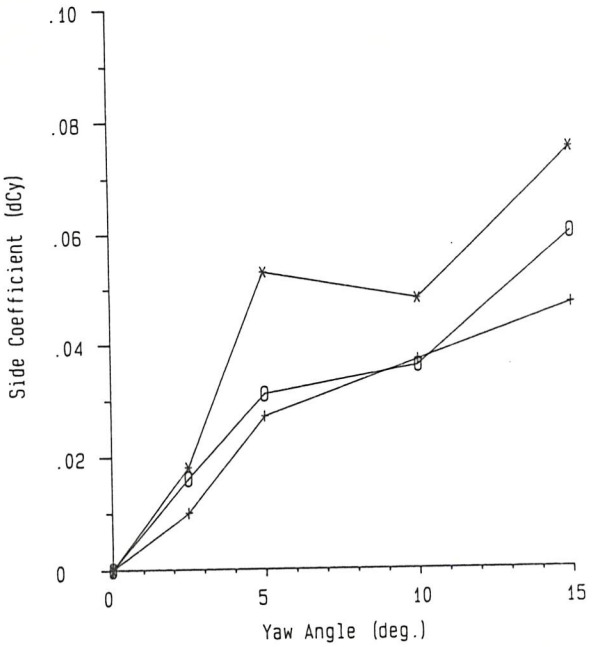

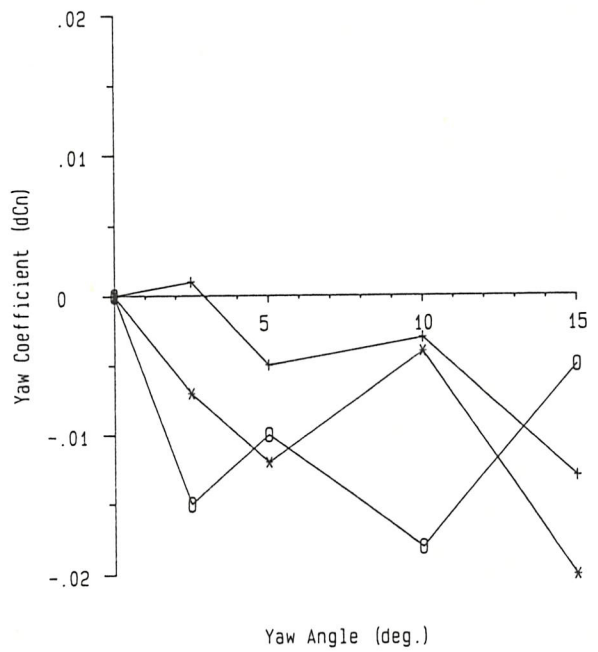

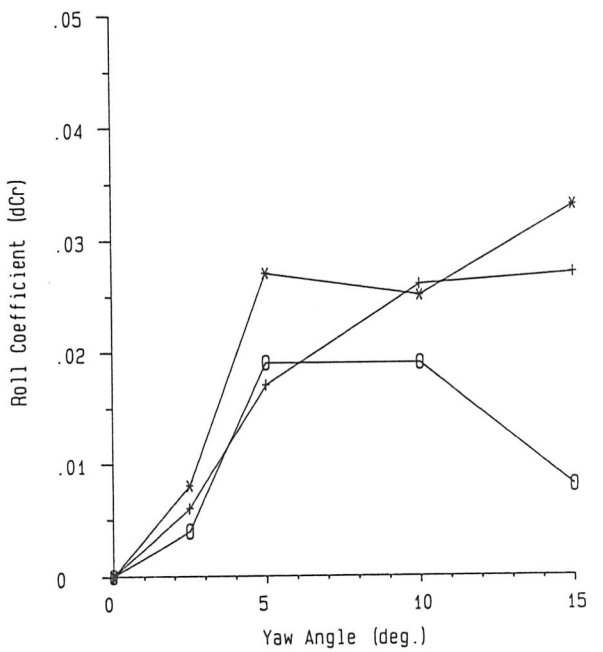

Model Configuration

\+ Baseline with Airdam (1)

* Baseline with Airdam (2)

0 Baseline with Airdam (6)

FIG. 43 EFFECT OF GROUND MOTION FOR 1:6 SCALE RIGID TRUCK MODEL IN 3.5m x 2.6m WIND TUNNEL

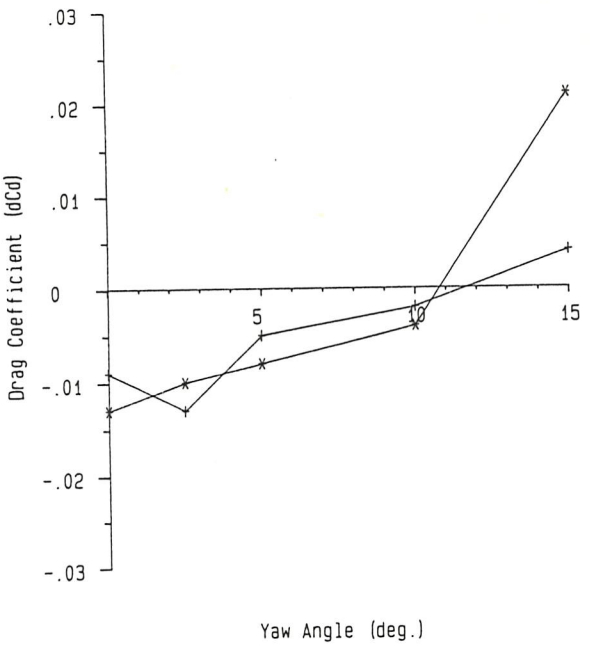

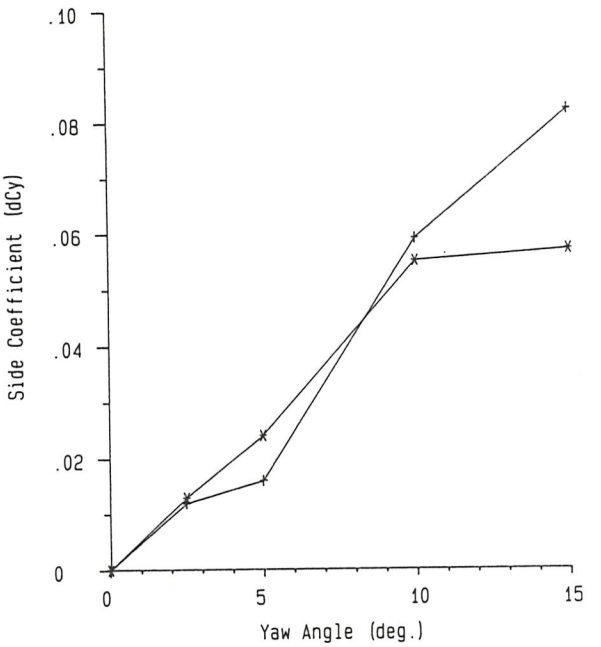

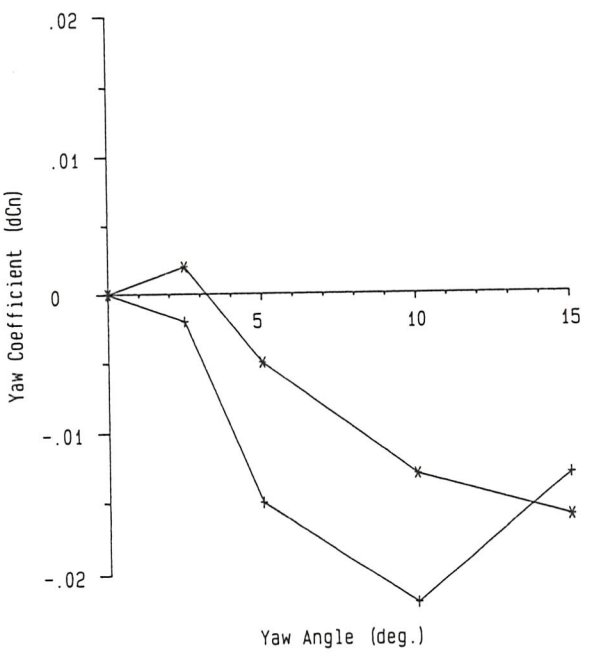

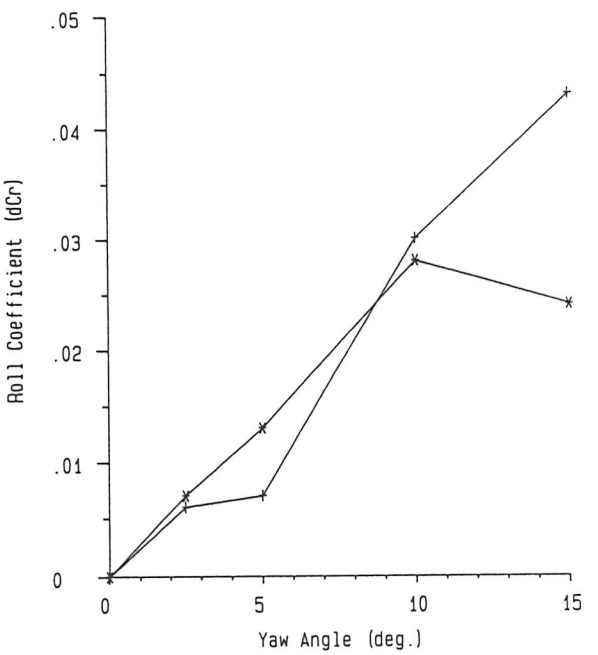

Model Configuration
+ Baseline with Side-Skirt (1)
* Baseline with Side-Skirt (2)

FIG. 44 EFFECT OF GROUND MOTION FOR 1:6 SCALE RIGID TRUCK MODEL IN 3.5m x 2.6m WIND TUNNEL

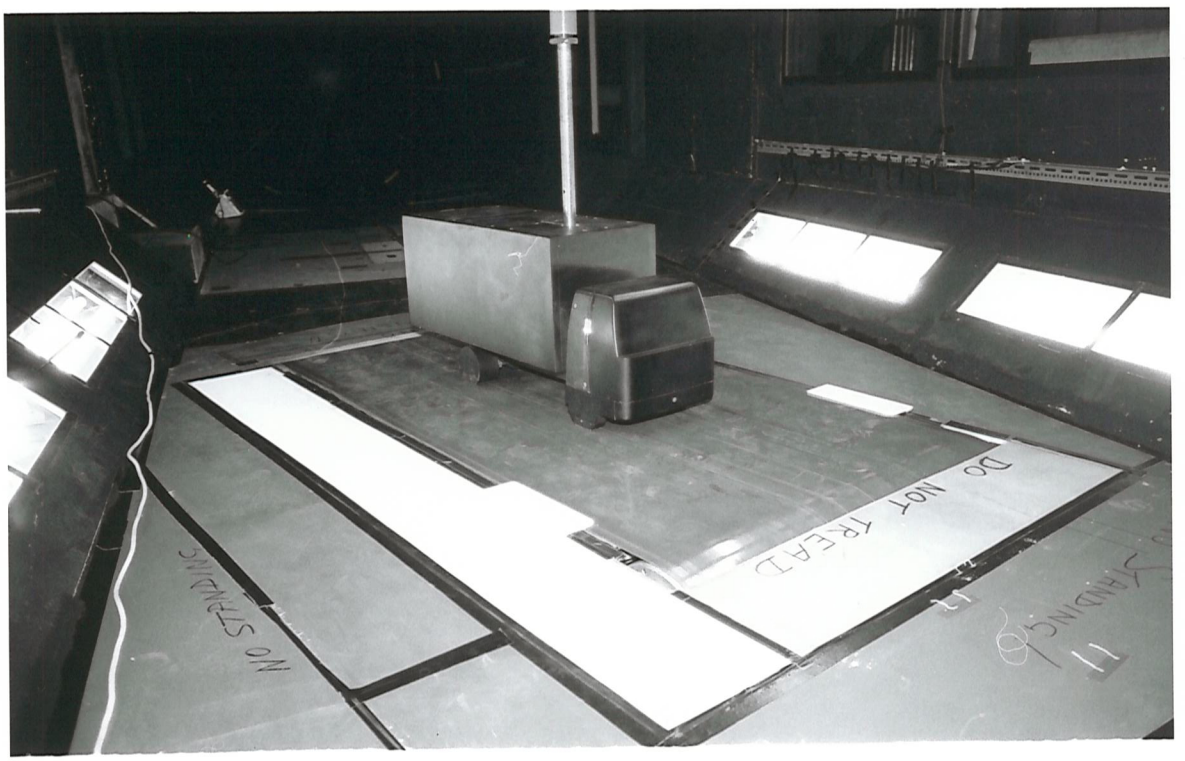

(a)

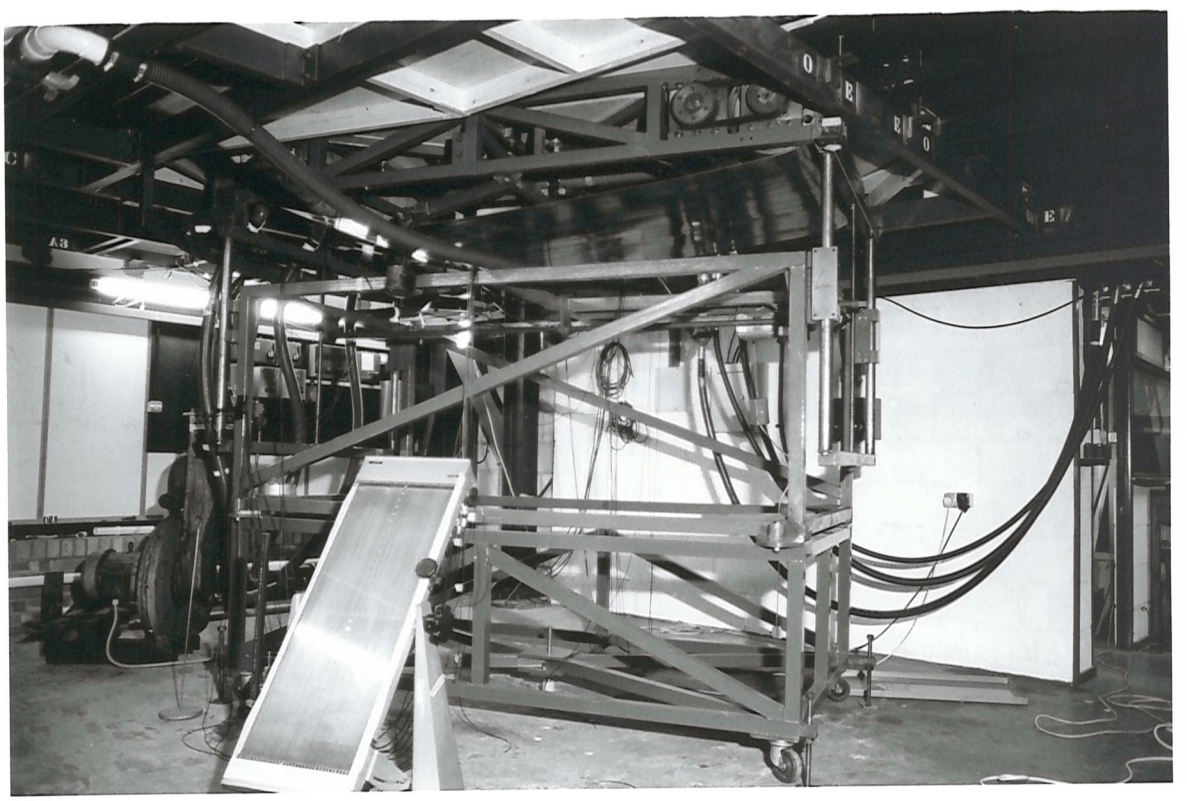

(b)

Plate 1

(a)

(b)

Plate 2

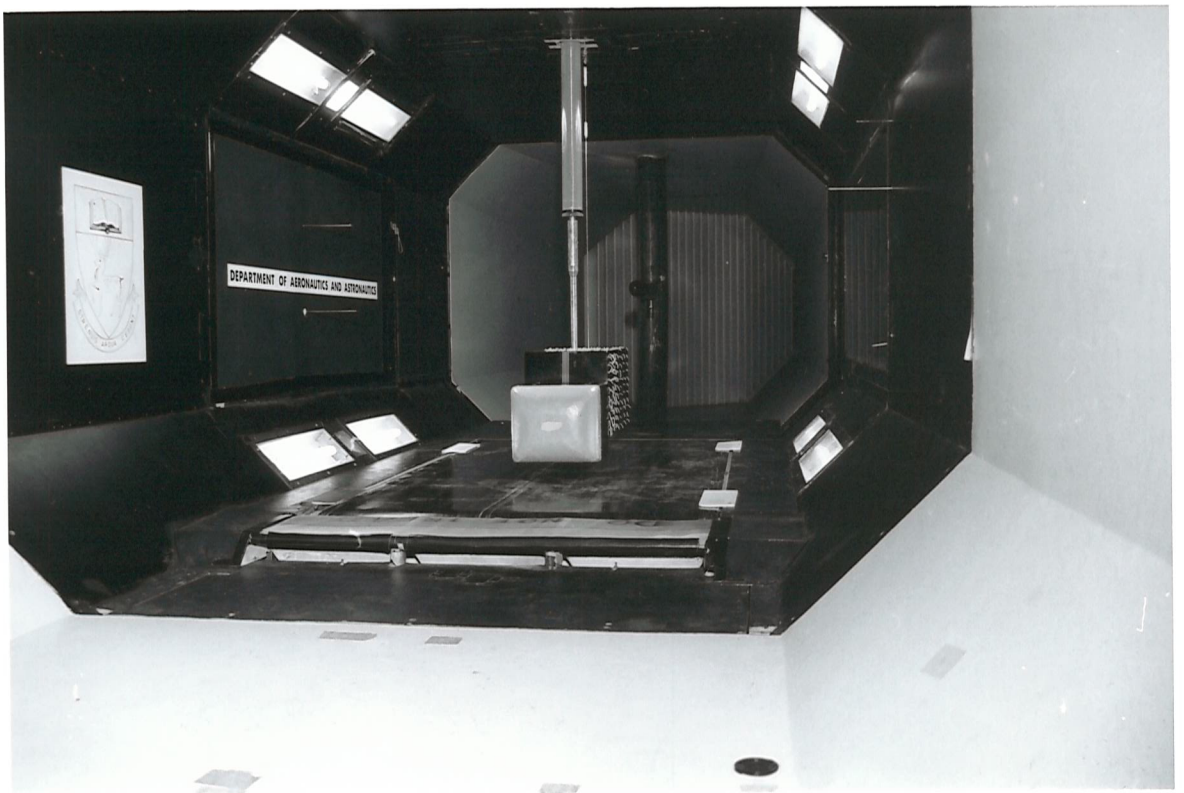
DEPARTMENT OF AERONAUTICS AND ASTRONAUTICS

(a)

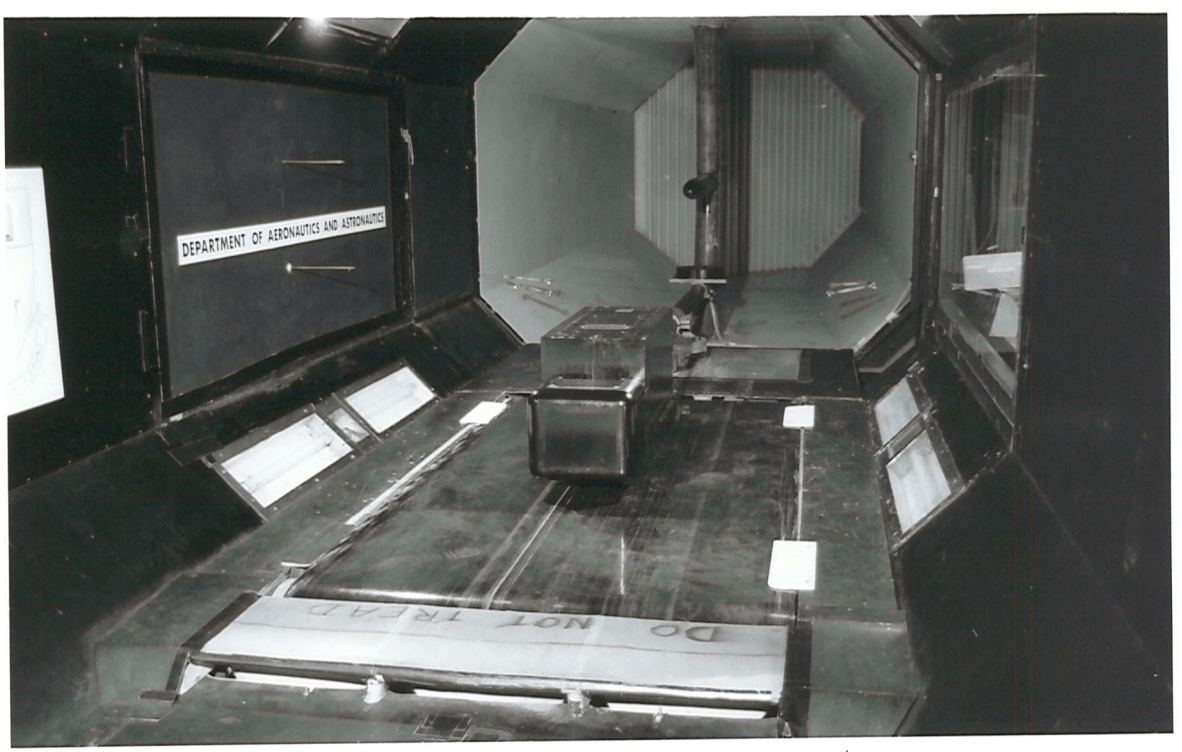
DEPARTMENT OF AERONAUTICS AND ASTRONAUTICS
DO NOT TREAD

(b)

Plate 4

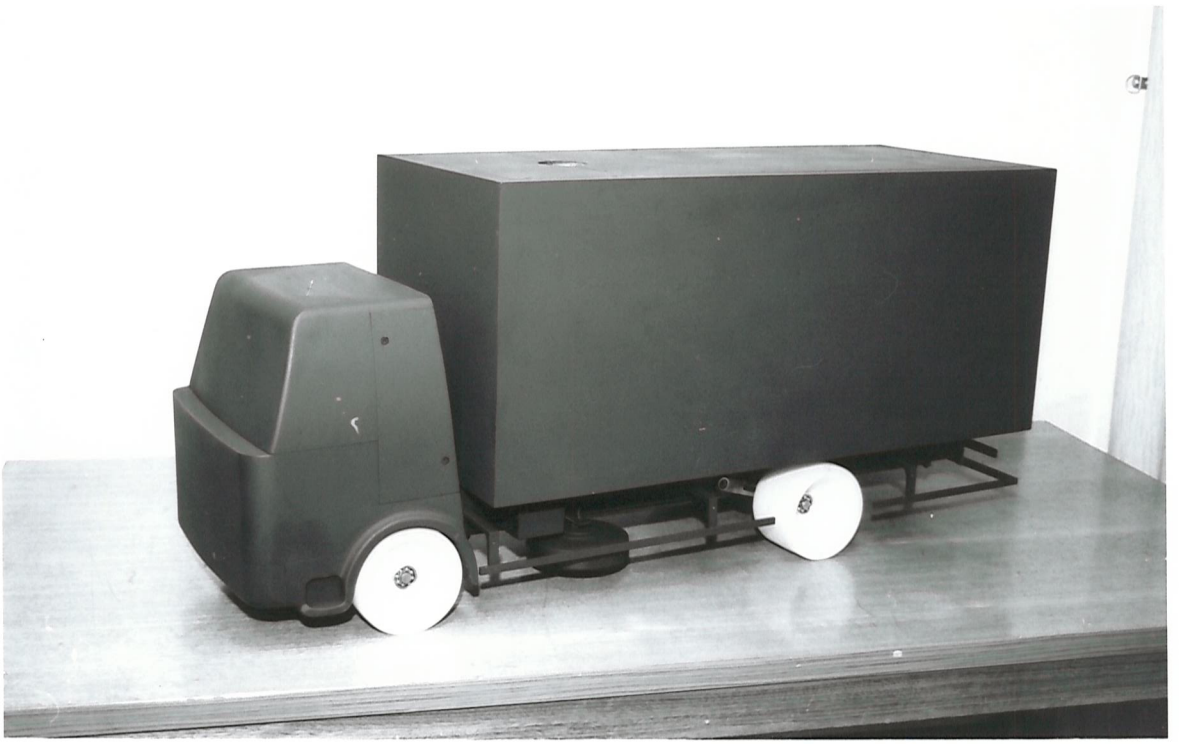

(a)

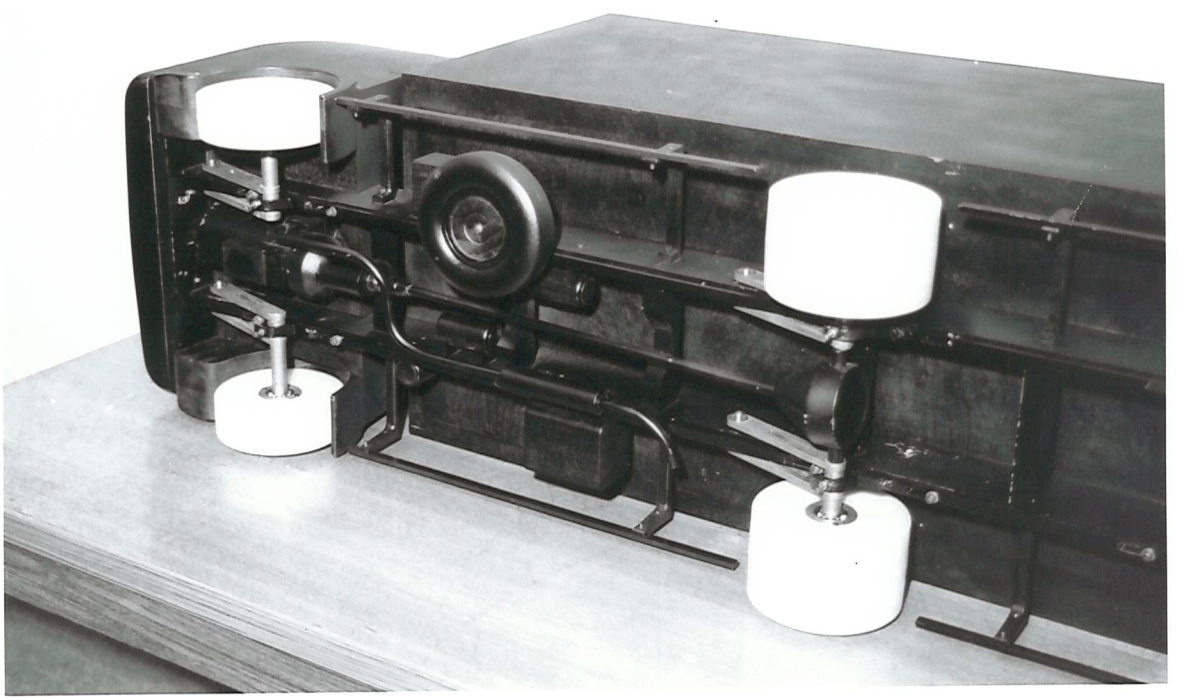

(b)

Plate 5